Homaeigohar, Shahin; Elbahri, Mady

Switchable Plasmonic Nanocomposites

Published in:
ADVANCED OPTICAL MATERIALS

DOI:
10.1002/adom.201801101

Published: 04/01/2019

Document Version
Peer-reviewed accepted author manuscript, also known as Final accepted manuscript or Post-print

Please cite the original version:
Homaeigohar, S., & Elbahri, M. (2019). Switchable Plasmonic Nanocomposites. *ADVANCED OPTICAL MATERIALS*, *7*(1), Article 1801101. https://doi.org/10.1002/adom.201801101

DOI: 10.1002/ ((please add manuscript number))

Article type: Review

Switchable Plasmonic Nanocomposites

*Shahin Homaeigohar, Mady Elbahri**

Dr. S. Homaeigohar, Prof. M. Elbahri

Nanochemistry and Nanoengineering, School of Chemical Engineering, Department of Chemistry and Materials Science, Aalto University, Kemistintie 1, 00076 Aalto, Finland.

E-mail: mady.elbahri@aalto.fi,Tel.: +358-50-431-9831.

Keywords: ((switchability, optical nanomaterials, nanocomposites, plasmonics, external stimuli))

Abstract

Smartness in nature is inspiring for engineers to design biomimetic devices acting based on switchable properties. In this regard, the nanomaterials able to show reversible optical properties have drawn immense attention from research and technology communities. In this review, we introduce diverse classes of switchable plasmonic nanocomposites (SPNs) according to their stimuli, structure, and composition. The SPNs perform relying on the reversible changes of the dielectric matrix' refractive index and physicochemical properties under the influence of various stimuli leading to alteration in the interparticle spacing of the encapsulated plasmonic nanoparticles thus their coupling intensity. Moreover, the stimuli

induced reversible reconfiguration of the plasmonic nanoparticles forming ordered or disordered structures is considered another operation mechanism for this group of advanced optical nanomaterials. The latter category involves a larger number of plasmonic nanoparticles and induces a more notable change in optical properties by the switching process. The enhanced controllability over synthesis, function and properties of the as-developed metamaterials could guarantee a better scalability, as well. Thus, it holds great promise for next generation of optical devices including optical switches, transducers, modulators etc. As a specific highlight for the future perspective, the switchable plasmonic molecules based nanocomposites will be introduced and the recent progress will be discussed. Ultimately, prospects, outlooks and the current bottlenecks in this field will be presented.

Table of Content

Abbreviatives List

Bovine Serum Albumin	BSA
Carbon Nanotube	CNT
Dynamic Self-Assembly	DSA
Electric Field	EF
Glass Transition Temperature	T_g
Glutathione	GSH
Graphene Oxide, Reduced Graphene Oxide	GO, rGO
Hexa(ethylene glycol)	HEG
Interpenetrating Polymer Network	IPN
Interparticle Spacing	IS
Liquid Crystal	LC
Localized Surface Plasmon Resonance	LSPR
Lower Critical Solution Temperature	LCST
Magnetic Field	MF
Merocyanine	MC
Nanoparticle	NP
Nanorod	NR

Nanosphere	NS
Nanotube	NT
Nanocrystal	NC
Nanowire	NW
Nanofiber	NF
Nanobipyramids	NBP
Near Infra Red	NIR
Near Ultraviolet	NUV
Poly(acrylic acid)	PAA
Poly(acrylonitrile-co- glycidylmethacrylate)	PANGMA
Polyaniline	PANI
Polyethylene Oxide	PEO
Polymethacrylic acid	PMAA
Poly(N-isopropylacrylamide)	PNIPAM
Poly(*N*-isopropylacrylamide-*co*-3-methacryloxypropyltrimethoxysilane)	p(NIPAM-*co*-MAPTMS)
Polystyrene	PS
Polystyrene-Poly(acrylic acid)	(PS-*b*-PAA)
Polyvinylalcohol	PVA
Polyvinylidene fluoride	PVDF
Poly(vinylpyrrolidone)	PVP
Plasmon Coupling	PC
Quantum Dot	QD
Refractive Index	RI
Spiropyran	SP
Surface Enhanced Raman Scattering	SERS
Switchable Plasmonic Nanocomposite	SPN
Transmission Electron Microscopy	TEM
Zero to Three Dimensional	0-3D

1. Introduction

Composite materials show a promising package of properties that are resulted from a combination of favorable surrounding medium's and filler's properties[1-6]. Such properties are not limited to the classic and predefined ones rather new properties and functionalities can emerge, in particular, when the filler's dimensions lie in the nanoscale, as seen in the nanocomposites. This area is dynamic and has been widely spotlighted globally, in particular, in the past decade. For instance, Faupel's group introduced various classes of functional metal-polymer nanocomposites in a review paper.[4] Behrens[7] reported about the progresses in the magnetic nanocomposites field and Elbahri's group[8-10] reviewed the various nanocomposites designed for solar absorbers, for structural coloration, antireflection coating, and environmental remediation. With respect to the nanoparticulate nanocomposites, Kango et al.[11] surveyed the surface modification approaches of inorganic nanoparticles that could be employed in construction of organic–inorganic functional nanocomposites. In this regard, a precious review was also authored by Goesmann and Feldmann[12] where they comprehensively studied various functional nanoparticulate materials. Last but not least, very recently, the colloidal nanocomposites with optical functionality have been thoroughly discussed by Hsu et al. [13].

In the last few years, the nanocomposite area has progressed fast and expanded to new dimensionalities (0-3D), Figure 1. Considering this fact, as a concrete, all inclusive definition, nanocomposites are multi-component materials whose properties are strongly associated with the composition, size, and arrangement of particles (i.e. the fillers) that could be largely affected by the surrounding medium's properties and structure. In this study, we review those kind of nanocomposites whose main nanoelement is plasmonic nanoparticles embedded within a polymer matrix or surface functionalized by active polymeric ligands and are able to show a switchable optical performance when subjected to different stimuli. These nanostructures are called as switchable plasmonic nanocomposites (SPNs).

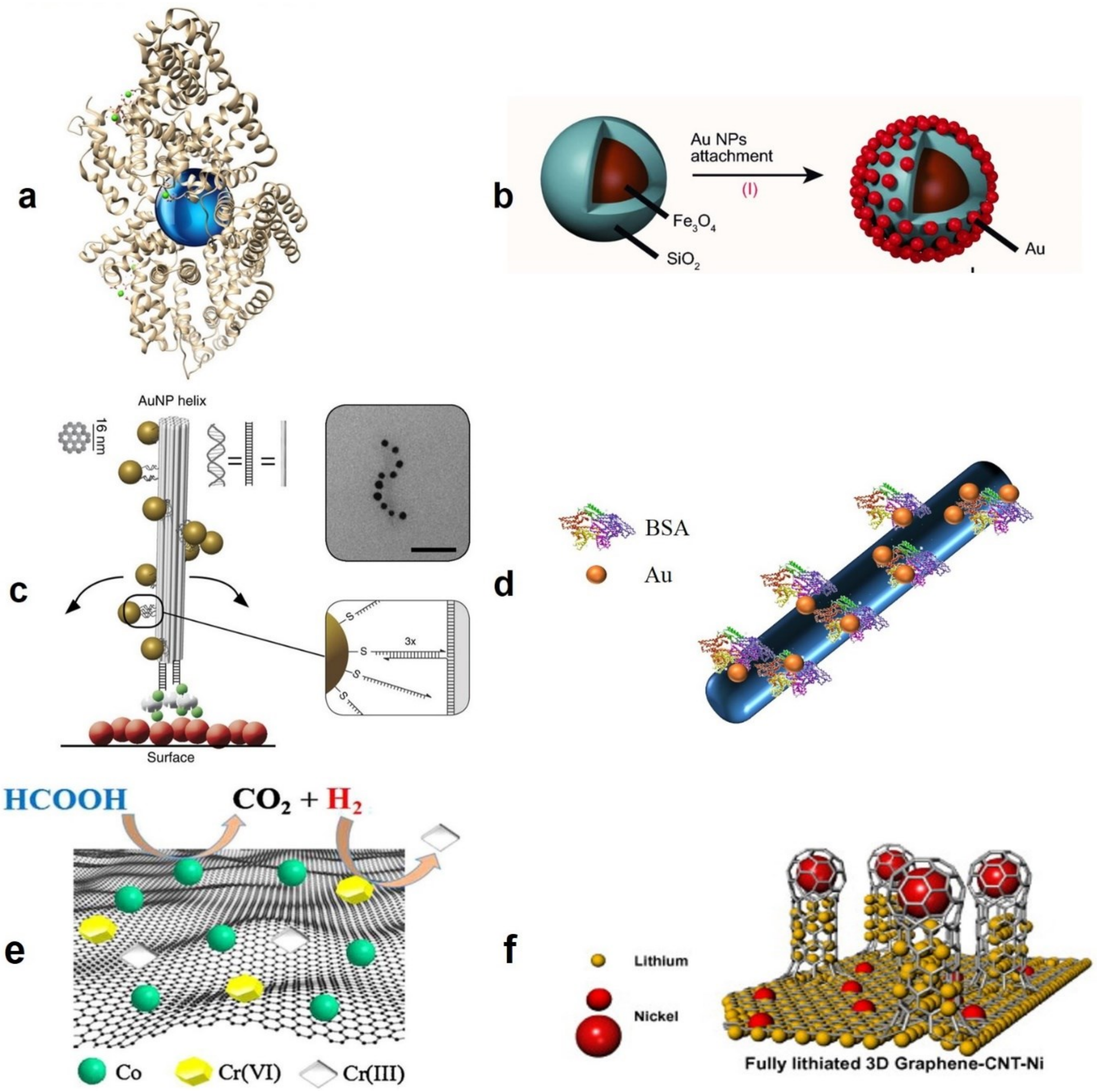

Figure 1. Nanocomposite systems in different dimensionalities. a) A 0D conjugate of plasmonic NP and BSA protein. Reproduced with permission.[14] Copyright 2017, John Wiley and Sons., b) A 0D superparamagnetic Au NPs/Fe_3O_4@SiO_2 core–shell system made via chemical adsorption of Au NPs to the amino groups pre-grafted on the SiO_2 surface. Reproduced with permission.[15] Copyright 2014, John Wiley and Sons. c) A 1D Au NP/DNA nanohybrid wherein the 10 nm Au NPs are organized in a secondary left-handed helix on the DNA origami bundle consisting of 24 parallel double helices. The zoomed area implies that the Au NPs functionalized with thiolated ssDNA are hybridized to the DNA origami. Further, the DNA origami is functionalized with biotin groups (green) whereby it can be attached to a BSA–biotin–neutravidin-coated surface (red, green, and grey). TEM image show a nanohelix that is attached non-specifically to a carbon-coated grid. Scale bar, 50 nm. Reproduced with permission.[16] Copyright 2013, Springer Nature. d) A 1D nanocomposite comprising a BSA biofunctionalized polymeric nanofiber decorated with Au NPs immobilized by the BSA ligands. Drawn based on the concept

presented in [17-19]. e) A 2D Co-rGO nanocomposite (the schematic shows the catalytic reduction mechanism of Cr(VI) by the nanocomposite. Reprinted with permission.[20] Copyright 2017, Elsevier. f) A 3D G-CNT-Ni nanocomposite employed as an anode material in the fully lithiated state. Reproduced with permission.[21] Copyright 2013, Elsevier.

Plasmonic nanocomposites have drawn extensive attention of academia as well as industry worldwide within the last couple of decades thanks to their immense potential for exotic optical applications. Interestingly, archaeological studies on the antiques of ancient civilizations have revealed that the people of very old era could employ such materials for various aesthetic purposes such as decoration, though they knew nothing about the origin of such materials' optical properties [22]. The ancient colorful sculptures (e.g. Tutankhamen's mask), tiles (the ever-living guards at Darius' palace in Susa and the Ishtar gate in Babylon), and glasses (e.g. the Roman Lycurgus cup) are some instances wherein different vivid colors stem from the plasmonic properties of the metal particles incorporated in a dielectric matrix[23-26]. Recently, chemical and microscopic analyses of the 16th and 17th century Italian and Spanish lusters and the 19th century Iranian painted tiles have also demonstrated the presence of nanoparticles (NPs) of copper (Cu), gold (Au) and silver (Ag) as the principal coloring elements.[27-30]

In 1904, Maxwell Garnett was the first scientist who theorized the physics behind the plasmonic phenomenon. In this regard, he benefitted from the works of his peers on staining by Ag and Au particles and theoretical analysis of colored glasses [31]. Thereafter, Gustav Mie offered a precise solution for Maxwell's equations and developed a simple method to explain the optical behavior of nanoparticles that is still practical. As mentioned by Caseri [32], the first report on polymeric nanocomposites was published by Lüdersdorff in 1833[33]. He described the synthesis of a nanocomposite based on reducing of a Au salt exposed to gum Arabic. Subsequently, co-precipitation of gum Arabic and Au in ethanol led to formation of a purple colored nanocomposite. As a more sophisticated plasmonic nanocomposite, Kirchner synthesized a smart plasmonic structure with switchable color in hydration/dehydration states. This plasmonic material based on a metal nanoparticles - gelatin nanocomposite was fabricated more than a century ago[34].

Since the first aforementioned cases of study on plasmonic nanocomposites, the relevant research has progressed and different efficient compositions and properties have been discovered. However, thanks to the advanced fabrication methods and facilities developed in the last two decades, a profound advance in the field has recently taken place. This blooming growth is owing to nanotechnology whereby a vast variety of nanocomposite/hybrid materials composed of metallic/ceramic nanoparticles and dielectrics have been synthesized and studied. Particularly, dynamic or switchable plasmonic nanocomposites as a new class of hybrid systems have been introduced. The switchable plasmonic nanocomposites, whose plasmonic resonance properties can alter instantly, have endowed a novel perspective to plasmonics in research and technological utilities. Reversible switching of material composition or arrangement of plasmonic metal nanostructures is indeed tricky. However, employing an active surrounding medium that can dynamically tune the configuration of plasmonic nanostructures and/or their optical properties is certainly a promising approach. In this regard, the materials able to perform as an active surrounding medium for the plasmonic nanoelements include liquid crystals (LCs), photochromic molecules, inorganic materials, and polymers[35]. When exposed to a stimulus e.g. light, temperature, or voltage, the dielectric function of the active neighboring medium or its physicochemical properties reversibly change and thereby affects the optical properties of the adjacent plasmonic nanostructures. Accordingly, nanohybridization of plasmonic (and in general optical/photonic) nanomaterials with switchable dielectric materials is a high potential route for creation of advanced optical devices in biosensing, nanomedicine, and optics[36-39].

The optical response of a plasmonic nanocomposite is defined by the size, shape, distribution (interparticle spacing (IS)) and chemistry of the embedded plasmonic particles. The response of the system can be adjusted by an external stimulus and the nanocomposite becomes smart provided that the matrix shows a switchable behavior. In other words, if the properties of the surrounding medium of the plasmonic NPs undergo a dynamic change, the dielectric of the NP´s hosting medium as well as the interspacing of them will change. Such alterations lead to the change of the nanocomposite's resonance. This concept has been implemented extensively to realize SPNs. Depending on the type of the stimulus, several classes of SPNs could be envisaged. The range of plasmonic nanocomposites, however, is not limited to optical responsive nanocomposites, acting based on reversible changes of the active surrounding media's properties. The dynamic reconfiguration of plasmonic NPs whose surface is decorated by active ligands and elements would open up new capabilities with respect to active engineering of aggregate structures and relevant properties. The classic approaches in SPNs mainly relying on the reversible change of the active surrounding media restrict the applicability considering the limited number of the involved NPs. Aside from low control on the properties and function, the emerged properties are not very different between the switching states, as well. In contrast, the dynamic reconfiguration based methods enable development of switchable nanocomposite structures with large metal-filling factors whose properties are notably superior over the classic ones' based on the weakly dispersive interactions of highly diluted metallic NP arrays[40]. The highly filled particulate polymer nanocomposites represent a new class of functional materials that function based on the closely spaced ultrafine nanoparticles embedded in a polymeric host. In such structures, various extraordinary properties arise from the strong and cooperative near field coupling between the neighboring nanoparticles, that synergistically bring about the macroscopic properties. Tailoring and controlling the function is, thus, realized through engineering of the near field coupling by precise adjustment of structure and reconfiguration mode of the NPs, field conversion, and interaction with external stimuli[19].

In this study, we aim to review the lately introduced types of SPNs in two categories of those performing based on the active surrounding media's reversible changes and those whose structures thus properties form by the stimuli induced reconfiguration of surface functionalized plasmonic NPs. Such kind of nanocomposites will be classified according to the applied stimulus type, i.e. the input signals including chemical, thermal, electrical, and optical in nature. Further, to encourage the progressive trend of this field, we aim to introduce active plasmonic polymeric nanocomposites whose polarization or conformation is altered by external stimuli induced isomerization of the embedded plasmonic molecules. This strategy can be regarded as an alternative for the switchable nanocomposite colloids performing via the reconfigurable coupling and enables creation of a new range of unique functional materials[41-44]. Finally, we will discuss our opinions on some important bottlenecks, prospects, and outlooks of this field.

2. Main operation mechanisms of SPNs

2.1. Reversible change of the interparticle spacing

Commonly, the composites' optical properties are described by the effective medium theory (Eq. (1))[45]:

$$\varepsilon_{eff}(\omega) = \varepsilon_m \left[1 + 3f \frac{\varepsilon(\omega) - \varepsilon_m}{\varepsilon(\omega)(1-f) + \varepsilon_m(2+f)}\right] \tag{1}$$

where ε_{eff} and f are the medium's effective dielectric function and the inclusion's filling factor in the composite, respectively. According to this equation, a resonance condition is realized when the denominator in ε_{eff} equals zero, resulting in a resonance peak in the extinction spectrum. For a nanocomposite system, the interaction between the NPs is taken into account and hence the optical response is explained with respect to the filling factor and an effective dielectric constant ε_{eff} is introduced. The most practical method for modelling the physical properties of nanocomposites is the effective medium approximation (EMA). In such a model, the properties of the nanocomposites are calculated by averaging the properties of each of its constituent materials. Despite its inaccuracy, for the nanocomposites with well-separation of

NPs (i.e. at a low filling factor), the EMA works well. However, it is unable to estimate the properties of a percolating or near percolation composite (i.e. at a high filling factor). One of the commonly used and most well-known EMAs is the Maxwell-Garnett theory (MG), wherein effective properties are theorized for a system comprising spherical fillers in a matrix. Although this approach is efficient in determination of the basic properties of nanocomposites, it fails for large filling factors as mentioned before, because it does not consider the interfacial area and ignores the dipolar coupling at the interface. Recently, to address such a bottleneck, the full wave simulations have been employed for the sake of modeling of high filling factor nanocomposites. As shown in Figure 2a, the simulations have been successful in modelling of the optical properties of the near percolation nanocomposites. In this method, the complex reflection and transmission coefficients carefully determined based on a slab of a nanocomposite are inverted to assign an effective permittivity[46]. The full wave simulations not only describe the effective properties of the highly filled percolating plasmonic nanocomposites fairly well, but also clarify the microscopic (represented by an interfacial plasmonic broad shoulder peak at around 610 nm) and the macroscopic light confinement effects along with the wavelength dependency of the absorption and near field radiation of the nanocluster.

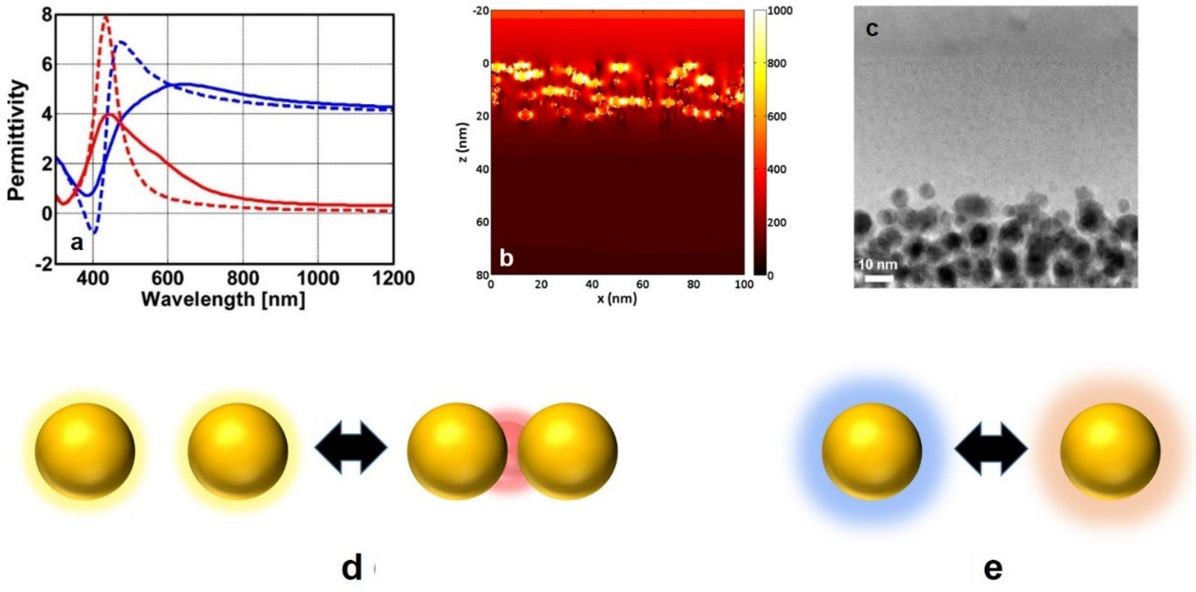

Figure 2. Effective optical properties of plasmonic nanocomposites. a) Effective properties of a nanocomposite (with 20% Ag NPs) calculated via full wave finite-difference time-domain (FDTD) simulations (solid lines) and the Maxwell-Garnett effective medium theory (dashed line). Blue and red lines represent the real and imaginary part of effective permittivity, respectively. b) Electrical field distribution calculated by the FDTD method in an ultra-thin Ag-SiO_2 plasmonic nanocomposite mounted on a SiO_2 coated silicon substrate subjected to 430 nm light. Reproduced with permission.[46] Copyright 2014, MDPI. c) Cross-sectional electron microscope image of a highly filled nanocomposite fabricated via physical vapor deposition. Reproduced with permission.[47] Copyright 2014, Royal Society of Chemistry. Two main operation mechanisms in SPNs as: d) reversible change of IS, and e) reversible change of the surrounding material's dielectric function.

The FDTD simulation of the Ag NPs embedded in a dielectric host when excited by a 420 nm light (plasmon resonance), Figure 2b, reveals the enhancement of the local EF of light near the NP's surface. In general, the electromagnetic radiation and interference effect within the highly filled plasmonic nanocomposites, Figure 2c, govern the macroscopic confinement of light within the host dielectric and the microscopic light confinement between the nanoparticles "hot spots" where the local EFs are strongly enhanced. Indeed, many of the SPNs to be introduced in this review act based on the reversible tuning of microscopic local EF via adjusting the IS of plasmonic NPs, in particular. The LSPR in plasmonic NPs is highly sensitive to existence of other adjacent plasmonic NPs. At a close distance, the LSPR modes of two adjacent plasmonic NPs are coupled via a near-field interaction, Figure 2d. The coupling subsequently leads to new modes of plasmon resonance showing a stronger electromagnetic field. The plasmon resonance modes' interferences can cause plasmonic Fano resonance and spectral splitting [48]. Thus, manipulation of a coupled SPR in an active manner provides the opportunity of having a wider adjustable spectral range, of switching localized EF intensifications, and also a variety of plasmonic responses. In this regard, the plasmon hybridization model can explain the dependence of the plasmonic dimers' dipolar coupling, to the IS[49]. Upon PC, the dipolar plasmon mode is divided into the bonding and antibonding hybridized plasmon modes[49]. The former mode includes two cooperative dipoles along the interparticle axis, bringing about a strong induced dipole and intensive coupling to the far field. In contrast, in the antibonding plasmon mode, the dipoles are antialigned and neutralize each other, i.e. forming a zero net dipole moment. As a result, far-field light is unable to excite the antibonding mode i.e. the "dark" plasmon mode. For this reason, the optical behavior of the plasmonic dimer is governed by its less energetic bonding mode. When light excitation occurs along the interparticle axis, the smaller the IS is, the more the plasmon resonance wavelength related to the less energetic bonding mode red shifts. Quantitatively, the fractional plasmon shift ($\Delta\lambda/\lambda_0$) (λ is the plasmon wavelength of the single metal NP, and $\Delta\lambda$ is the shift in the plasmon wavelength induced by the PC), decreases quasi-exponentially with the IS divided by the particle size (equation 2)[35, 39, 50]:

$$\frac{\Delta\lambda}{\lambda_0} = Ae^{-d/(sT)} \tag{2}$$

where *d* is the IS, *s* is the size of the particle i.e. the particle's length in the direction of the interparticle axis (for a nanodisk or nanosphere this is the diameter), τ is the decay length of the EF from the particle surface, and *A* is the maximal fractional plasmon shift, related to the dipolar coupling intensity. The parameters of τ and *A* are mostly regarded as constants for a given size scale, for a specific shape and orientation. Despite proper applicability of the above equation in estimation of the shift of the LSPR peak for a specific plasmonic dimer depending on the IS, in the case of the anisotropic NRs in the end-to-end mode, it needs to be modified[51]. Accordingly, in the above equation, the component of *d*/*s* should be substituted with $(V_{\text{spacing}}/V_{\text{nanorod}})^{1/3}$, where V_{spacing} and V_{nanorod} represent the IS' and the NR monomer's volume, respectively. Given that the volume ratio nearly equals *d*/*L*, where *L* denotes the NR length, the above equation can be modified as:[35, 39, 51]

$$\frac{\Delta\lambda}{\lambda_0} = A'e^{-(\frac{d}{L})^{1/3}/r} \tag{3}$$

where A' is the maximal fractional plasmon shift.

2.2. Reversible change of the surrounding material's dielectric function

The second important operation mechanism of the SPNs relies on the critical correlation of LSPR wavelength and strength to the surrounding material's dielectric function, Figure 2e. For a spherical metal NP, whose LSPR behavior can be explained according to the Mie theory, with a diameter of $d << \lambda$ of the incident light (i.e., $d/\lambda < \sim 0.1$), the EF extent around the NP is fixed. In such a circumstance, the metal NP is in fact an ideal dipole. According to the Mie theory, the extinction cross-section $\sigma_{ext}(\lambda)$ of the metal NP with the aforementioned characteristics, the sum of the absorption and scattering cross sections, can be expressed as[39]:

$$\sigma_{ext}(\lambda) = \frac{18\pi V \varepsilon_d^{3/2}}{\lambda} \frac{\varepsilon_2(\lambda)}{[\varepsilon_1(\lambda)+2\varepsilon_d]^2+[\varepsilon_2(\lambda)]^2} \tag{4}$$

where V is the NP volume, λ is the light wavelength, ε_d is the surrounding medium's dielectric constant, and $\varepsilon_1 + i\varepsilon_2$ is the metal's complex dielectric function. $\sigma_{ext}(\lambda)$ will be at its highest magnitude if $\varepsilon_1 = -2\varepsilon_d$ and ε_2 is negligible. In fact, under such conditions, LSPR occurs in the metal NP. The relationship between the LSPR peak wavelength and the surrounding medium's dielectric function can be characterized utilizing the Drude model as (equation (5))[39, 52]:

$$\varepsilon_1 = 1 - \frac{\omega_P^2}{\omega^2+\gamma^2} \tag{5}$$

where ω_P and γ are the plasma frequency and damping frequency of the bulk metal, respectively, and $\gamma \ll \omega_P$ within the visible and NIR regions. As mentioned above, for the LSPR, $\varepsilon_1 = -2\varepsilon_d$ and thus the LSPR frequency can be described as[52]:

$$\omega_{LSPR} = \frac{\omega_P}{\sqrt{2\varepsilon_d+1}} \tag{6}$$

Converting frequency to wavelength by $\lambda = 2\pi c/\omega$, the equation (6) turns to[52]:

$$\lambda_{LSPR} = \lambda_P\sqrt{2\varepsilon_d + 1} \tag{7}$$

where λ_P is the wavelength correlated to the bulk metal's plasma frequency and $\varepsilon_d = n_d^2$. As a result, it can be deduced that when the dielectric constant or RI of the dielectric medium rises, the LSPR peak of the spherical metal NP red shifts.

The Gans theory, also, explains the longitudinal plasmon wavelength of a metal spheroid or NR as[39]:

$$\lambda_{LSPR} = \lambda_P \sqrt{\varepsilon_\infty + (\frac{1}{P} - 1)\varepsilon_d} \quad (8)$$

where ε_∞ is the metal's high-frequency dielectric constant and P is the depolarization factor along the spheroid or NR's long axis. As simply deduced from the equation, also in the case of the metal NR, when the dielectric medium's dielectric constant is enhanced, the LSPR peak is red-shifted.

Table 1 lists some of the recently developed SPNs reported in the literature that operate in accordance with the two main above mentioned mechanisms.

Table 1. Some of the recent (since 2014) examples of the SPNs in the literature

Optical nanoelement	Switchable surrounding material	Stimulus	structure	Operation mechanism	Ref.
Au NPs	PNIPAM	temperature	microsphere	IS change	[53]
Ag nanoprisms	PNIPAM	temperature	microsphere	IS change	[54]
anisotropic Au NPs with octahedron, concave cube, and bipyramid shapes	thiol-terminated PS or PS-*b*-PAA shells	solvent polarity or temperature	core-shell	RI change	[55]

Au NPs	chitosan hydrogel	pH	film	IS change	[56]
Au NRs	a HEG derivative	temperature	ligand coated NRs	IS change	[57]
Au NPs	3D DNA NTs with integrated Azo molecules along the edges	UV/Vis irradiation	Azo-NTs anchored with AuNPs	IS change	[58]
Ag/Au NPs	p(NIPAM-*co*-MAPTMS)	temperature	microgel	RI change	[59]
anisotropic Au NPs, such as rods and platelets	LC	voltage	dispersion	IS change	[60]
anisotropic Au–SiO_2−dye NRs	LC	voltage	dispersion	RI change	[61]
Ag NPs	PNIPAM/PAA IPN	temperature/pH	microgel	IS and RI change	[62]
Ag NPs	PNIPAM/PAA IPN	pH	microgel	IS change	[63]
Au NPs	PANI	proton-doping	core-shell	IS change	[64]
Au NRs	PANI	proton-doping	core-shell	RI change	[35]
Au NCs, including NSs, NRs, and NBPs	PANI	proton-doping	core-shell	IS and RI change	[65]
Au NRs	smectic LC	temperature	dispersion	RI change	[66]
Au NRs/ (CdSe/ZnS) core–shell QD	chiral nematic LC	temperature	dispersion	IS change	[67]
Au NSs, Au NRs	LC	light (photothermal)	film	----	[68]

Au NRs	nematic LC	voltage	suspension	RI change	[69]
Au NPs	PNIPAM	temperature	core-shell	IS and RI change	[70]
Au NRs	LC oily streaks	light	film	IS change	[71]
Au NRs	nematic LC	light/voltage	dispersion	N-LC alignment by the Au NRs	[72]
(PEO45-b-PS670) BaTiO3	nematic LC	voltage	dispersion	RI change	[73]
Au NPs	2, 3, 6, 7, 10, 11-hexabutyloxytriphenylene discotic LC	temperature	dispersion	RI change	[74]
dodecanethiol functionalised Ag NPs	chiral nematic LC	voltage	dispersion	The enhanced intrinsic field created by silver NPs	[75]

3. Different classes of SPNs depending on the applied stimulus

Active modulation of plasmonic nanostructures is a blooming area in nanoplasmonics, assuring progress in the design and construction of state of the art active devices, such as transducers, optical switches, filters, modulators, and phase shifters at different wavelengths[76]. In SPNs, the arrangement of the optical nanofillers and/or dielectric function of the surrounding media can be controlled via external stimuli, Figure 3. This feature confers high freedom in the modes of assembly and arrangement of the optical nanoelements as well as reversibility of the assemblies. Besides the environmental factors including pH, polarity and composition of the solution and temperature, external stimuli, such as light, EF, mechanical stress, and MF, are used to induce switchability in optical properties. Here, we introduce different stimuli responsive plasmonic systems offering reversible optical properties including those acting based on active surrounding media and on reconfiguration of plasmonic NPs. In this regard, the most frequently studied stimuli such as pH, solvent, temperature, light, metal ion doping, proton doping, EF, and MF are discussed.

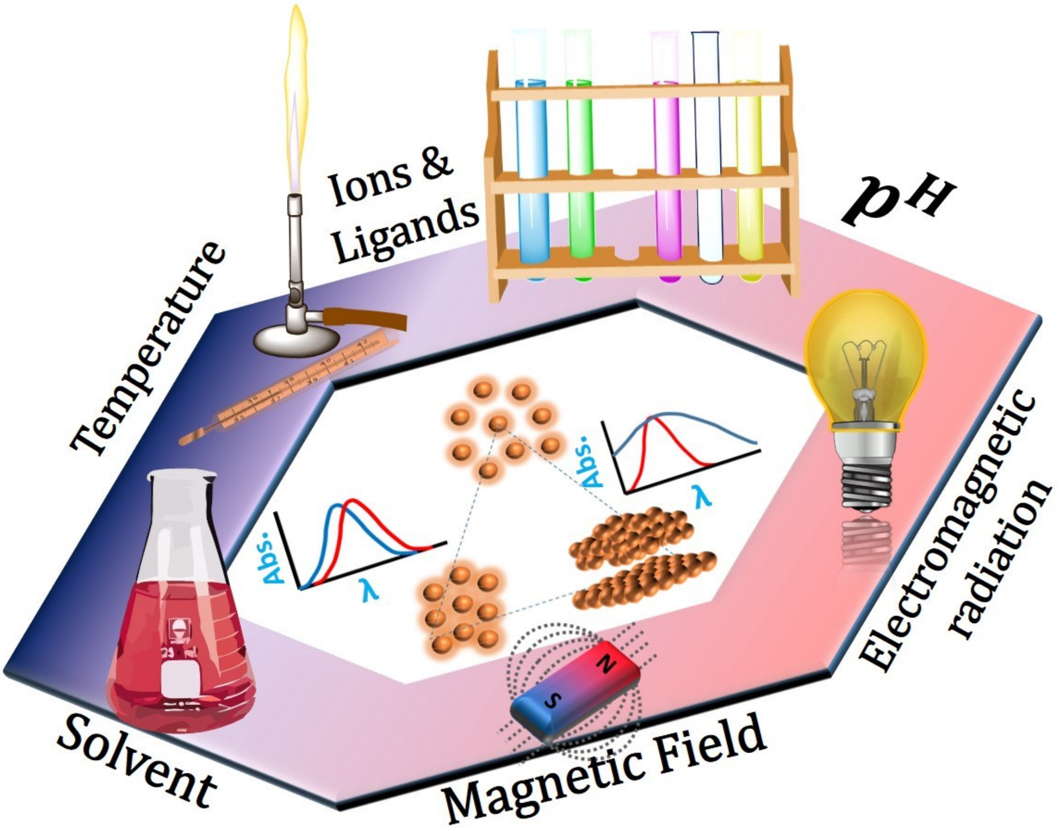

Figure 3. Various stimuli responsive SPNs in two categories of classic low filled ones and reconfiguration based high filled ones.

3.1. SPNs based on the stimuli induced control of the surrounding media

3.1.1. Temperature induced control of the surrounding media

The thermochromic nanocomposites are favorable for applications such as thermal sensors or thermo-sensitive coatings. In general, temperature can affect the NPs embedded in a polymer matrix thus the resulting optical properties of the nanocomposite in several ways. A thermal treatment can lead to either enlargement of primary particles by fragmentation of the finer particles, a process called the Ostwald ripening, or particle agglomeration[77]. The former effect is mainly applicable in a liquid facilitating mobility of the fragments rather than in a solid medium. However, long thermal treatments at high temperatures could realize such an effect even in a solid polymeric matrix, in case the polymer is not thermally degraded.[78] In general, color changes based on the Ostwald ripening of spherical particles are not reversible[77].

As the second possibility of thermochromism in a NP system, the IS thus the emerged optical feature could be reversible by a thermal process provided that tiny spacings do not give rise to formation of clusters whose primary particles are stuck to each other firmly. Carotenuto et al.[79, 80] observed such a reversible thermochromism in a nanocomposite based on PS and Ag NPs as large as 2–3 nm. The nanocomposite was synthesized in situ by thermal decomposition of silver dodecylmercaptide incorporated into the PS matrix. When heating up to T_g of PS i.e. 80–100 °C, the nanocomposite's color changed from brown to yellow. Oppositely, upon cooling the system to below PS's T_g, the color reversibly changed to brown. This situation was the case for other nanocomposites based on Ag NPs incorporated poly(vinyl acetate), poly(methyl methacrylate), a polycarbonate or poly(phenylene oxide)[79]. In fact, thermal expansion of the polymer matrix at T_g makes distance between the NPs and thus changes the color. In contrast, below T_g, the polymer matrix' shrinkage leads to a shorter IS thus restoring the primary color. In this regard, surface functionality of the NPs could help the reversibility by avoiding any significant interaction of the NPs when approaching each other. For instance, surface dodecylmercaptide groups of the Ag NPs could facilitate the color reversibility. Whereas, the neat Ag NPs are more likely susceptible to a mutual interaction and resist against the switchability[77]. On the other hand, the surface functionality of the NPs can enhance their bonding with the polymer chains. This feature can have two beneficial effects: First, agglomeration of the NPs is hampered and second reversibility of the resulting properties during expansion and contraction is optimized.

The thermoresponsive polymer of PNIPAM shows an extraordinary switchable volume phase transition around its LCST. In fact, the thermoresponsiveness of PNIPAM is resulted from its amphiphilic structure comprising hydrophilic secondary amine groups able to form hydrogen bonds with water molecules and hydrophobic isopropyl groups that are hydrated below the LCST. The polymer-polymer and polymer-solvent interactions govern the phase transition of PNIPAM[81]. The materials from this family are typically classified as smart materials and considered for a diverse range of advanced applications including optics[82, 83]. PNIPAM and its derivatives have been employed as a thermoresponsive matrix for plasmonic NPs. The reversible temperature induced change of IS thus their optical properties by these materials is a promising feature that has drawn wide attention of research community. The most frequently studied plasmonic NPs in PNIPAM optical nanocomposites are Au ones. For instance, Gehen et *al.*[84] developed a SPN based on thermoresponsive PNIPAM brushes grafted on Au nanodot arrays. The optical behavior of the system is based on the local RI changes when PNIPAM undergoes a transformation from the hydrophilic (swollen) state to the hydrophobic (collapsed) one by temperature. Alteration of the temperature from 16°C to 52°C leads to the red-shift of the plasmon resonance due to the mentioned RI variation. Karg et al.[85] prepared the nanocrystal superlattices based on Au-PNIPAM core-shell particles whose spacing varied from 50 to 500 nm. Such nanocrystal superlattices are able to diffract visible light (440-560 nm) notably with peak half-widths of the order of 10 nm. The Bragg peak’s location can be readily controlled by the particle volume fraction. Temperature is employed to trigger crystallization or melting of the superlattice in a reversible manner, mainly because of the thermoresponsiveness of the polymer shell. The crystals are melted due to temperature induced shrinkage of the responsive PNIPAM shell, leading to a considerable loss in the particle volume fraction. In another study, Ding et al.[86] modulated plasmonic scattering from Au NPs employing a thermoresponsive PNIPAM spacer layer enabling their separation from a mirror surface. The PNIPAM layer (d = 70 nm thick) is grafted onto the Au mirror via a surface-initiated atom transfer radical polymerization method, and coated by a layer of scattering Au NPs. This structure creates an optical cavity between the scattering NPs and underlying mirror that can modulate the plasmonic scattering fast and in large area. Figure 4a&b implies that the nanohybrid films generate scattering colors that are so strong that can be perceived even by naked-eye, varying from green at 25 °C to orange at 35 °C. Ding et al.[87] also developed AuNP@PNIPAM core-shell structures by a ligand exchange method. The PNIPAM shells play two roles in this system. They ease the placement of 15 nm diameter Au NPs at the interface of water and hexadecane. Moreover, they act as a spacer between the Au NPs whose function is adjusted by temperature. Thus, they form a reversibly tunable plasmonic Au NP monolayer at the interface. Tuning the NPs packing density at Liquid-liquid interface, the plasmon wavelength can shift as large as 100 nm. As Gawlitza et al.[88] state that in a Au NPs/PNIPAM microgel system, the cross linker density can affect the loading amount of the Au NPs, thus the optical properties. The larger cross-linker concentration, the shallower penetration of the Au NPs, thus lower loading of the Au NPs. Accordingly, PC will decline with a lower NP loading but is enhanced with less integrity of the microgel network. This fact can be the basis of the development of nanocomposites with controllable PC. More precisely, in a nanocomposite with low Au NP loading and highly cross-linked microgel, weak PC is observed, while for a nanocomposite system containing a high Au NP loading density and with slightly cross-linked microgel matrix, the PC is stressed.

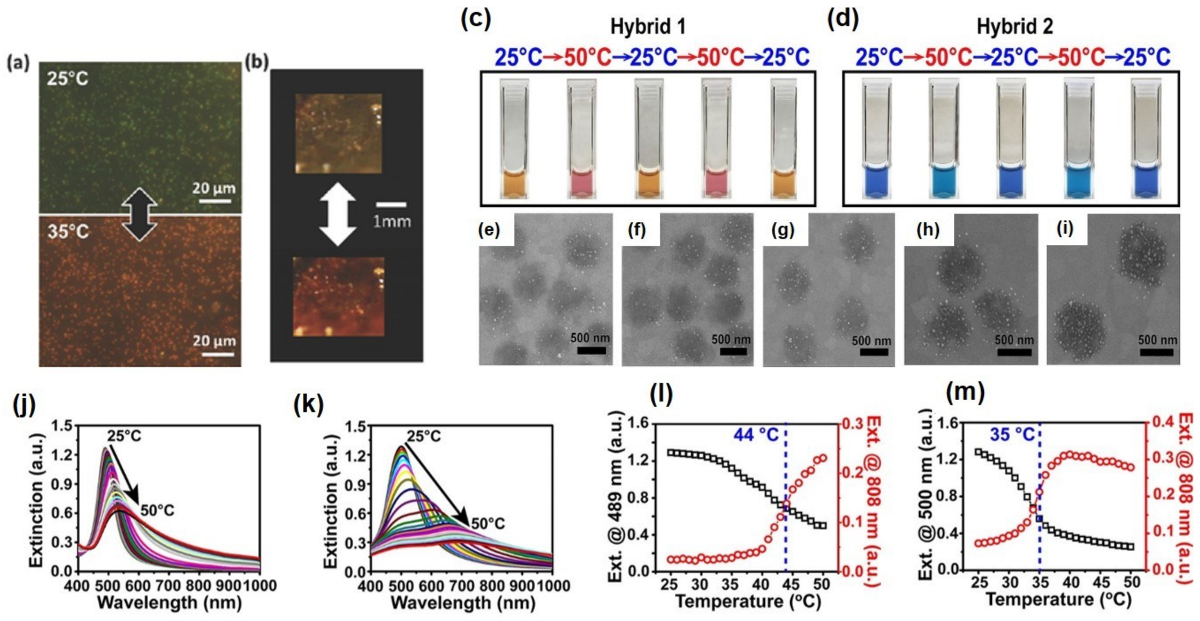

Figure 4. Thermoresponsive SPNs. The generated color of the scattering image based on Au NP/PNIPAM/Au mirror reversibly changes between 25 °C and 35 °C a) under dark-field microscope and b) to the naked eye. Reproduced with permission[86]. Copyright 2016, John Wiley and Sons. (c,d) Reversible thermochromic switching of two hybrid microgels based on Ag nanoprisms with average edge lengths of 30 ± 5 nm (hybrid 1) and 55 ± 14 nm (hybrid 2), when the temperature of the solution varies between 25 and 50 °C. (e–i) SEM images of hybrid 1 samples containing ascending filling factor of the Ag nanoprisms (white dots) embedded into PNIPAM microgels (dark zones). The volume ratio of Ag nanoprism to PNIPAM microgel are as: (e) 1:1, (f) 2:1, (g) 4:1, (h) 8:1, and (i) 16:1. The extinction spectra of the hybrid solutions containing the (j) minimum and (k) maximum loading amount of the Ag nanoprisms vary with increase of temperature. While for the samples in (j) the extinction peak shifts slightly from 489 nm at 25 °C to 535 nm at 50 °C, for the samples in (k) this shift is from 500 to 686 nm. The samples' extinction changes at 489 and 500 nm (black squares) and 808 nm (red circles) versus temperature are demonstrated for the (l) lowest and (m) highest Ag nanoprism loadings. The blue dashed line represents the temperature whereat the largest change in the extinction takes place. Reproduced with permission[54]. Copyright 2018, American Chemical Society.

In addition to gold, PNIPAM based nanocomposites have been synthesized by using other NPs to extend the domain of colors and optical characteristics. For instance, Samai et al.[54] developed SPNs consisting of PNIPAM and anisotropic plate-shaped Ag nanoprisms. Such nanohybrids offer intensive, switchable optical extinction and scattering properties when subjected to different temperatures. Figure 4c&d shows the solutions containing the Ag nanoprism/PNIPAM microgel nanohybrids cyclically subjected to 25 and 50 °C. In the two nanohybrid systems, Ag nanoprisms are in two different sizes. Figure 4e-i demonstrates the morphology of the nanohybrids containing tens to almost one hundred nanoprisms in each microgel (proportional to the chosen loading ratio). The nanohybrids' optical behavior is highly dependent on the loading density and size of the Ag nanoprisms in the polymer. Figure 4j&k illustrates the temperature-controlled extinction spectra of the nanohybrids including solutions. While at 25 °C, the extinction spectrum of the nanohybrid with low amount of the nanoprisms shows a negligible red shift (11 nm) and a minimally wider LSPR peak at 489 nm, versus the pure nanoprisms, at the higher temperature of 50 °C, the extinction peak wavelength shifts from 489 to 535 nm. This wavelength shift is as large as 186 nm, from 500 to 686 nm for the nanohybrids with the highest nanoprism loading amount. Figure 4l,m implies that the nanoprism loading influences the transition temperature whereat the most notable changes in optical properties take place. The nanohybrids with higher nanoprism loading offer larger changes at lower temperatures. Increase of the nanoprism loading facilitates near-field coupling between them, thus the LSPR peak red-shifts notably and is broadened. This parameter along with high temperature leading to collapse of the PNIPAM matrix decreases the IS and promotes the PC.

Liquid crystals (LCs) are materials, intermediate between the typical liquid and crystalline solids. LCs can flow as does a liquid while the constituting molecules are aligned as in a crystal. LCs show the lowest elastic constants and the highest birefringence compared to any other materials. Interestingly, their large birefringence covers the whole visible-IR spectrum and beyond. Thanks to their specific organic composition, they can be chemically fabricated and upscaled. In this regard, they are readily adapted with nearly all technologically important optoelectronic materials [89]. LC's optical properties are extensively dependent on the orientation of anisotropic molecules and adjusting the orientation by temperature can lead to the thermochromism of LCs[90]. Utilizing LCs as a single phase in switchable plasmonic nanocomposites has been researched by several groups, e.g. for the reversible control of the AuNR assemblies[91] and for application in different active plasmonic devices, such as switches, modulators, color filters, absorbers, etc.[89]. This rearrangement caused by the spontaneous order-disorder transitions of LCs subjected to heat, light, and electrical fields leads to coupling of the AuNRs' optical properties, beneficial for creation of active plasmonic devices. As Lee et al.[91] demonstrated the LC director field can be reversibly controlled at the nanoscale by employing micron sized ring confinement via the interaction of elastic energy at various temperatures. Such control enables tuning of its core replacement energy to dynamically isolate the Au NRs at the microscale, resulting in shifts of equal to or even over 100 nm in the SPR peak, i.e. 10 times larger than the highest previously reported value for AuNR composites. To address the bottlenecks of dichroic dye guest-host LCs such as instability, surface precipitation and difficult engineering of the dyes, Liu et al.[72] replaced dichroic dyes with Au NPs in a LC host. They made nematic dispersions of aligned anisotropic Au NPs by polymer passivation of their surfaces. This surface treatment could weaken tangential boundary conditions thereby enabling alignment of anisotropic host molecules. As a result, long-range ordered colloidal dispersions were obtained that realized cooperative optical and electrical switching of rod- and platelet-shaped NPs. Similarly, Zhang et al. [60] reported development of switchable plasmonic nanocomposites comprising LCs and relatively dilute dispersions of aligned anisotropic Au NPs, such as rods and platelets instead of dichroic dyes. Such materials can be employed for switchable optical devices including plasmonic polarizers and color filters. The Au NPs used in such a system enable achievement of optimum polarization or scattering and absorption properties in a range from the visible frequencies to the IR ones. Other than chiral nematic LCs, cholestric LCs have been also used as a host for plasmonic NPs. For the first time, Querejeta-Fernandez et al.[92] benefitted from cellulose nanocrystals (CNC) based films to host and to organize plasmonic Au NRs, thereby developing a chiroptical material. Their suggested method could be beneficial in the main following terms: (i) the chiroptical activity of Au NRs that was notably superior over that for individual chiral objects present in solutions; (ii) parallel alignment of the CNCs and NRs‘ long axes, that were perpendicular relative to the left-handed helix‘ orientation, creating a novel plasmonic chiral pattern; (iii) a cooperation between the structural and optical properties of the CNC host and Au NRs; (iv) the possibility to adjust the circular dichrosim of the nanocomposite; among others.

3.1.2. pH induced control of the surrounding media

pH is another environmental parameter, particularly in chemical and biomedical media, that can affect the conformational status of the hosting matrix of plasmonic NPs, thus their arrangement and the resulting optical properties. As a fact, pH values vary in the human body's different tissues and cellular compartments. For instance, majority of tumor tissues and also inflamed or wound tissues show acidic pH. Employing such pH discrepancies, the pH responsive microgels that respond to minor environmental pH changes, whereby offering different physicochemical properties, could be suggested for applications in controlled drug delivery and disease recognition [63]. In this regard, Liu et *al*.[62, 63] developed a SPN based on Ag NP-loaded microgels. The microgel was composed of an interpenetrating polymer network including individually cross-linked PAA and PNIPAM. When the pH value declines from 6 to 4, the hydrodynamic diameters of the nanocomposite microgels decrease, and thereby the LSPR peak of the Ag NPs significantly redshifts. This behavior i.e. the pH dependent PC and red shift of the LSPR peak of the incorporated Ag NPs was employed in the SERS sensing of 4-mercapto benzoic acid. The pH dependent PC effect can be controlled by the Ag NPs' shape, size, and density. Lately, Liu et al.[56] developed a colorimetric sensor comprising Au dimers within a chitosan hydrogel film. The reversible pH induced volume change of the chitosan hydrogel affects the Au IS and their PC effect, Figure 5a. The Au dimer/hydrogel nanocomposites were synthesized by crosslinking of the hydrogel monomers containing the recognition functional groups and the Au dimers in the precursor solution. The volume expansion of the hydrogel increases the IS of the Au dimers and weakens their PC effects. Accordingly, as shown in Figure 5b-d, with decrease of pH, the Au dimers' PC peak gradually blueshifts, whereby the films' color changes from deep blue to bright red. For the specific colorimetric sensing application proposed in this study, the PC peak shifts is associated to the level of hydrogel swelling, directly influenced by the concentration of target analytes i.e. glucose. Such a colorimetric sensor offers a promising optical sensitivity and stability, and performs reversibly, particularly at high pH values.

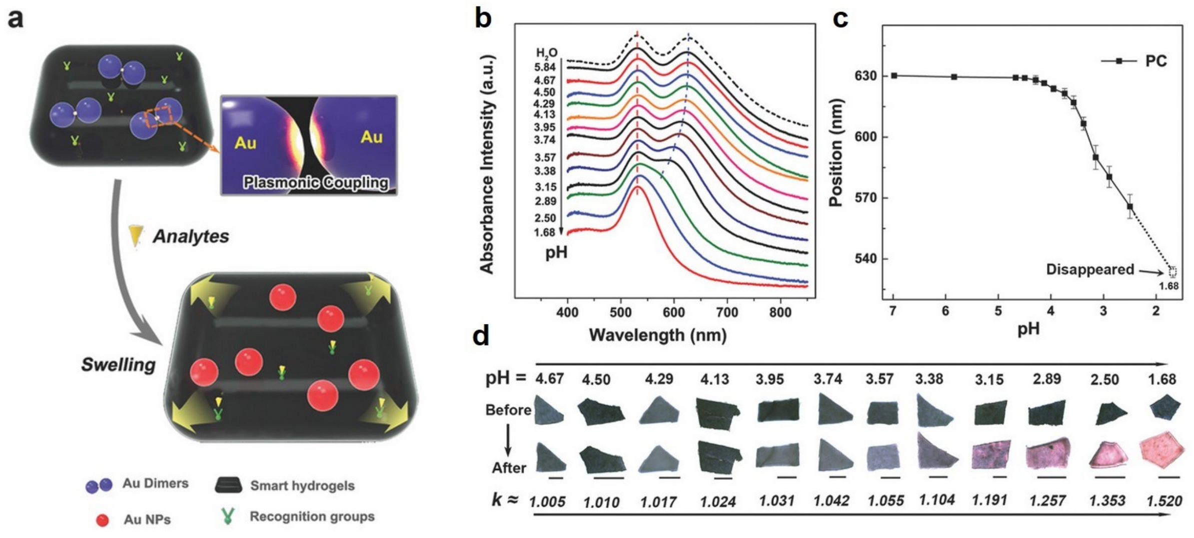

Figure 5. pH responsive SPNs. a) Schematic demonstration of the sensing mechanism of the Au dimer/chitosan nanocomposite based on the PC peak shift. b) The absorbance spectra of the Au dimer/chitosan nanocomposite after immersion in different pH buffer solutions, implying emergence and shift of the PC peak. c) the graph of the extracted positions of PC peaks of the spectra shown in (b). d) The camera (optical microscope) images of the Au dimer/chitosan nanocomposites before and after immersion in different pH buffer solutions. The scale bars: 200 µm; *k*: the swelling ratio of the nanocomposite film. Reproduced with permission[56]. Copyright 2018, John Wiley and Sons.

3.1.3. Metal ions doping induced control of the surrounding media

The stimuli-responsive polymer gels able to capture metal ions and form an ionic bond have also been studied for the sake of creation of SPNs. Particularly, various ionized polymers have been developed that adsorb multivalent ions when coupled with ionized side chains and thereby tailor the swelling/deswelling performance of the microgels[93]. In this regard, methacrylic acid is attacked by bivalent ions e.g. Cu^{2+}, Cd^{2+}, and Zn^{2+} . The as-formed metal-polyacid compounds involve two carboxylate groups per ion within a long pH range. Muratalin and Luckham [94] investigated the extent of metal responsiveness of PNIPAM-*co*-1-vinylimidazole (NIPAM/VI) microgels exposed to different Cu^{2+} ions concentration. The monomer, 1-vinylimidazole, is well-known for showing both metal- and pH-responsiveness. Thus, copolymerizing this monomer with NIPAM brings about colloidal multi-responsive microgels. As reported by them, the swelling degree of these microgels can be adjusted simply by changing Cu^{2+} ions concentration. In a more recent study, Zhang et al.[95] developed a multiresponsive spiropyran-modified PNIPAM-based microgel that could respond to Cu^{2+} ions via forming a coordinate bond with the phenoxide anions. Accordingly, in the SPN the isomerization of the monomers (SP to MC and vice versa) can be activated by Cu^{2+} ions. As a plasmonic SPN, Zuo et al.[93] developed a metal and pH responsive SPN made of Au NPs/poly(*N*-isopropylacrylamide-*co*-3 methacryloxypropyltrimethoxysilane)/poly(acrylic acid) as a core–shell structure. In this system, the Au NPs were incorporated into the polymer microgels via seed-mediated growth. The pH and metal induced swelling/deswelling of the microgel led to re-arrangement of the Au NPs thus altering the electromagnetic coupling between them as an indication for pH sensitivity (Figure 6a-d). Additionally, the coordination bonding between the PAA chains' carboxyl groups (in the shell layer) and Cu^{2+} ions could be tuned depending on the copper ion concentration at different pH values, Figure 6e. This feature allowed regulation of the LSPR of the Au NPs. As mentioned earlier, the LSPR intensity strongly varies with the particle shell's dielectric constant and its loss would decline the LSPR absorbance. When the coordination bonding is raised, the water infiltrated into the PAA network is dramatically replaced by Cu^{2+}, thus lowering the dielectric constant of the Au NPs surrounding medium. This effect causes a dramatic decrease in the highest absorption peak proportional to the Cu^{2+} concentration. In addition to the loss of dielectric constant, the coordination bond between Cu^{2+} and PAA chains leads to loosening of PAA chains, thus enlargement of the distance between the AuNPs.

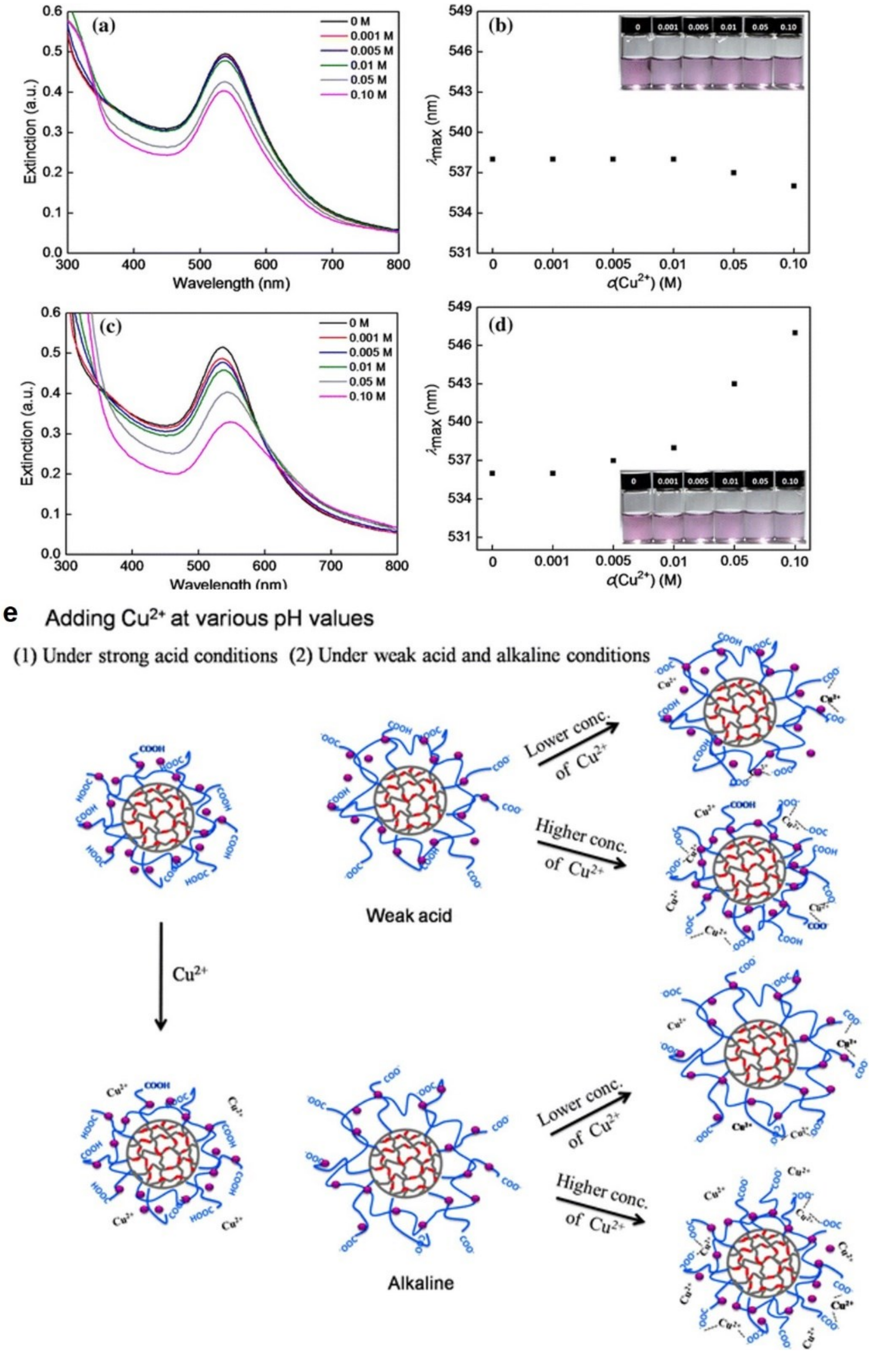

Figure 6. Metal Responsive SPNs. UV–Vis extinction spectra of the P(NIPAM-*co*-MPTMS)/PAA–Au SPNs subjected to different Cu^{2+} concentrations and the LSPR absorption peak (λ_{max}) versus Cu^{2+} concentration at pH = 3 (a, b), and pH = 5 (c, d). The camera images, *insets,* show the corresponding suspensions. e) Schematic illustration of the metal ion dependent regulation mechanisms for the P(NIPAM-*co*-MPTMS)/PAA–Au SONs. Reproduced with permission[93]. Copyright 2017, Springer Science+Business Media New York.

3.1.4. Proton doping induced control of the surrounding media

As mentioned earlier, one of the main mechanisms for induction of switchable optical properties in SPNs is changing the dielectric function of an active surrounding medium by an external stimulus, e.g. light, temperature, or electric potential. Such an alteration itself imposes changes in the plasmonic properties of neighbouring metal nanostructures. Besides pH-, thermo- and photoresponsive materials, the electroactive ones are of most interesting candidates for active media in SPNs. Their attractiveness stems from this fact that they facilitate an immediate switching of LSPR when exposed to electrical (or electrochemical) stimuli. This possibility holds a great promise for sophisticated real life applications in electrochromic smart windows, 3D and flat-panel displays[96, 97].

With respect to the electroactive SPNs, many materials such as graphene,[98-100], liquid crystals[101], silver[102] , metal oxide semiconductors[97], and conductive polymers[103, 104], have been suggested as the active media encapsulating plasmonic nanostructures. In such electroactive materials, influential factors including the charge carrier concentration, arrangement, and/or electronic structure determine their dielectric functions fluctuations, thereby tuning the plasmonic properties of the encapsulated metal nanostructures. Thanks to optimum stability, inexpensiveness, and easy production, conductive polymers have attracted wide attention for the large-scale manufacturing of relevant electrochromic devices[96]. Among conductive polymers, PANI is a classic and one of the most applicable semiconducting polymers owing to its inexpensive fabrication, optimum environmental stability, and customizable conductivity. With respect to the most latter feature, the proton-doping magnitude or the oxidation state can be relied to adjust the conductivity of PANI up to eight to nine orders of magnitude. In fact, there is an extremely fast reversibility (as fast as microseconds) between the reduced nonconductive state and the oxidized conductive one of PANI. As a result of tuning the PANI conductivity, its dielectric function will change proportionally. This relationship between the proton doping and dielectric function of PANI has been employed in manipulation of the plasmonic properties of the encapsulated metal NPs. Lacroix et al.[104-106] showed this phenomenon by developing a switchable structure based on deposition of a PANI layer, electrochemically polymerized, on Au NP arrays synthesized by electron-beam lithography. As reported by them, the extinction spectra of the Au NP arrays are controlled electrochemically in terms of wavelength (with a shift of 70 nm) and intensity (a variation of 4.5 dB). While in this study, the Au NPs due to their lithographically-mannered structure are incompletely covered by the PANI layer, in a core/shell structure, based on a plasmonic metal core and a PANI shell, the plasmonic properties could be tuned in a more controlled way. Such a structure enables utilization of colloidal metallic NCs as the plasmonic cores, with much more enhanced plasmonic properties than those of the earlier mentioned structure suffering from grain boundaries and existence of an adhesive metal layer that cause a large plasmon damping. In this regard, Jiang et al. [35] developed Au NR core/PANI shells through surfactant-assisted oxidative polymerization for performing as active plasmonic switches. Figure 7a-c shows the TEM images of the core/shell nanostructures with different shell thicknesses of 4 ± 1 nm, 16 ± 2 nm, and 39 ± 6 nm, respectively. Such nanostructures show an extraordinary switchability by proton doping (Figure 7d), with the modulation depth and scattering peak shift as large as 10 dB and 100 nm, respectively. The proton doping and de-doping process are carried out by injection of HCl and NaOH solutions, respectively. The reaction between HCl and PANI leads to formation of the proton-doped emeraldine form of PANI, i.e. a p-type semiconductor with higher electrical conductivity. In turn, proton dedoping takes place by providing NaOH to counteract the acid and to recover the undoped PANI's emeraldine form with lower conductivity. In such nanostructures, the polymer shell thickness determines the modulation depth i.e. the thicker the PANI shells, the higher modulation depths are. The switching time is as short as several ten seconds, and compared to the switching-on process (by proton de-doping), the switching-off one (by proton doping) takes a shorter time. Jiang et al. also deposited Au NRs into macroscale monolayers on glass slides and subsequently coated them with PANI shell. This category of core/shell based monolayers also offer interesting switching behaviours. As shown in Figure 7e, the extinction spectra implies a red-shift of 11 nm for both the monolayers composed of 5- and 30-nm PANI-coated Au NRs, verifying the successful PANI coating. The extinction spectra for a Au NR/5-nm PANI nanostructure monolayer shows a maximum extinction variation of ~0.5 dB and a peak shift of ~10 nm, Figure 7f. An enhanced maximum modulation depth of ~1.5 dB and a plasmon shift of ~90 nm was achieved for a Au NR/ 30-nm PANI based monolayer (Figure 7g). As Jiang et al. believe the (Au NR core)/(PANI shell) nanostructures can be employed in facile, inexpensive development of advanced plasmonic switches with applicability in smart windows, information displays, anti-counterfeiting inks, and pH-responsive photothermal systems for cancer treatment.

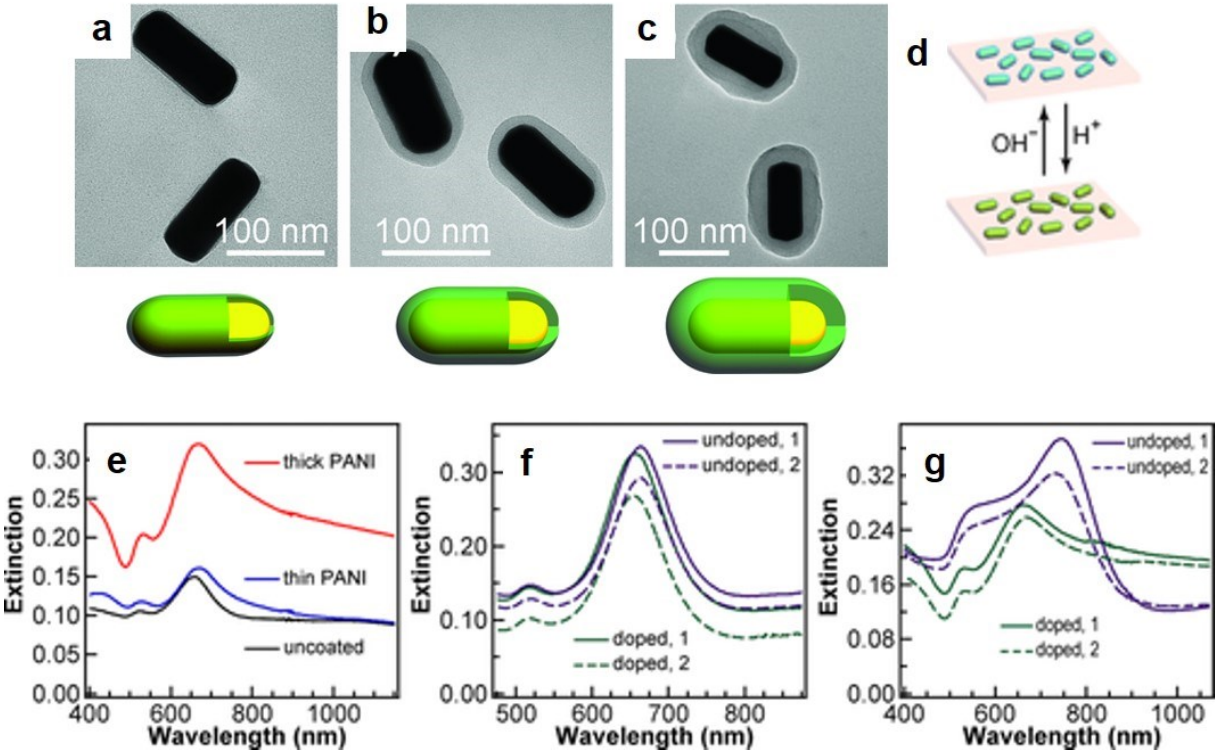

Figure 7. Proton doping responsive SPNs. a–c) Top and bottom rows include TEM images and schematics of the Au NRs encapsulated in PANI shells as thick as 4, 16, and 39 nm, respectively. d) Schematic illustration of the switching performance of Au NR/PANI core-shells (deposited on glass slides) by proton doping and dedoping. e) Extinction spectra of the monolayers consisting of the Au NRs and the Au NRs with 5-nm and 30-nm PANI shell. f) Extinction spectra of a monolayer of Au NR/5-nm PANI core-shell during the proton-doping and dedoping processes in two cycles. g) Extinction spectra of a monolayer of Au NR/30-nm PANI core-shell undergoing proton-

doping and dedoping in two cycles. The areal density of the Au NR monolayers in (e) and (g) is 12 per μm^2, and that in (f) is 20 per μm^2. Reproduced with permission[35]. Copyright 2014, John Wiley and Sons.

Similarly, Lu et al. [96] synthesized nanostructures composed of colloidal Au NS, NR, and NBP based cores encapsulated within a PANI shell. They studied the electrochemical switching behaviour of such core-shell nanostructures individually and collectively. In the former case, a reversible plasmonic shifts of ≈20 and ≈100 nm were recorded for the Au NS and NR based core-shells, that was notably stable for over 200 cycles. Additionally, the plasmonic switching time was as short as less than 10 ms. The Au NCs/PANI core-shells also cooperatively offered optimum electrochemical plasmonic switchability. A reversible plasmonic shift of 20, 50, and 150 nm was recorded for the ensembles based on the PANI-coated Au NSs, NRs, and NBPs, respectively. In another study, Jiang et al. [64] realized active control of the PC in homodimers of Au NP/PANI core-shell nanostructures. For this sake, they tuned the PC via adjusting the proton-doping magnitude of the PANI shell. This mode of modulation of the plasmon coupling in the dimers leads to significant spectral shifts, highly dependent on the IS. In the case of the dimer whose PANI shell thickness is 10 nm and there is a 0.5 nm IS, the stronger scattering peak shifts as large as 231 nm when subjected to the active modulation. In this regard, electrodynamic simulations imply that the dipolar bonding plasmon shift controls the location of the main, notable scattering peak for the dimers with various ISs. Additionally, the quadrupolar bonding plasmon mode can be switched on and off by tuning the proton-doping level of the dimers whose IS does not exceed ∼3 nm.

3.1.5. Light induced control of the surrounding media

3.1.5.1. Photoresponsive SPNs

Photoswitching is another interesting way to reversibly tune the optical properties of nanocomposites for advanced applications such as gas sensor[42], smart windows[107], information storage, logic gates, non-destructive readout, and biological probes [108-117]. In this regard, photoswitchable molecules including spiropyrans and bistable bisarylethenes are able to be photo-interconverted between two states of ring-open and ring-closed[118-120]. This process affects on the dipole moments of the molecule that can be switched on (open form) or off (closed form) by light and UV irradiation, respectively, for instance[42].

Within the past few years, several SPNs based on a combination of photochromic molecules and metal nanolayers or nanoparticles have been suggested. In such systems, each component offers particular properties when light irradiated. While SPR i.e. local field enhancement occurs in the metal phase, the photochromic molecule shows a photoswitching effect, as stated above. These two optical behaviors affect each other, due to close proximity of the constituents of such a nanohybrid system. With respect to the interplay between metal nanostructure and photochromic molecules, various researches have been taken place. These researches deal with three main groups of hybrids based on metal and photochromic molecules including colloidal suspensions of Au or Ag NPs functionalized with photochromic molecules, ultrathin layers of photochromic molecules deposited on a metal surface, Au or Ag NP dropped on a substrate and subsequently coated with a photochromic thin layer [121]. In this review, the first two groups will be discussed later within the frame of the SPNs functioning based on reconfiguration of plasmonic NPs and of the progressive trends, respectively.

The third group of the SPNs consisting of metal NPs and photochromic molecule are those made of plasmonic NPs deposited on a substrate, subsequently covered by a molecular layer of photochromic molecules. In this regard, Spangenberg et al.[121] developed hybrid materials comprising photochromic molecules of diarylethenes and Au NPs. In this structure, not only photochromism is fully maintained when the sample is exposed to cyclic UV-visible light irradiation, but also induced by the cooperation between the components, the Au NPs‘ SPR is notably and reversibly enhanced. The latter effect is attributed to the photoinduced change in the RI of the surrounding medium. Wang et al.[122] studied the intrinsic intersystem crossing

(ISC) of photochromic molecules in order to tailor their plasmon-enhanced fluorescence. ISC takes place when in the proximity of an intensive spin–orbit coupling, an extra nonradiative decay route forms and thus enables the excited electron transfer from the first singlet state to the triplet one. Wang et al. employed nanohybrids consisting of photochromic spiropyran (SP) molecules and Au NPs as single and aggregates, to show that (1) ISC-induced plasmon-raised fluorescence of photochromic molecules can allow for extensive tuning of emission of light from the hybrid, and (2) ISC can raise the plasmonic induced fluorescence of molecules particularly when electromagnetic field is enhanced notably and the ISC rate is quick enough. In this regard, the SP-originated merocyanine (MC) molecules resulted from the photochemical ring-opening process can efficiently provide ISC because of zwitterionic nature of them. Whereas, ISC in the quinoidal MC molecules that are obtained via thermal ring-opening process is minor. Based on such findings, photomodulation of fluorescence can be largely realized when the ISC within MC molecules located at the aggregates of Au NPs, i.e. the location of highly intensified plasmonic hot spots, is switched, Figure 8a&b. Figure 8c&d shows the fluorescence lifetime imaging microscopy (FLIM) images of the PMMA film doped with MC in the presence and absence of Au NPs after UV irradiation wherefrom the zwitterionic MC molecules' fluorescence lifetime can be extracted. According to the images, the zwitterionic MC molecules present in the PMMA film show a fluorescence lifetime of around 400 ps. While, the presence of Au NPs reduce the fluorescence lifetime down to ≈150 ps, as witnessed by SEM image (Figure 8d, specifically the region marked by the black dashed rectangle) because of the strong EF enhancement at the interparticle gaps. Figure 8e illustrates the dark-field optical microscopy image of the previous sample coated with an undoped PMMA film. When the dark-field image is compared with the FLIM one, it is deduced that the fluorescence signals of declined lifetime stem from the broader orange zones that show more intensive optical scattering. The plasmon-raised fluorescence effect tailored by the ISC property of photochromic molecules can be regarded as a promising new concept enabling the spontaneous emission of fluorophores near plasmonic nanostructures. This strategy can expand the applications of active molecular plasmonics in information processing, biosensing, and bioimaging.

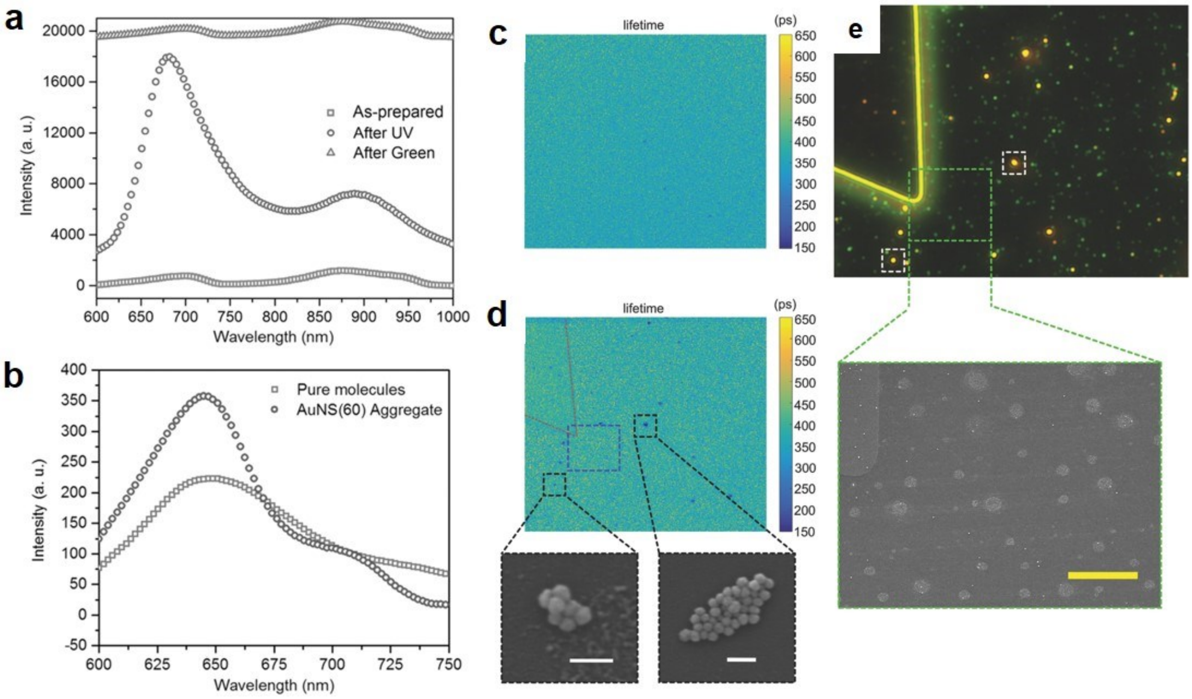

Figure 8. Plasmonic enhanced fluorescence of photoswitchabe molecules. a) The graph implies significant photoswitchable fluorescence enhancement by a hybrid material comprising MC molecules and an AuNS aggregate. b) The fluorescence spectra recorded near (blue circles) and far (green squares) from the AuNS aggregate covered by the SP-doped PMMA film when subjected to green light irradiation. The former spectrum was measured by removing the scattering by the AuNS aggregate. The fluorescence lifetime imaging microscopy (FLIM) image of the MC-doped PMMA film c) without AuNSs and d) with 60 nm AuNSs after UV irradiation. SEM images of AuNS aggregates were taken from the spots of the shorter lifetime marked by the black dashed rectangles. e) Dark-field optical image of the same area of the sample as shown in (d). SEM image was taken from the area highlighted by the green dashed rectangle, corresponding to the blue dashed rectangle in the FLIM image of (d). The white dashed rectangles are relevant to the black dashed rectangles in the FLIM image of (d). The whitish circular regions in the SEM image are made of PMMA left on the glass substrate. White scale bars in SEM image of (d) are 200 nm and yellow scale bar in SEM image of (e) is 5 μm. Reproduced with permission.[122] Copyright 2017, John Wiley and Sons.

3.1.5.2. Photothermoresponsive SPNs

In addition to photoswitchable molecules as a single additive in SPNs, SPR of the plasmonic NPs could trigger reversible optical properties by changing the hosting matrix' and/or an included chromophore's structure. In this regard, Murphy et al.[123] developed a Au NP/PNIPAM nanocomposite that was activated by indirect heating via nanosecond laser flash photolysis. In this system, when the LSPR of the Au NP cores is excited photothermally, the PNIPAM shell rapidly collapses in the laser's 10 ns pulse width. Interestingly, the polymer shell reswells as soon as 100 ns. Morones and Frey[124] developed a SPN of PNIPAM–Au NP. They adopted a room-temperature synthesis approach for the Au NPs by using PNIPAM as the capping and stabilizing factor and ascorbic acid as the reducing factor. Optical measurements after heating revealed a small red shift owing to the local changes in RI of the Au NPs. In this system, temperature raised indirectly when the SPR of the Au NPs was optically excited. Accordingly, the polymer was thermally stimulated, though kinetically at a lower rate compared to when direct heating is applied. Yan et al.[125] biomimicked a chameleon-like material showing the thermo-photochromic property based on a nanocomposite structure comprising photonic poly(N-isopropylacrylamide-co-methacrylic acid) copolymer and Au and Ag plasmonic NPs, Figure 9a. As mentioned above, the plasmonic NPs can raise the light (Vis and NIR) absorption and the light-to-thermal conversion efficiency of the visible light within the thermosensitive film. The thermal- and photo-chromic performance of this system is caused by the molecular conformation change of PNIPAM upon raising the temperature as shown in Figure 9. A high temperature induces a conformation change from intermolecular (state 1) to intramolecular (state 2) hydrogen bond leading to shrinkage of the material. This system shows a reversible glowing color change induced by temperature and light, as do chameleons. Weiss, Huang and co-workers[126] employed the photoswitchable molecules coupled with a plasmon resonance supporting structure to realize a smart plasmonic system. As a molecular switch, spiropyran (1′,3′,-dihydro-1′,3′,3′-trimethyl-6-nitrospiro[2*H*-1-benzopyran-2,2′-(2*H*)-indole]) was selected which was co-deposited along with PMMA on a nano disk array of gold. Upon UV illumination of the coating, the molecules switch from their closed form to open form and absorb the light. The researchers have observed that upon the switching, the plasmon resonance peak of the nanodisk can be tuned. This is because of the fact that the refractive index of the coating changes when subjected to UV/visible light and consequently the SPP of the LSPR of the composite shifts. Cao et al.[127] synthesized a series of PVA/thermochromic dyes/Au NCs films with photothermochromic behavior that could be used as sunlight driven smart windows. The dye molecules and Au NRs cooperatively enhance the absorption of solar energy, thereby raising the film's temperature. Eventually, the color of a glass substrate covered with the PVA/dyes/Au NCs film reversibly varies when the sunlight switches, Figure 9b.

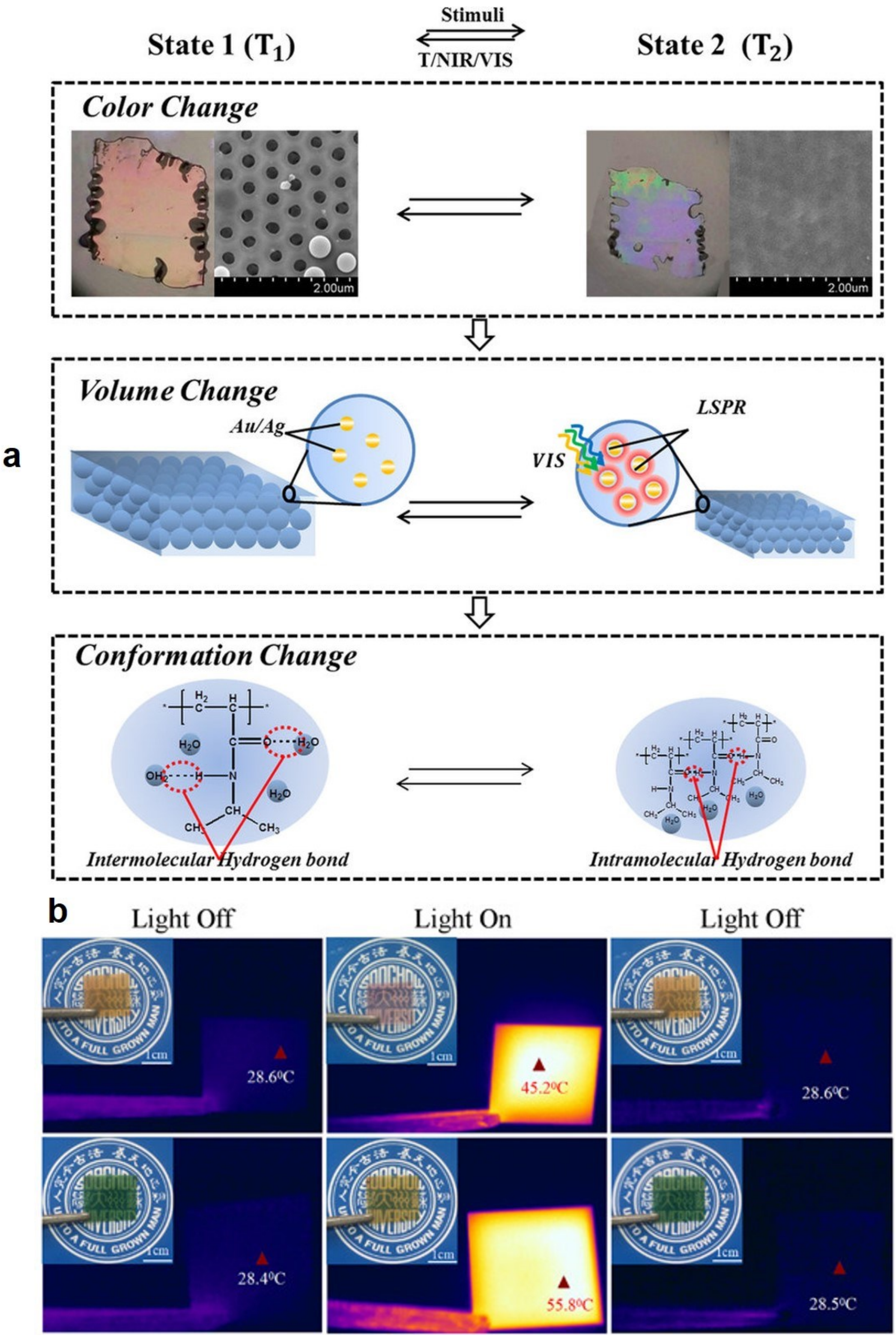

Figure 9. Photothermoresponsive SPNs. a) The biomimetic chameleon with photothermoresponsiveness that shows reversible color (upper row), volume (middle row), and conformation changes (lower row) under the influence of plasmonic NPs. Reproduced with permission.[125] Copyright 2016, Springer Nature. b) PVA/dyes/Au NCs films show tunable colors with adjusted switching temperature at light off, on, and then off. Reproduced with permission.[127] Copyright 2018, John Wiley and Sons.

3.2. SPNs based on stimuli induced reconfiguration of the plasmonic NPs

As schematically shown in Figure 10, other than the classic scheme of SPNs‘ function based on reversible change of the surrounding media’s properties that eventually affects on either RI of the system or IS of the plasmonic NPs, there is a second option of the SPNs performing based on the stimuli induced reconfiguration of the plasmonic NPs. As mentioned earlier, in contrast to the classic class of SPNs, the dynamic reconfiguration of NPs allows for creation of switchable structures with large metal-filling factors and thus the materials whose properties are notably optimized versus the poorly dispersive dielectric properties supplied by the highly diluted plasmonic NP arrangements.

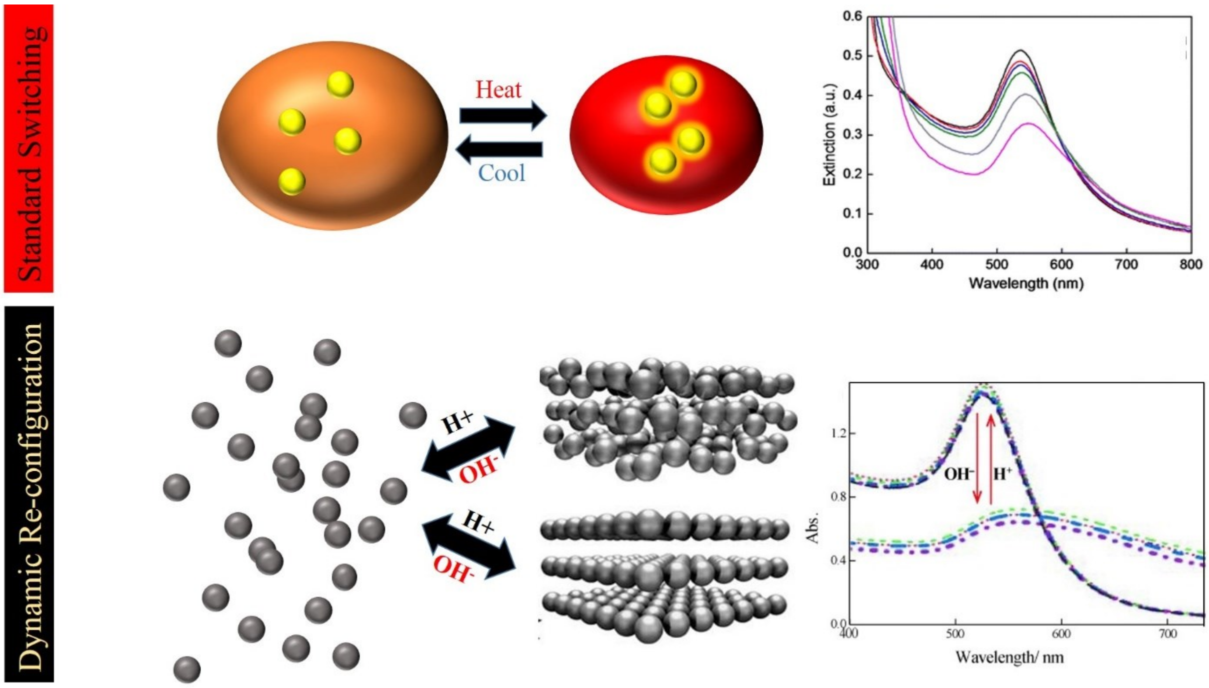

Figure 10. Two main schemes to obtain SPNs including: (Top) Standard switching strategy based on active tuning of the surrounding medium’s properties. (Note that the obtained structure after switching is still chaotic and involve a limited number of NPs and the obtained properties are not significantly different compared to those resulted before the stimulus application, here temperature as an example). (Bottom) Dynamic reconfiguration strategy based on active assembly of plasmonic NPs by assistance of the stimuli responsive surface agents (Note that the approach can lead to either ordered or non-ordered assemblies involving a large number of NPs and thus the obtained properties differ notably after the stimulus application, here pH as an example). The adopted graphs are from [93] and [128].

3.2.1. Temperature induced reconfiguration

Temperature induced dynamic self-assembly (DSA) of plasmonic NPs is another remarkable topic that has drawn attention in research and academia. SA of NPs into organized structures is indeed a cherished goal for a diverse range of researches, with respect to materials science, particularly for metamaterials research. In this regard, achieving this objective facilitates the scalable production of metamaterials. So far, the suggested SA methods that have been beneficial for creation of metamaterials have been successful in development of solely static structures, thus restricting applicability of such advanced materials[40]. To address this challenge, vast attempts have been done in the past years by using DSA of NPs via different methods[129-131]. However, majority of these techniques are based on solvated environments, bringing about very low NP-filling fractions, or only 2D structures. Thus, proposing new DSA approaches providing reconfigurable, densely packed NP assemblies with large metal-filling fractions is of utmost importance. In this regard, one strategy could be synthesis of thermally tunable metamaterials, as reported by Lewandowski et al.[40] In their interesting study, they succeeded to make a dense LC coated Ag NP aggregate (Ag@L) that employs heat as a stimulus for switchable spatial rearrangement between lamellar and isotropic phase, Figure 11a-d. Such reconfiguration leads to changes in the nearest IS of the NPs and enables active control of cooperative interactions between NPs. As shown in Figure 11e, the switchability is confirmed by the position shift of the aggregate's plasmon band maxima. As the authors state, tunability of up to 20 nm was obtained when the system was cooled and heated slowly (tens of minutes). For the sake of verification of the obtained results and to ascertain that the optical properties stem solely from the reconfiguration of NPs, the aggregate's extinction spectra achieved by slow cooling/heating was calculated via full-wave electromagnetic simulation. As shown in Figure 11f, an optimum harmony exists between the modelling and experimental results. On the other hand, by rapid switching (as fast as ten of seconds) during a fast cyclic thermal treatment between 120 and 30 °C only a 14 nm shift was recorded, Figure 11g. It is worthy to mention that such a numerical analysis also enables extraction of metamaterial properties of the slowly switched system, indicating tunable ENZ performance, Figure 11h&i. The spectroscopic ellipsometry measurements also stressed a very good agreement between the dielectric functions of the Ag@L sample having lamellar order with the theoretically predicted properties (Figure 11j).

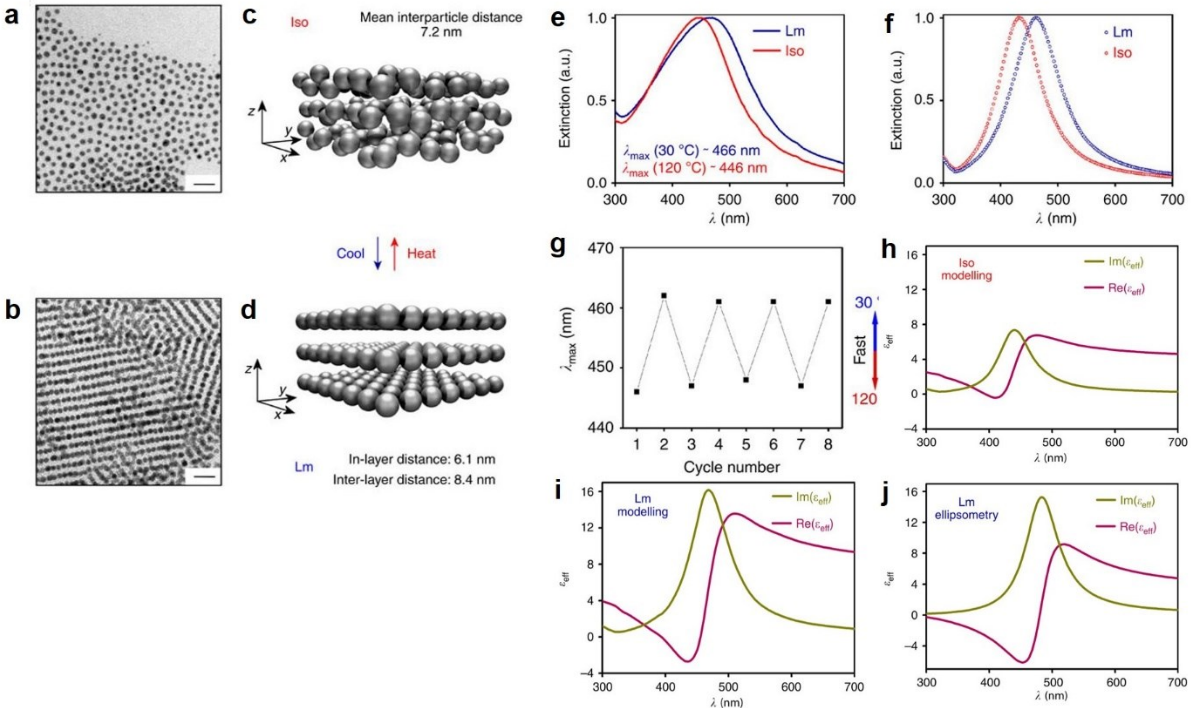

Figure 11. Thermally switchable metamaterials. TEM image of the structures containing thermally annealed Ag@L NPs implying patterns relevant to the isotropic (Iso) (a) and lamellar (Lm) structures (b), scale bar, 20 nm. (c) Schematic illustration of the NP arrangements in Iso and (d) Lm structures according to TEM images. e) Extinction spectra of the Ag@L NP aggregate measured at 30 and 120 °C implying a shift of plasmon band maxima (λ_{max}). (f) Simulated extinction spectra of the Lm and Iso structures. (g) Reversible shifting of λ_{max} position when the system is subjected to successive fast heating/cooling cycles. (h) Theoretically predicted imaginary (Im($\varepsilon_{\mathrm{eff}}$)) and real (Re($\varepsilon_{\mathrm{eff}}$)) parts of the dielectric function of the system in the Iso and (i) Lm structure. (j) Dielectric functions calculated based on spectroscopic ellipsometry measurements. Reproduced with permission.[40] Copyright 2015, Nature Springer.

3.2.2. pH induced reconfiguration

In addition to the film shaped SPNs, the ones as suspended nanohybrid particles could be also influenced by pH. While the dispersion mode of NPs are largely influenced by suspension conditions including temperature and the NP concentration, pH plays also a critical role for the NPs whose surface is treated with the stabilizers that are protonated and/or deprotonated in a solution. In this regard, surface modifiers such as GSH[132, 133], PMAA[134], and PAA [93, 135, 136] have been employed to endow pH-responsiveness to NPs. In this regard, Li et al.[135] developed a pH induced switchable system based on the Au NPs tethered by random copolymers of poly(styrene-*co*-acrylic acid). In this system, pH reversibly alters the surface charge of polymer tethers whereby adjusting the attractive and repulsive forces between the NPs. In fact, presence of the –COOH groups within PS hydrophobic segments and variation of their ionization degree via pH induced deprotonation can decline their hydrophobic interaction. Accordingly, pH can somehow program the assembled nanostructures of Au NPs. Under alkaline condition, the carboxyl groups of the polymer tethers strongly lose proton, giving rise to electrostatic repulsion between the polymer segments and end-to-end arrangement of the anisotropic NPs as *e.g.* 1-D chains. In contrast, under acidic condition, a lower electrostatic repulsion exists due to less deprotonation of –COOH groups, thus the side-to-side arrangement of the NPs prevails and thus clusters and stacked chains of Au NPs are dominant. This approach enables the controlled design of plasmonic NPs as the given pre-defined nanostructures with an adjusted PC effect. A same concept was applied by Torri et al. [136] in development of a pH responsive Au NP based nanohybrid system. They succeeded to construct a novel pH-triggered coassembly system based on the Au NPs tethered with oligo(ethylene glycol) (OEG) ligands. With the help of anionic polymer of PAA that acted as an external mediator, the coassembly formed via hydrogen bonding in water. As schematically shown in Figure 12a, the pH induced protonation of PAA led to hydrogen bonding between the tethered Au NPs and polymers. Accordingly, the Au NPs' plasmonic properties and assembly size were determined by both the amount and molecular weight of PAA. With no PAA, the color of the EG6-AuNPs solution (15 nM) is steadily red also when pH declines from 13 to 1.5. For this sample, the EG6-AuNPs' extinction spectra of remains almost unchanged (Figure 12b-i,ii). Also, DLS graphs show one maxima located at ~10 nm, irrespective of pH, implying that EG6-AuNPs are homogenously suspended in water (Figure 12b-iii). In contrast, when PAA is included into the solution (150 μM), the EG6-AuNPs solution's color (15 nM) switches from red to purple at low pH values (Figure 12c-i). In addition, the extinction spectra red-shifts roughly at pH 2 (Figure 12c-ii) thanks to the PC occurring by the assembly of Au NPs. The DLS graphs also witness the coassembly of EG6-AuNPs using PAA depending on the solution's pH (Figure 12c-iii).

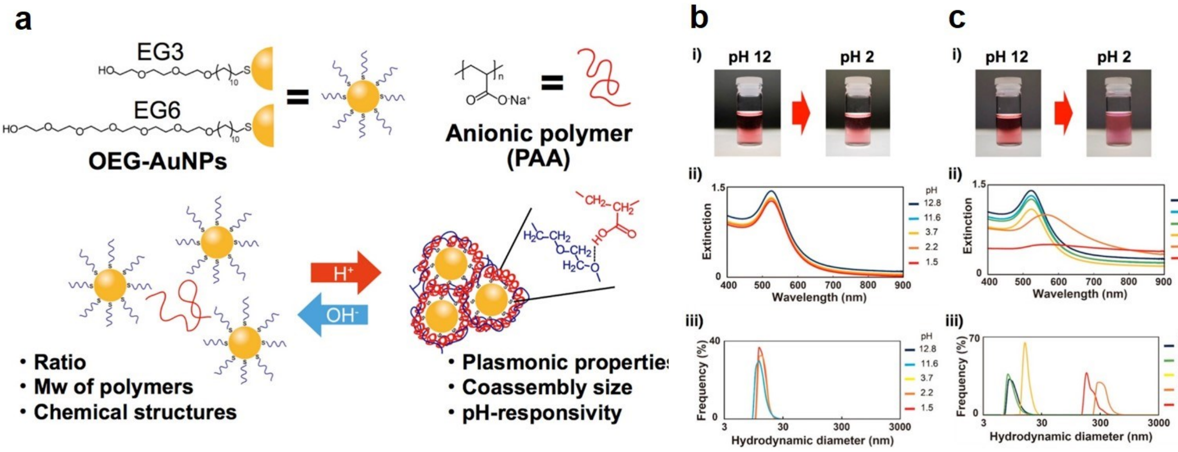

Figure 12. pH responsive Au NPs assemblies. a) Schematic illustration of the mechanism behind the pH-induced assembly and disassembly of the OEG-Au NPs by protonation/deprotonation of external anionic polymer of PAA. The performance of EG6-AuNPs subjected to different pHs in a solution free of (b) or containing PAA (c).(i) Camera images of the solutions, (ii) extinction spectra, and (iii) hydrodynamic diameter of the NPs as measured by DLS. Reproduced with permission[136]. Copyright 2017, American Chemical Society.

Catenanes or rotaxanes i.e. interlocked circular DNA nanostructures could be employed for creation of pH induced SPNs. The reversible reconfiguration of such structures that takes place by e.g. changing pH is the main mechanism in operation of new DNA switches. Such a feature enables them to act as active scaffolds adjusting chemical functions and locating functional agents, as well. A particular applicability of the reversibly reconfigured catenane DNA structures is for the pre-defined arrangement of Au NP aggregates. This behavior enables reversible tuning of IS and phonon resonance in Au NP assemblies, and could be employed in pH sensing application. This possibility allows also the plasmonic tuning of the fluorescence behavior of Au NP/fluorophore hybrid loads as a part of the scaffold, and functioning of logic gates[137]. Figure 13a&b shows the pH-triggered reversible construction of the cytosine-rich i-motif system under an acidic condition. The i-motif structure returns to primary configuration of random coiled when pH rises to neutral. This reversible transformation is the principle of the design of switchable DNA structures. For instance, as shown in Figure 13a, in a system comprising the C-rich sequence **21** and a partly complementary sequence **22,** a fluorophore (i.e. F=Rhodamine green, RhG) and a quencher (i.e. Q=Dabcyl, Dab) are positioned on the 5′- and 3′-tails of strand **21,** respectively[128]. When pH is low i.e. acidic (≈ pH 5.0), stabilization of the i-motif structure of strand **21** approaches the fluorophore/quencher pair to each other, leading to quenching of the fluorophore’s fluorescence. Whereas, at neutral pH, the i-motif structure is separated and the duplex between nucleic acids **21** and **22** is thus formed. The large spacing between the quencher and fluorophore enhances the fluorophore’s fluorescence. This performance is reversible and when the system is exposed to the cyclic pH change of pH 5.0 and pH 8.0, the i-motif and duplex DNA structures are interconverted, as witnessed by recording the fluorophore’s fluorescence intensities (Figure 13b)[128].

As mentioned above the reversible interconversion of DNA structures can be employed for active control of the optical behavior of plasmonic NPs, i.e. SPNs. For instance, Wang et al. [138] employed the pH-induced transformation of a duplex nucleic acid structure to the i-motif one to devise a smart nanospring. When this system was exposed to cyclic pH change of acidic (pH 6.0) and basic (pH 8.0), it could reversibly switch between compact and relaxed spring modes. This ability was profited in order to adjust the aggregation or de-aggregation of

Au NPs chains. For this sake, Au NPs were tethered with a single nucleic acid (**26**), that could play a complementary role for the linking strands **23**, **24**, and **25**. The functionalized Au NPs were subsequently hybridized with the DNA nanospring. At pH8, the hybridization gave rise to relaxation of the spring system. In contrast, at a lower pH, i.e. pH 6.0, the functionalized Au NPs were separated and the nanospring became compact. When the system is further neutralized i.e. at pH 8.0, re-extended the Au NPs decorated spring to end up with the chains with IS of ≈ 10 nm.

The pH-induced reversible transition between DNA's i-motif structures and random-coil strands can be also employed to control the Au NPs aggregation. In contrast to the single Au NPs that show a LSPR band (ca. λ=530 nm), the aggregated ones offer a wide plasmonic coupling effect (λ>560 nm). Correspondingly, individual NPs emerge a purple color that is shifted to blue for the aggregated ones. This phenomenon has been based for a diverse range of sensors or biosensing platforms[139]. The pH-induced aggregation of Au NPs, namely type I and II, is schematically illustrated in Figure 13c. The Au NPs, I and II, are those tethered with the C-rich nucleic acid **31** and the nucleic acid **32**, complementary to strand **31**, respectively. At pH8, when the nucleic acids **31** and **32** are hybridized, the Au NPs are aggregated. In contrast, at pH 5, the strand **31** gets the rigid i-motif form that hinders the aggregation. As shown in Figure 13d, by cyclic exposure of the system to neutral and acidic pH, the assembly of the Au NPs can be switched "ON" and "OFF", respectively. Liu et al. [140] employed the DNA structures as active scaffolds to rearrange Au NP aggregates and also to turn On and OFF the fluorescence properties within the conjugates of fluorophore/Au NP based on reversible tuning of the spacing between these components. Zhao et al. [141] constructed a switchable pH probe operating on the basis of the PC effect of i-motif functionalized Au NPs assembly. A cyclic and strongly sensitive response was achieved when pH changed between 4.5 and 7.5. When morpholino oligomers (MO), i.e. a neutral analogue of DNA, is incorporated into the Au NPs aggregate, the pH probe is stabilized even when there is a low salt concentration. Thanks to the Au NPs' strong optical signal, pH in the local medium can be readily measured in the micro- or nanofluidic channel and even on an individual assembly of i-motif-MO functionalized AuNPs. Thus, measurement of the LSPR spectrum of the Au NPs enables precise identification of chemical properties in the highly confined space of biological systems.

As seen above, to date, dynamic control of plasmonic metamolecule ensembles has been realized solely by using single structural species. To extend the domain of programmable DNA chemistry for nanoplasmonics, there is a need to involvement of over one responsive element that can be programmed to respond to a particular stimulus. Accordingly, the system can perform several operations via a precisely designed "sense-activate" approach, e.g. for advanced plasmonic sensors. In this regard, reconfigurable chiral plasmonic metamolecules coupled with DNA origami has been shown by Kuzyk et al. [76]that can be selectively controlled. They employed pH-responsive DNA "locks" as active agents to govern the chiral plasmonic metamolecules structure in an extensive pH range. Thanks to existence of specific protonation sites, the triplex DNA secondary structures utilized in the locks show a pH responsive behaviour. As shown in Figure 13e, a DNA triplex can be synthesized via pH-dependent sequence-specific parallel Hoogsteen interactions (shown by dots) that take place between a single-stranded DNA (ssDNA) and a duplex DNA. The latter agent is formed via pH-independent Watson-Crick interactions (shown by dashed lines). While the CGC triplets need that the N3 of cytosine existing in the ssDNA becomes protonated [average pK_a (K_a: acid dissociation constant) of cytosines in the protonated state in a triplex structure is ~6.5]. This is interpreted as they are stable only under acidic condition, while the TAT triplets are unstable only when pH increases up to over 10 due to the deprotonation of thymine (p$K_a \approx 10$). Tuning the ratio of TAT/CGC triplets, allows for the design of the DNA locks that are opened or closed in a given pH range. Accordingly, this behaviour enables pH-triggered reconfiguration of the plasmonic metamolecules simply by tuning the amount of TAT/CGC triplets in the DNA locks, Figure 13f. Such pH control over oligonucleotides brings about merits including simpler implementation, prompt modulation, and cleanliness in terms of no waste release preserving the entire system. With respect to the DNA based plasmonic systems, recently, several precious review and perspective papers have been published[142-144].

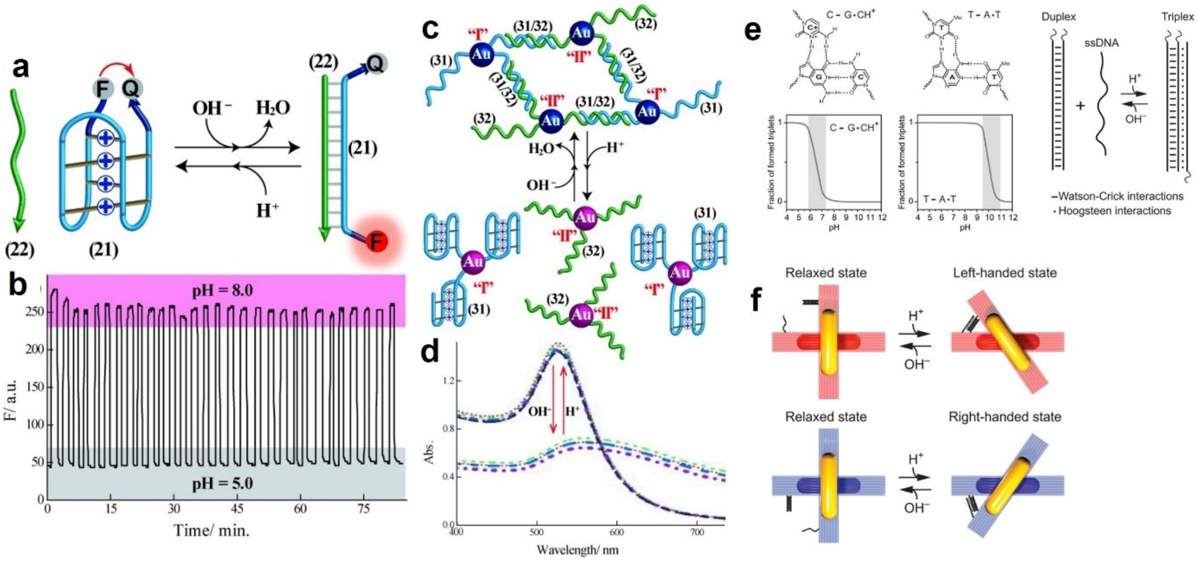

Figure 13. pH responsive DNA based SPNs. a) pH-induced interconversion of i-motif and duplex structures, tracked via recording the fluorescence intensities of a fluorophore label in the presence of a quencher. b) Monitoring the cyclic fluorescence intensity variations of the fluorophore induced by the i-motif structure (stable at pH 5.0, low intensity), and the reconfigured duplex structure (stable at pH 8.0, high intensity). c) Cyclic pH-induced reversible aggregation/de-aggregation of Au NPs. d) Absorption spectra corresponding to the individual and aggregated Au NPs, under acidic and alkaline conditions, respectively. Reproduced with permission[128]. Copyright 2015, John Wiley and Sons. Operation mechanism of the pH-responsive plasmonic metamolecules. e) The CGC and TAT triplets can be made by the combination of Watson-Crick and Hoogsteen interactions (top left). The CGC triplets are formed only when cytosines are protonated, and are stable only under acidic condition (bottom left). Whereas, the TAT triplets are stable at pH values below 10 and unfold due to deprotonation of thymines. Right: pH-triggered DNA lock. f) pH responsiveness of the DNA origami–based chiral metamolecules, switched between the relaxed and the LH/RH state by opening or closing the pH-induced DNA locks. Reproduced with permission.[76] Copyright 2018, American Association for the Advancement of Science.

3.2.3. Light induced reconfiguration

Compared to other stimuli, for reconfiguration of plasmonic NPs, light offers several advantages including convenient operation, remote manipulation, noninvasiveness, and no adverse effect on the solution system[145]. The polymers or lipid vesicles responding to light have been spotlighted for controlled drug release, biosensing, and as chemical reactors. Conventionally, the light responsive vesicles are designed by incorporation of photoreactive antennas (e.g. plasmonic NPs or chromophores such as azobenzene) into thermoreactive polymer membranes. When exposed to light, the plasmonic NPs or chromophores are able to transform the absorbed light i.e. photons to heat via non-radiative ‘‘photothermal effect’’. This process raises temperature locally and eventually disrupts the vesicles. A beneficial photothermal effect requires involvement of a large number of antennas in the process provided. In this regard, combining photoswitchable molecules such as azobenzene with plasmonic NPs have shown promising light responsiveness for reconfiguration of such nanostructures[146]. As reported by Wei et al.[147] the AuNPs decorated with azobenzene ligands can undergo a reversible aggregation when subjected to light irradiation. However, such light-triggered assembly method of plasmonic NPs necessitates highly complicated synthesis of photoresponsive chromophore ligands for the functionalization of the NPs. To address this challenge and as one step further towards controlled assembly of the plasmonic NPs as vesicles, self-assembly of the plasmonic NPs tethered by amphiphilic polymer brushes into nanovesicles have been suggested. When the plasmonic NPs are subjected to the light whose wavelength resonates with their LSPR, the vesicles are promptly damaged thus releasing their content, induced by the strong localized heating. In this regard, He et al.[146] functionalized Au nanoflowers by amphiphilic block copolymer of poly(ethyl oxide)-b-polystyrene (PEO_{45}-b-PS_{455}) via a ligand exchange process that further allowed for formation of related vesicles. The intensive PC among the Au nanoflowers resulted in a notable rise in the NIR absorption of the vesicles. Thus, the vesicles responded to NIR irradiation and thereby released the hydrophilic molecules encapsulated. Bian et al.[148] developed a system composed of the dodecanethiol and oleylamine capped AuNPs which via UV-induced oxidation of mercapto groups to sulfonic ones could arrange themselves as vesicles, as shown in Figure 14a. As a newer study, Zhang et al.[145] reported about the AuNPs surface functionalized with hydrophilic and hydrophobic segments of poly(ethylene glycol) (PEG) and polymethacrylate containing photoresponsive spiropyran units (PSPMA), respectively. The mentioned ligands were immobilized onto the Au NPs via sequential “grafting to” and “grafting from” methods. While, the PEG chains endow high hydrophilicity thus stability to the Au NPs in solution i.e. less chance for formation of large aggregates, the PSPMA chains provide high hydrophobicity and photoresponsiveness by the SP-MC isomerization under visible and UV light, respectively. Such amphiphilic Au NPs, can be reversibly self-assembled into aggregates with a given density of NPs (oligomers) when subjected to light irradiation.

Combining plasmonic NPs, photoswitchable molecules and DNA structures, Yan et al.[149] have introduced a new kind of photoresponsive DNA-functionalized Au NPs coupled with azobenzene-modified oligonucleotides. The *trans*-azobenzene compounds can rigidify duplex DNA under visible light. Whereas, the UV-induced photoisomerization of *trans*-azobenzene to *cis*-azobenzene can lead to separation of the duplex. This feature enables photo-regulation of the Au NPs aggregates, Figure 14b. For this study, two types of Au NPs functionalized by different nucleic acids (type I and II) were synthesized. The former type was based on nucleic acid **54**, with *trans*-azobenzene photoisomerizable tethers, while the latter one contained nucleic acid **55**, partial complementary to strand **54**. This combination not only enables the classic directed assembly and sensing behaviours related to the oligonucleotide-functionalized NPs, but also offers reversible photoswitching of their assembly behaviour, Figure 14c. When both the NPs are mixed, the *trans*-azobenzene cooperative rigidification of the duplexes **54**/**55** takes place which gives rise to the NPs aggregation. UV-irradiation of the aggregates facilitates *trans* to *cis* photoisomerization of the azobenzene units and also destabilization of the DNA duplex, thus separating the Au NP aggregates. In contrast, irradiation of blue light reverses the isomerization, and causes the NPs to assemble again. The photoisomerization process is readily reversed for several times. Figures 15d&e imply after one hour of UV irradiation, the solution's extinction increases to 1.5, with a sharp LSPR at 526 nm. The reason is dissociation of the large aggregates and resuspension of the single Au NPs. After blue light irradiation for 2 h, the NPs completely sediment due to formation of large aggregates, and thus the solution's extinction approaches nearly zero.

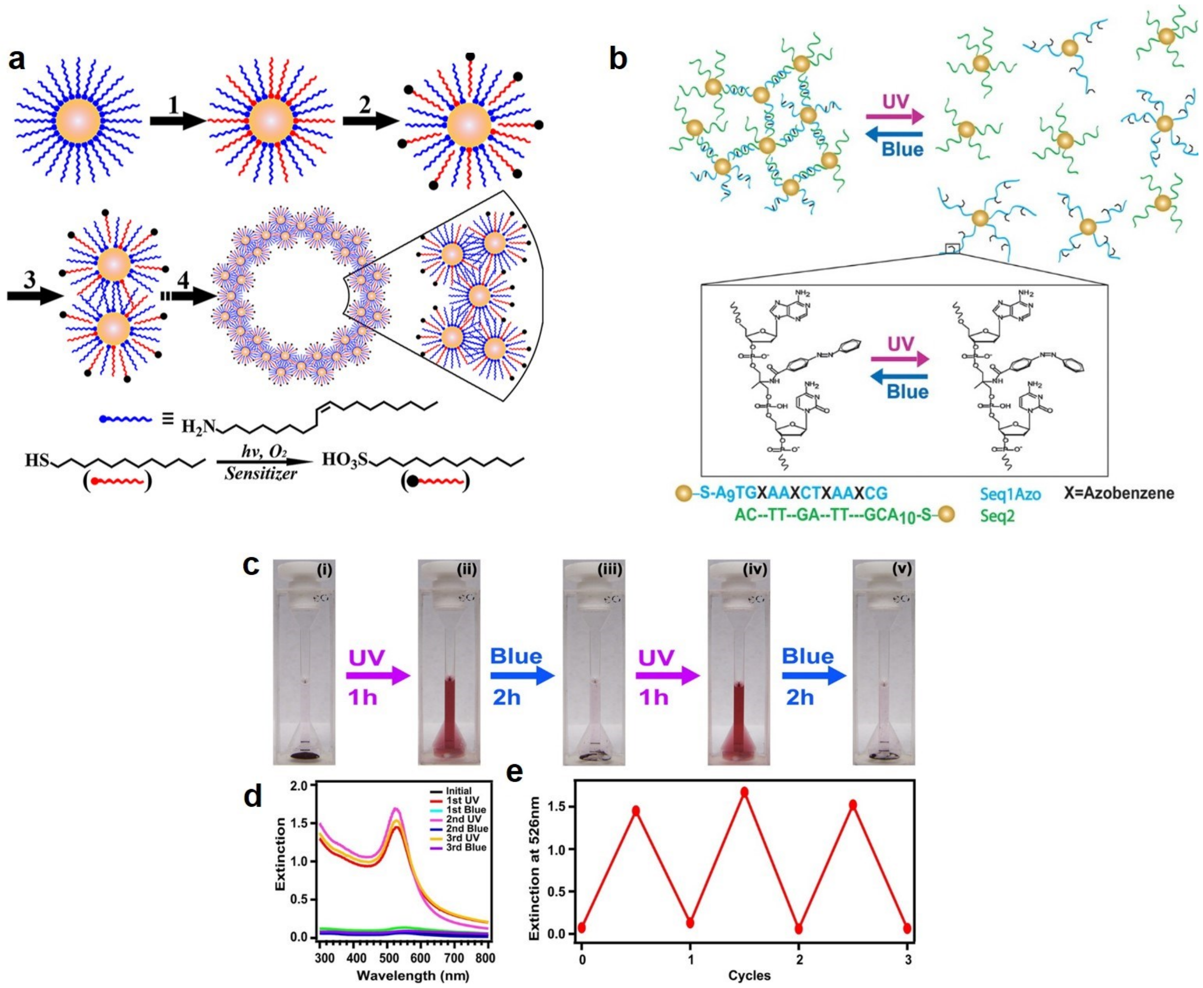

Figure 14. Light induced reconfiguration of plasmonic NPs. a) Schematic shows the photoinduced assembly process of Au NPs into vesicular nanostructures when the mercapto groups are oxidized to the sulfonic ones under UV-irradiation: 1. exchange of ligands with thiols; 2. UV-irradiation; 3. reconfiguration of ligands and assembly of NPs; 4. large scale assembly. Reproduced with permission.[148] Copyright 2014, John Wiley and Sons. b) Functionalization of Au NPs with thiol-terminated DNA containing azobenzene. The NPs carrying complementary sequences are hybridized in a controlled manner by UV and blue light irradiation leading to azobenzenes' trans–cis photoisomerization. Photoinduced reversible assembly of DNA–NP conjugates containing azobenzene-functionalized oligonucleotides. c) Camera images show the solution including the Au NPs with Seq1Azo and Seq2 attachments after cyclic UV and blue light irradiation. d) UV–vis spectra for the solution shown in (c) for

three cycles of photoswitching. The spectra show an extinction peak located at 526 nm after each time irradiation that is plotted in (e). Reproduced with permission.[149] Copyright 2012, American Chemical Society.

3.2.4. Electric field induced reconfigurations

As a fact, metal NPs are highly responsive to an applied electric field when compared to non-metallic NPs, thus subjecting them to an electric field could be an important strategy to tune their assembly thus optical properties in a switchable manner. This approach has been implemented for control of the NP aggregates in a suspension through dielectrophoresis, and indirectly in nematic liquid crystals (NLCs)[150]. The latter applicability lies within the scope of this paper and related to SPNs and is discussed in more detail here. Sio et al.[151] reported about the dynamic tuning of the LSPR of the arbitrarily distributed Au NPs deposited on a glass layer coated with Indium Tin Oxide (ITO). The NPs were subsequently covered with a LC material. When subjected to an external electric field, the hybrid-aligned LC layer is re-oriented and also a carrier accumulation layer near the ITO substrate forms. The RI of both LC and accumulation layers are affected by the electric field and thereby imposing a “dancing behaviour” of the Au NP's plasmonic resonance spectral position. Re-orientation of the NLCs along the applied electric field’s direction, could change the effective birefringence of the system, whereby shifting the substrates’ colors when the applied voltage increases from 0 to 10 V.

In the latest years, using an electric field to customize the alignment thus optical properties of anisotropic NPs, e.g. NRs and nanoplates, has been spotlighted[150]. For instance, Zhang et al.[60] synthesized the Au NRs decorated by an orientation molecule called: N,N-dimethyl-N-octadecyl-3-aminopropyltrimethoxysilyl chloride (DMOAP). To govern the alignment of the DMOAP functionalized Au NRs via tuning the NLCs’ orientation, an external electric field of 20 V was applied. The DMOAP-modified Au NR/LC system is an electrical SPN wherein the NRs with the negative scalar order parameter can be arranged individually or assemble into 1-D chain nanostructures. The elastically arranged ensemble of NPs, whose performance is vastly dependent on NP's shape, size, among others, provides new opportunities for creation of mesoscopic nanocomposites with coupled SPR states that are switchable by electric fields. Provided that P ‖ n (P is the direction to NPs' polarization and n is the LC director implying the local average orientation of rod-shaped organic molecules), a 500-nm absorption peak emerges when no electric field is applied. The peak red shifts by an electric field of 20 V, implying that the NRs are aligned under the influence of the orientation of NLCs. Interestingly, the optical properties obtained in the presence and absence of an electric field were different proportional to the orientation of the electric field of the light.

As an advanced class of anisotropic optical nanostructures, 1D assembly of NRs has shown extensive potential for a variety of applications including sensors, catalysis, photoelectric devices, and data storage. Such applicabilities stem from the LSPR and high surface energy in an ordered structure. In this regard, one high potential approach to produce ordered NRs assemblies is by 2D confinement e.g. in anodic aluminium oxide (AAO) channels or carbon nanotubes. Related to this concept, Wang et al. [152] have reported a simple yet effective approach enabling control of the polystyrene-tethered AuNRs (AuNRs@PS) assemblies via EF-induced confinement in AAO channels (Figure 15a). As shown in Figure 15b&c, the AuNRs@PS can be well-organized in different forms depending on the EF's orientation, PS's molecular weight ($M_{\text{w-PS}}$), and AAO channel's pore size (D_{C}). In addition, the optical properties of the as-formed nanostructures can be tailored by manipulating IS.

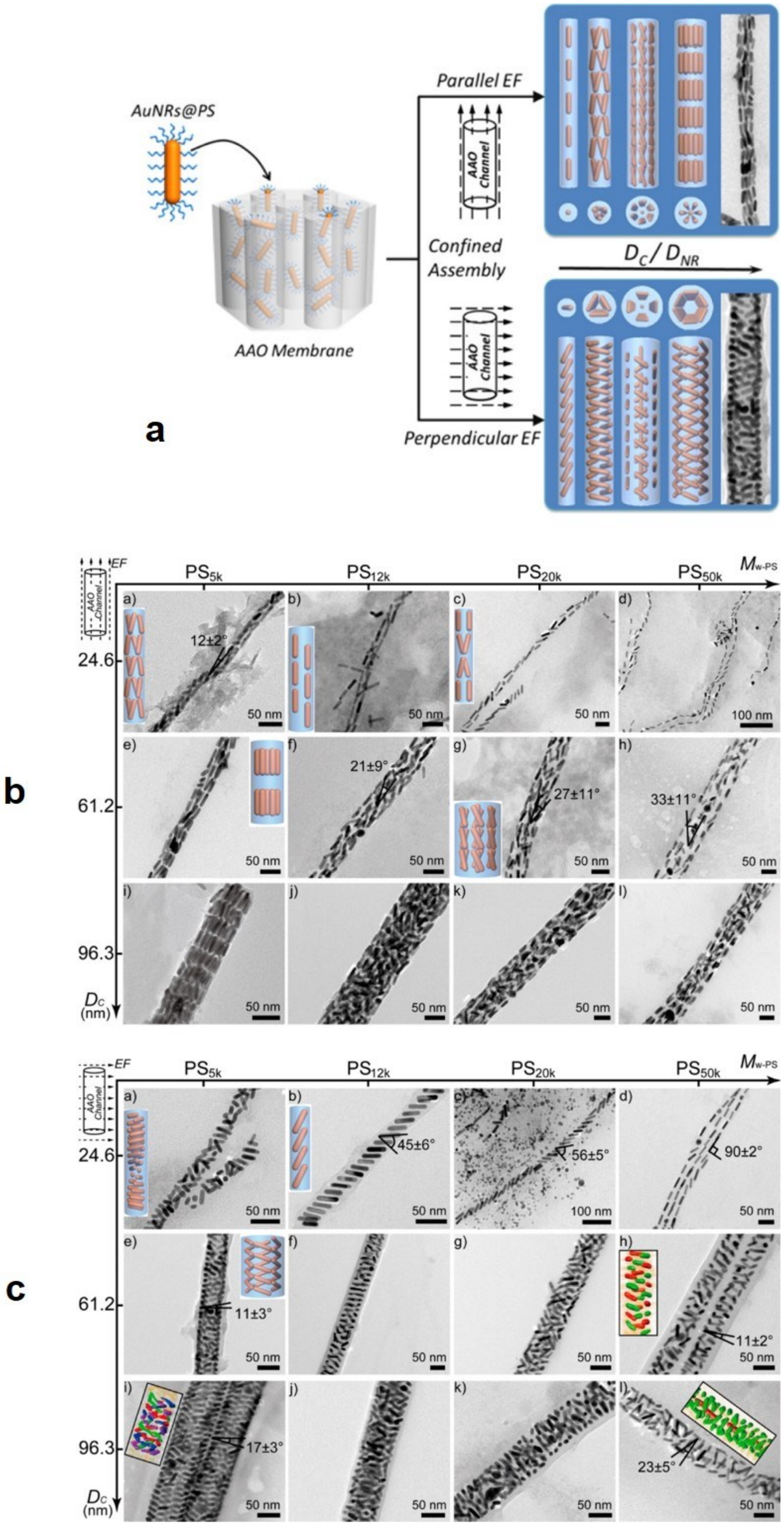

Figure 15. Electric field assisted alignment of nanoparticles in SPNs. a) Schematic illustration of the EF-induced confinement of PS-tethered Au NRs in AAO cylindrical channels. Via this approach hybrid assemblies as

e.g., 1D chain, side row, single helix, triple helix, and hexagonal structures, were developed. TEM images show Au NRs@PS assemblies subjected to b) parallel EF and c) perpendicular EF relative to the direction of the AAO channel and obtained by changing pore size (D_C) and PS's molecular weight ($M_{w\text{-}PS}$). The pore sizes are 24.6 nm, 61.2 nm, and 96.3 nm for the first to third row, respectively, and depending on the M_w, AuNRs@PS$_{5k}$, AuNRs@PS$_{12k}$, AuNRs@PS$_{20k}$, and AuNRs@PS$_{50k}$ assemblies are formed in AAO channels. Reproduced with permission[152]. Copyright 2016, American Chemical Society.

For the sake of inducing the optical performance of SPNs, the SPR peak's location, width, and intensity must be tunable. In the previously discussed reconfiguration approaches wherein the NPs do not touch a substrate (*e.g.*, in dilute solutions), the SPR peak position can be adjusted by the NP size, shape, composition, and RI of the neighbouring medium. The active dielectric neighbouring media include pH-responsive or conductive polymers, light-responsive materials, e.g. photochromic molecules, etc. as previously discussed. In the other case of SPNs i.e. those established on underlying films of *e.g.*, metal or oxide electrodes, an intimate contact could hybridize the dipolar plasmonic mode, depending on the energy level, into the weak antibonding and strong bonding states. The antibonding state associated with the electromagnetic field spreading away from the substrate enhances the RI sensitivity of the surrounding medium. The splitting of the plasmon peak of the hybridized modes is dependent on the RI of the surrounding medium and substrate. Thus, with respect to the design of SPNs on solid substrates, there is a need to accurate production of a high density of uniform NP aggregates and the accurate determination and control of the localized, intensified field, that are both challenging for the complex aggregates and shapes. With respect to the former necessity, as a promising technique for the organization of nanostructures, the Langmuir–Blodgett (LB) technique can produce monolayers of the respective elements at the interface of air–water with given areal density and regional packing that can eventually be transferred onto solid substrates as highly thin solid films. As shown in Figure 16a-d, utilizing the LB based Ag nanocube monolayer that was subsequently covered by an electrochromic polymer, reversible RI changes depending on the applied electrical potential is realized[153]. This feature can reversibly shift the SPR peak positions of the Ag nanocubes, Figure 16e-g. Such SPNs are able to offer frequent reversible, adjustable plasmonic optical behaviours (absorption and scattering) with an orthogonal shift in plasmon resonance. As verified via electrochemical tunability studies coupled with *in situ* spectroscopic measurements and finite-difference time-domain (FDTD) simulations, the notable SPR shifts are induced by the relative changes of the environmental RI of the electrochromic polymer overlay arose from reversible electrochemical oxidation and reduction processes (Figure 16h). Instead of an electrochromic polymer, as the surrounding medium, ITO branches were employed to encompass Ag NPs by Jeong et al. [154]. Such electrochromic SPNs were designed to perform in transparent (an optical transmittance of 73.76%), mirror (a reflectance of 79.77%) and black (a reflectance of 8.78%) states (Figure 16i-k). In this device, the 3D ITO branches were developed via electron beam (e-beam) evaporation on an ITO coated glass substrate. Ag NPs were synthesized between the ITO coating and the ITO branches set apart by a 200 μm polyimide layer. Applying a positive voltage to the ITO coating leads to reduction of Ag^+ ions in the electrolyte on the ITO branches. The Ag NPs are able to show LSPR by light irradiation thus hampering the reflection and providing a totally black state. The FDTD method can explain the entirely black mode induced by Ag NPs‘ LSPR. Figure 16l-n demonstrates that in the ITO coating with Ag film, the EF is distributed uniformly across the device and the transmission is poor at the interface of the Ag film and air. In this case, the Ag film reflects light, leading to the mirror state. At the presence of only the ITO branches, the EF’s distribution is uniform across the device, enabling the transparent state i.e. the generated electromagnetic wave propagates with no significant absorption and scattering. In the last case, i.e. the ITO branches with Ag NPs, incident light is predominantly absorbed around the top, and thus the field magnitude in the Ag NPs is more profound around the top of the ITO branches than their bottom. Also, an intensive field is concentrated between the NPs in the horizontal and vertical orientations. This behaviour means that for occurrence of LSPR, the Ag NPs need to be deposited on the surface of the ITO branches and to be isolated by them to cause effective light trapping, thus LSPR. Consequently, the resulting intensive LSPR can capture the electromagnetic energy and form a pure black mode with minor reflectance and significant absorption. The electrochromic devices, as discussed above, can be rarely used for flexible electronics, because they are mainly constructed based on ITO substrates that lose their conductivity after a given number of bending cycles. To address this challenge, Wang et al.[155] made a flexible smart window based on co-assembly of Ag and $W_{18}O_{49}$ NWs modified with PVP in a large area. They created multilayer ordered NW networks via the LB technique, wherein the Ag NWs acted as the conductive element and $W_{18}O_{49}$ NWs as the spacer between the Ag NWs. The highly transparent $W_{18}O_{49}$ NW network not only assists to the formation of transparent conductive electrodes but also allows the electrochromic performance. This hybrid network was able to show adjustable conductivity (7–40 Ω/sq) and transmittance (58–86% at 550 nm). Such a device, in contrast to the ITO-based electronics, can be curved with a radius of 1.2 cm for over 1000 times with no notable loss of conductivity ($\Delta R/R \approx 8.3\%$) and electrochromic behaviour (90% retention), implying its optimum mechanical pliability.

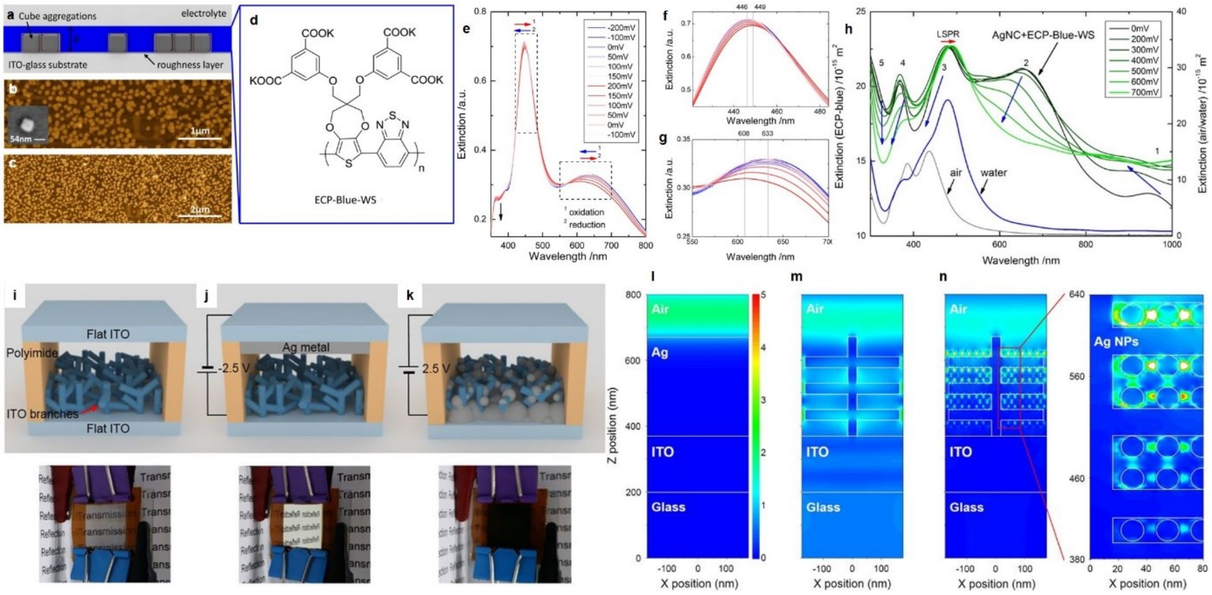

Figure 16. Electric field assisted tuning of plasmonic properties of SPNs. a) Schematic illustration of the SPN comprising Ag nanocube (54 nm) aggregations as an LB monolayer on an ITO-glass substrate. The nanocubes are coated by a layer of water-soluble electrochromic polymer (ECP-Blue-WS) in an electrolyte solution. b&c) AFM images of a monolayer of Ag nanocubes at different magnifications. d) Chemical structure of the ECP-Blue-WS repeat unit. The reversible plasmonic shifts of Ag nanocubes covered with ECP-Blue-WS when subjected to electrochemical oxidation and reduction of the polymer coating (d = 55 nm) e). UV–vis spectra of one switching cycle: (f) monomer peak and (g) aggregation peak. h) Simulated graph implies the oxidation of ECP-Blue-WS coating on a single Ag nanocube (from black to light green lines). The blue arrows point to the peak position and amplitude shift direction of the polymer under oxidation. The red arrow points to the opposite plasmon resonance shift under oxidation. The below curves imply the extinction cross-sections of the same nanocube monomer in air (gray line) and water (blue line). Reproduced with permission.[153] Copyright 2014, American Chemical Society. Schematic illustration (top row) and camera images (bottom row) of the electrochromic device in different operating states of i) Transparent, j) mirror and k) black. Finite-difference time-domain (FDTD) simulations. The x–z plane cross-section of electric field distribution at wavelength (λ)=420 nm for glass/ITO with (l) Ag film, (m) ITO branches and (n) ITO branches with Ag NPs. Reproduced with permission.[154] Copyright 2018, Springer Nature.

Recently, Montelongo et al.[156] introduced a reversible electrotunable liquid mirror operating based on voltage-induced self-assembly/disassembly of negatively charged (12-Mercaptododecanoic acid; MDDA) functionalized Au NPs (16 nm) at the interface between two immiscible electrolytes. The operational mechanism of such a system is based on capillary force driven positioning of the NPs at the interfacial region. Stimulating coupled plasmon resonances, a packed monolayer of large Au NPs can reflect back the light. However, the negative surface charges of the NPs hamper formation of a dense layer and lower reflectivity. Accordingly, to create a plasmonically coupled monolayer, a critical density of the NPs at the interface is required that not only enhances reflectivity but also does not lead to the NPs aggregation (Figure 17a (i and iii)). This objective could be met by construction of a ‘potential energy well’ at the interfacial region (Figure 17a (v)) capturing the NPs. Yet, when the NPs electrostatically repel each other the energy well is shallow. To address this challenge, the repulsion is reduced via screening by the electrolyte, thereby the well is deepened, i.e. the creation of mirror- like packed NP arrays (Figure 17a (ii, iv, and vi) is enabled. Nevertheless, this ‘chemical’ approach is largely limited by the highest electrolyte concentration minimizing the agglomeration chance for the NPs present in the bulk or at the interface. The authors developed a ‘physical’, *in situ* control strategy in an electrochemical cell (Figure 17b). In this method, the aqueous solution drives negative polarization versus the organic one, thereby moving the NPs towards the interface (Figure 17b (iii and iv)). Accordingly, the NPs are forced to bear each other in close proximity, i.e. the density and reflectivity is promoted (the reflectance peak is red shifted) (Figure 17b (v)). In contrast, polarizing the aqueous solution returns the NPs into the bulk, thereby lowering the reflectivity peak and ‘blue-shifting’ it (Figure 17b (vi)). Such an electrochemical adjustable plasmonic nanosystem can be reversibly shifted from a notably reflective ‘mirror’ to a transmissive ‘window’ and vice versa.

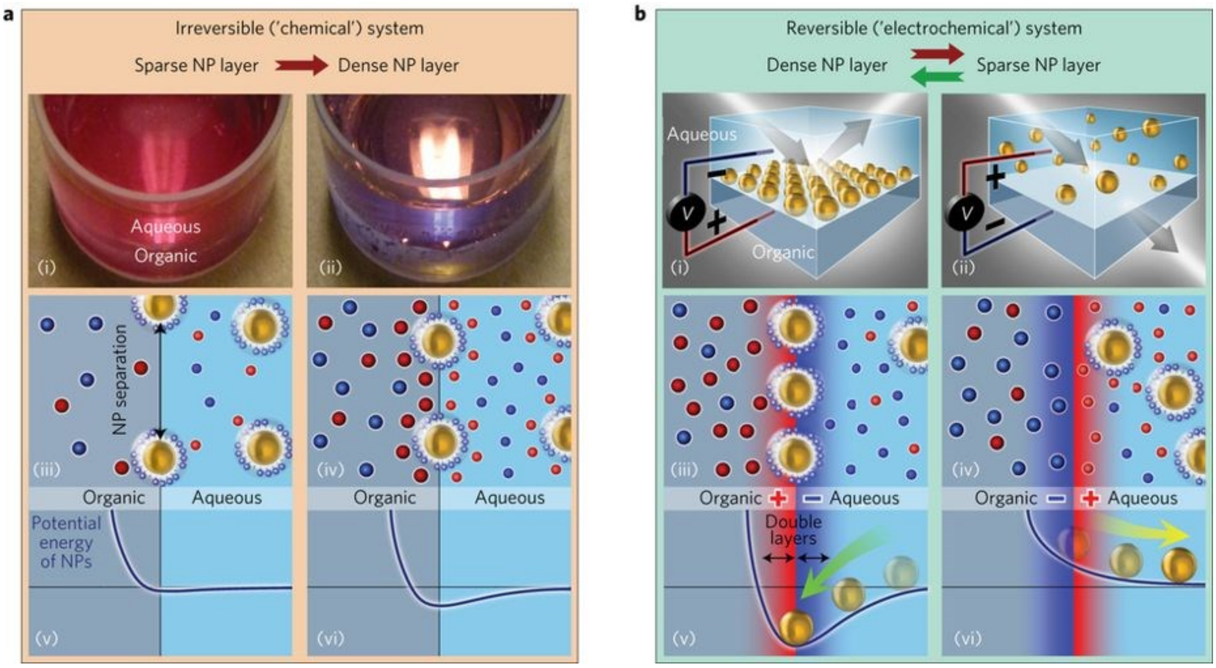

Figure 17. An electrochemically switchable liquid mirror/window. a) Via adjusting the electrolytes concentration, the Au NPs adsorb at the interface between the aqueous and organic phases, forming a dense reflective layer, as seen in the camera images (i) and (ii). When the concentration of electrolytes rises, the electrostatic repulsion between the NPs, functionalized by negatively charged ligands, declines, enabling

formation of denser layers, as schematically shown in the cartoons (iii) and (iv) wherein cations, anions and NPs are drawn as red, blue and gold spheres, respectively. The schematics (v) and (vi) imply the potential energy well for the NPs at the interface, intensified when the NPs' electrostatic repulsion declines with the increase of electrolyte concentration. b) The reversible control of the assembly and disassembly of the NPs to/from the interface when the polarity of the applied potential drop across the interface changes. In this mode, the system is located in an electrochemical cell. Under such circumstances, the NP layer can be even more packed compared to that formed by the spontaneous assembly, or can be fully disassembled from the interface, as schematically shown in (i) and (ii), and (iii) and (iv). Formation of two back-to-back electrical double layers at the polarized interface, leads to a deeper (v) or shallower (vi) potential well, depending on the sign of the applied voltage, thus switching on/off the electrotunable nanoplasmonic liquid mirror. Reproduced with permission.[156] Copyright 2017, Springer Nature.

The electric field induced reconfiguration is an advanced approach for dynamic plasmonic structural coloration, as well. The commercial black-and-white electronic papers are in fact electrophoretic displays based on tiny ink particles with positive and negative charges, encapsulated within microcapsules suspended in a fluid, displaced by applying an electric field[157]. When an electric field is exerted, the ink particles move inside the microcapsule to approach the display surface and create solely a black and white image on the screen. To promote the quality of the image in terms of color, the mentioned classic approach must be modified. In this regard, such a challenge has been recently addressed by utilizing four kinds of pigment particles with different colors of yellow, cyan, magenta, and white in a fluid[158, 159]. The pigment ink particles are also different in size, polarity, and their charge strength. Thus, any alteration in the voltage can lead to movement of different pigment particles towards the display surface and thereby generating diverse color combinations, i.e. a large variety of reflective vivid colors. The mentioned pigment particles are ink-containing polymeric capsules. As an upgrade to such a system, a diverse range of plasmonic NCs or the related compositions could be employed as the pigments to provide the electrophoretic display with full color facility. This modification can notably enhance the reflective display's resolution, longevity, and color contrast, and also offer higher display refreshing rates[160]. Regarding the dynamic plasmonic coloration a precious review paper has been recently authored by Shao et al.[160]

3.2.5. Magnetic field induced reconfiguration

Similar to electric field, magnetic field can also be employed as an external stimulus to influence locally on the NPs assembly or in general dispersion mode in a suspension. In this regard, plasmonic NPs are normally functionalized with magnetic components to acquire magnetism and thereby can be controlled in various assemblies by an applied magnetic field. Such kind of magnetic/plasmonic particles, possessing magnetic and plasmonic properties together, have been studied particularly with respect to biomedical applications, such as magnetic resonance imaging, photothermal treatment, and drug delivery[150].

Xue et al. [161] developed a system based on 1D chains of magnetic/plasmonic Fe_3O_4@Au NPs (Figure 18a, left) with core–shell structure. It is worthy to note that the NPs were coated with an ultrathin polymeric (surfactant) layer to preserve a nanogap between adjacent particles constituting a 1D chain. Alignment of the NPs was realized by using a set-up of magnetic assisted self-assembly, shown in Figure 18a, right. The Fe_3O_4 superparamagnetic core allows for magnetophoretic adjustment of the NPs and realizes the coupling between them as the driving force for their assembly. Additionally, the plasmonic shell is responsible for provision of extraordinary optical and photothermal behaviours of the assembled structures. According to the optical measurements, upon formation of a chain, the absorption spectrum red shifts. Also, as shown in Figure 18b, a strong plasmonic coupling takes place between adjacent NPs, while localization and increment of photothermal transduction happen at the chain center. The opportunity of controlling the magnetic and optical performance of colloidal plasmonic NPs by application of an external field holds great promise for development of advanced imaging, sensing, theranostic, and optofluidic applications.

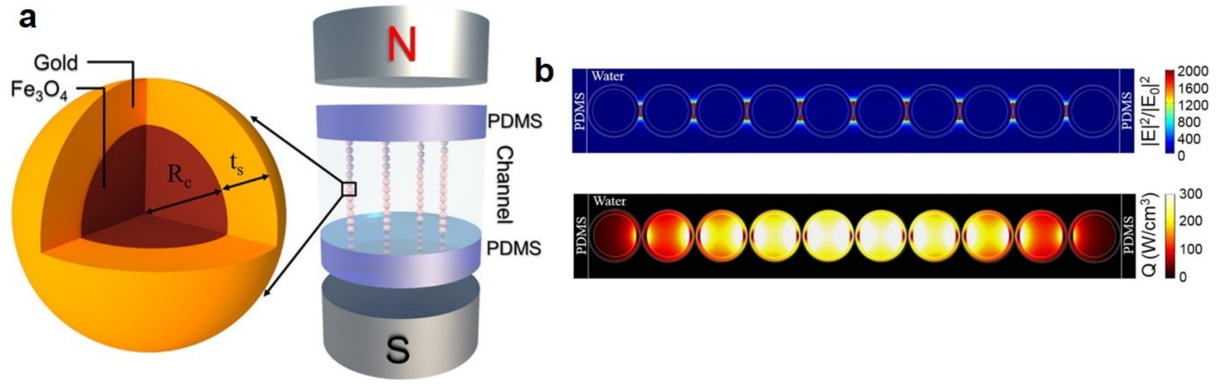

Figure 18. Magnetic field assisted alignment of hybrid NRs. a) Schematic illustration of magnetic/plasmonic Fe_3O_4@Au NPs (left) (note that the NPs are coated with an ultrathin polymer layer), and self-assembly of 1D particle chains when the NPs are exposed to a uniform magnetic field (right). b) Plasmonic coupling and photothermal transduction: (top) local field enhancement $|E|^2/|E_0|^2$ and (bottom) thermal power density in a single chain composed of 10 polymer-coated Fe_3O_4@Au nanoparticles. Reproduced with permission[161]. Copyright 2017, American Chemical Society.

3.2.6. Solvent induced reconfiguration

The reconfiguration of plasmonic NPs tethered with amphiphilic block copolymers by selective solvents has also brought about a new possibility of formation of complex hierarchical nanostructures. Such components comprising a stiff core made of a metal NP that is tethered with amphiphilic block copolymer chains simulate structurally the micellar architectures based on a hard core and a corona of several pliable amphiphilic block copolymer chains. The strategy of employing plasmonic NPs as a template for accumulation of several block copolymer chains in a controlled manner enables easy yet reliable production of micelle-like architectures with well-defined chemistry at only one stage. Moreover, the Au NPs as the "micelle" cores impart LSPR properties to such building blocks. Thus, through a controlled strategy, these particles are arranged in a way that allows modulation of PC between them, thereby the cooperative properties of aggregates. In this regard, He et al.[162] have successfully synthesized Au NPs tethered with amphiphilic block copolymer chains of poly(ethyl oxide)-*b*-polystyrene with a thiol group at the PS end (PEO-*b*-PS-SH). Subsequently, they assembled such NPs into different superstructures such as single-molecule micelles, clusters containing given density of the NPs, and vesicles comprising a monolayer of the NPs in the membrane in a water/tetrahydrofuran (THF) mixture, Figure 19a-d. In fact, when water, i.e. a weak solvent for PS, is added, the PS blocks are shrunk thus lowering the system's total free energy, leading to structuring of the NPs as single-molecule micelles, clusters, and vesicles. The morphological transition of the superstructures was determined by the polymer tethers length and the NP core size. The solvent induced dynamic reconfiguration of the particles led to their controllable PC thus a strong LSPR peak's red-shift and a largely improved LSPR absorption in the NIR range, as shown in Figure 19e&f. Such superstructures could show a promising potential for in *vitro* and *vivo* cancer imaging and photothermal treatment. Choueiri et al.[163] demonstrated applicability of this concept i.e. bottom-up surface patterning of colloidal particles for the Au NPs tethered with PS. When suspended in DMF, i.e. a strong solvent for PS, the 20-nm-diameter Au NPs functionalized with PS-50K are covered by a uniformly thick PS shell. In contrast, when the solvent quality for the PS ligands is lowered e.g. by adding water, the PS layer is transformed into a surface patch. The construction and structure of the patch were dependent on the polymer length, nanosphere diameter, and polymer grafting density. Recently, Kim et al.[55] reported a same behavior for anisotropic Au NPs of octahedron, concave cube, and bipyramid shapes that were coated with a layer of thiol-terminated PS. Such core-shell nanocomposites offer distinct shell segregations when exposed to a variation in solvent polarity. By addition of polar solvents e.g. a dimethylformamide and water mixture (1 vol.% of water), the PS shells on the Au NPs are mainly accumulated on the highly curved zones of the core particle.

With respect to anisotropic plasmonic NPs, despite routine adoption of aqueous systems for their preparation in controlled size and shapes, their reconfiguration is facilitated in case the NPs are suspended in organic solvents. To relocate from water to an organic solvent, the NPs should be surface functionalized by ligands of alkylamines, octadecylamine, bidentated thiols, thiolated polystyrene etc. In this regard, a facile and prompt technique relying on a composition of PEG-SH and 1-dodecanethiol (DDT) i.e. a hydrophobic capping agent has been reported by Serrano-Montes et al.[164] to transfer different types of Au and Ag NPs whose sizes could vary up to 200 nm and whose shapes were as diverse as spheres, nanorods, and nanostars from a water based dispersion into chloroform. These organic-plasmonic NP dispersions readily spread out on water, whereby are assembled at the air/water interface into large NP assemblies that can be subsequently deposited onto solid substrates. Such superstructures provide strong PC, thanks to a dense close packing in them, assuring their effectiveness for SERS application.

As seen above, the majority of dynamic reconfiguration based systems are based on dispersion systems that could be limited in terms of applicability and stability over long times. In contrary, as a breakthrough, Elbahri et al.[17-19] devised a switchable plasmonic system that could operate via solvent/pH induced reversible conformational change of BSA protein stuck to polymeric (PANGMA) NFs. In this pioneering study, upon hydration, the protein could be swollen and capture Au NPs, Figure 19g. Subsequently, the reversible conformational change of BSA induced by water allows for different arrangement of the NPs and thus different optical properties. While in the dry state, BSA is as folded with α-helix structure, it is transformed to β-turn and unfolded when hydrated. This behavior can reversibly change the morphology of the bionanocomposite as swollen and thus the adsorbed Au NPs' configuration. The Au NP/BSA/PANGMA NF bionanocomposite performs well as a switchable angle-insensitive broadband black absorber whose absorbance in the visible frequencies could be as large as 100%. The bionanocomposite in dry state shows a red color due to the presence of the adsorbed Au NPs. Whereas, when it is immersed in water, the color turns to black. The black color is correlated to the adjustable conformation, as witnessed by cryo-SEM. As seen in Figure 19h, the black nanocomposite could be simulated to a swollen interconnected porous nanofoam. Such a structure implies occurrence of a phase segregation in the completely wet membrane. In fact, the bionanocomposite is identified by the existence of hydrophilic zones incorporated in the hydrophobic polymer host. The hydrophobic matrix exerts notable limitations on the hydrophilic amorphous zones, hampering their expansion by minimizing deformation parallel to their surfaces. Due to the low segmental mobility, an osmotic pressure is distributed across the matrix resulting in the creation of pores. Development of the pores is inhibited by the vitrification of the polymer host that embraces them. Accordingly, the interplay between the two opposite forces leads to the creation of porous structures resided by the nanoparticles. However, the color transformation is highly reversible as witnessed by ten consecutive experiments, Figure 19i. As seen here and in Figure 19j (top), upon hydration, the color of the bionanocomposite is transformed from red, represented by a reflection loss at 537 nm, to black without any distinct reflection feature in the visible frequencies range. The hydration induced conformational change of the protein decorated with the Au NPs leads to a smaller IS in this bionanocomposite, thus reinforcement of the local plasmon enhancements and notably coupling them in an extensive spectral domain [165-168]. As a fact, for the neighboring NPs (at the percolation threshold), intensive near field coupling takes place and energy is highly captured [169]. This phenomenon i.e. light capture is notably enhanced when the NPs within the porous structure of the bionanocomposite diffract or scatter the light.

Homaeigohar et al.[17] further investigated the pH responsiveness of the Au NPs/BSA conjugate on the polymeric NFs. It is well known that under highly acidic conditions, that is, a pH below 4, the acidic moiety of the protein component is highly protonated, thereby the protein is denaturated. The secondary and tertiary structures of the protein are disrupted leading to an unfolding or straightening effect. These transitions bring about an increased local separation of the domains as the conversion of the compact heart shape of the protein to a linear bead form. Such an expansion could alter the plasmonic state of the nanoparticles stuck to the protein, thereby acting as signal transduction. In the ideal case, this transition should be reversible upon increase of pH, that is, a switchability in plasmonic behavior of the metal nanoparticles. As shown in Figure 19j (bottom), while the plasmonic red color of the bionanohybrid after exposure to the acidic medium is drastically weakened, it is recovered as soon as the pH rises to 7 in a neutral aqueous medium. The weak and intensive plasmonic red colors observed at different pH values represent denaturation and renaturation of the protein, respectively. This color change occurs owing to coupling/decoupling between the nanoparticles induced by the interparticle distances, Figure 19k. While in the naturated state, an intensive near field coupling between closely spaced nanoparticles occurs, in the denaturated state as the distance between the nanoparticles changes, the effect is diminished.

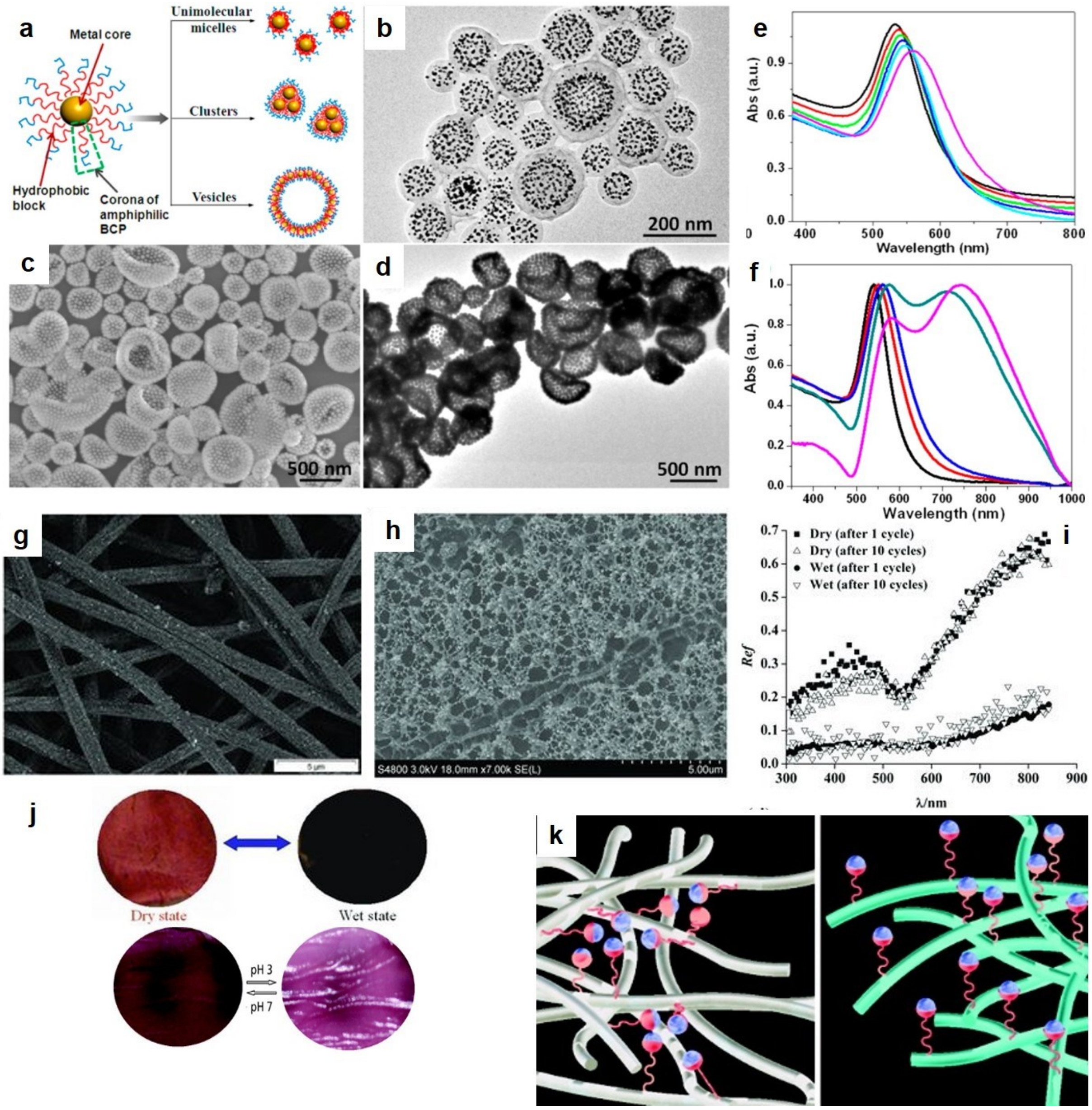

Figure 19. Solvent responsive SPNs. a) Schematic illustration of the amphiphilic block copolymer tethered Au NPs and their resulting assemblies. b) TEM image of vesicular assemblies of PS-34-Au-5 (34 and 5 show

PS' molecular weight and Au NP's diameter, respectively). (c) SEM and (d) TEM images of vesicular assemblies of PS-34-Au-40. UV–vis spectra of (e) Au-20, and (f) Au-40 using different M_w of block copolymer, increasing from left to right, along with the red-shift of plasmonic peaks. Reproduced with permission.[162] Copyright 2013, American Chemical Society. g) SEM image shows a bionanohybrid structure made via adsorption of Au nanoparticles onto the BSA/PANGMA nanofibers. h) Cryo-SEM image showing the surface of the wetted (water soaked) membrane. i) The measured reflection spectra of the bionanocomposite in dry and wet states. Ref and λ represent reflection and wavelength, respectively. Reproduced with permission[19]. Copyright 2012, John Wiley and Sons. j) Reversible color transformation of the bionanocomposite induced by hydration and pH. k) The sketch illustrates plasmonic coupling between nanoparticles in the naturated state (pH 7) left and plasmonic decoupling for the denaturated one (pH 3), right. Reproduced with permission.[17] Copyright 2013, ICE Publishing.

4. Progressive Trend: The switchable plasmonic molecules based nanocomposites

So far, we have reviewed the SPNs acting based on reversible changes of the plasmonic metal NPs' spacing and surrounding medium. As a new generation of plasmonic nanocomposites, incorporation of plasmonic molecules that undergo stimuli induced reversible changes into polymeric hosts can boost the area of advanced, dynamic optics. According to the quasi-static approximation, it is well known that when electromagnetic radiations strike dipoles (i.e., atoms, molecules and nanoparticles), a collective electron displacement occurs where the electric field within the dipole moves the electron cloud away from the positive core (Figure 20a). In the most straightforward situation, an oscillating dipole's alternating surface charges create a plamonic response even when only organic molecules are involved, as demonstrated by Elbahri et al.[41]. In fact, similar to polarizability that generates plasmon in a metallic structure, electronic polarization of oscillating molecules allows the possibility of collective electron displacement that can be further enhanced for the conjugated molecules containing delocalized electrons in the π–$\pi*$ orbitals. Under electronic polarization, in particular, the dynamic polarizability is highlighted where the molecules behave as a set of classical oscillators despite considering their electronic transitions. In other words, the molecules perform as transition oscillators with eigenfrequencies equal to the frequencies of transitions between the atomic energy levels i.e. “electronic transition” and with a damping constant as described by the conformity principle[170]. According to the spectroscopic conformity principle, the dynamic polarizability is explained as:

$$\alpha(\omega) = \frac{e^2}{m}\sum_n \frac{f_{n0}}{\omega_{n0}^2 - \omega^2 - i\omega\delta_{n0}} \tag{9}$$

where δ_{n0}, ω_{n0}, and f_{n0} are the damping constant, eigenfrequency and the oscillator strength.

In case the external field frequency approaches one of eigenfrequencies of the transition oscillators, so that the resonance condition i.e. $|\omega - \omega_{n0}| \leq \delta_{n0}$is met and one resonant summand in the sum (Eq. 9) is kept, the expression for resonant polarizability can be extracted from Eq. 9 as follows[170]:

$$\alpha_{res}(\omega) = (\frac{e^2}{2m\omega_{n0}})\frac{f_{n0}}{\omega_{n0} - \omega - i\delta_{n0}/2} \tag{10}$$

It is obvious that, the resonant polarizability is a complex value whose real part can be both positive (in the case of molecules and dielectric dipoles) and negative (for metals). Its imaginary part is also related to the damping constants of the transition oscillators and responsible for absorption of radiation. While, the real part determines the reflection and refraction of an electromagnetic wave in a medium. Accordingly, at the resonance, two processes namely absorption and specular reflection progress. Contrary to the common belief, the specular reflection is not related to the arrangements of dipoles, rather it depends on the dynamic polarizability and hence can occur in the disordered glassy composite systems, as demonstrated by Elbahri et al.[41].

To elaborate this concept, here, a molecular composite model system composed of the photochromic spirooxazines molecules embedded in a PS matrix is taken into account. Such molecular switches operate based on isomerization between two different states, when exposed to an applied stimulus e.g. light. The photochromic system provides a monomolecular chemical reaction to avoid any complications due to diffusion. As mentioned earlier, SPO as a photochromic dipole, in the closed or "OFF" state shows absorption merely in the UV range. As shown in Figure 20b, when SPO (in the closed form) is irradiated by UV light, its C-O bond cleaves, and subsequently is converted to its planar MC isomer (open or "ON" state). Such photochromic dipoles are known for their absorption based switchable properties. However, in the ON state, they can cooperatively oscillate and thereby specularly reflect light. As a game changing study, Elbahri et al.[14, 41] could manifest, specifically, the mechanism of the specular reflection and Brewster phenomenon caused by the cooperative coupling of the photochromic molecular dipole antennas. The latter effect is caused by the dipolar interaction between the radiating dipoles (SPO in this study) and the hosting matrix with a net dipole moment (Figure 20c). The Brewster wavelength could act as an important indication for largely localized polarity of matrix. Figure 20d demonstrates the reflection spectra measured at the oblique angles of 45° and 65° (related to the Brewster dip) for the films composed of 30 wt.% SPO incorporated in apolar PS and polar PVDF matrices. As deduced from the graphs, the reflection peaks and dips red shift whose magnitude depends largely on the dipole moments of the matrix. While the shift of the reflection peaks (at 45°) is only 11 nm, the reflection dip at the Brewster condition (at 65°) shifts as large as 40 nm.

As a breakthrough that challenges the common wisdom justifying the RI dispersion behaviour solely by the imaginary part (electronic transition and absorption) of the oscillated molecules, we stress here that RI consists of two parts taking place independently yet simultaneously under the resonance condition. In this regard, the dispersive curve of the real part is governed by the photochromic molecules' dynamic reflection. This postulate can be proved by determination of the RI variations based on the absorption and reflection coefficients through direct numerical simulations, as shown in Figure 20e. For such calculations, the RI was restored according to the following equation (Eq. 11)[171]:

$$n = \frac{1+R}{1-R} + \sqrt{\frac{4R}{(1-R)^2} - k^2} \quad (11)$$

where k is calculated by;

$$k = \frac{\lambda}{4\pi} \times \frac{A}{d} \quad (12)$$

where, A is the normalized absorption coefficient, R is the normalized reflection coefficient, λ is the wavelength and d is the thickness. As clearly seen, the outcomes are in a desirable harmony with those achieved experimentally (Figure 20e&f). Figure 20e illustrates the light modulation of refractive index of a photoswitchable nanocomposite of SPO(20-30%)/PS by UV illumination. The imaginary part of refractive index, correlated to molecular absorption, is peaked at 560 nm, while the real part undergoes an anomalous dispersion whose peak appears at 660 nm. It is worthy to note that the dispersive curve of the real part is largely influenced by SPO molecules' dynamic reflection. Accordingly, by tailoring the specular reflection, interferences, absorption and the real and imaginary parts of the photoswitchable molecules' RI, a new road map for the molecular plasmonic photonic coupling is realized. Such a strategy can be based in the fabrication of a new family of optically active photoswitchable devices. In this context, the molecular photonic coupling can be either weakened with enhanced absorption or reinforced with generation of new colors based on splitting response (when the photonic resonance of the surrounding material is concurrent with the imaginary and real part of the photoswitchable molecules, respectively) (Figure 20g).

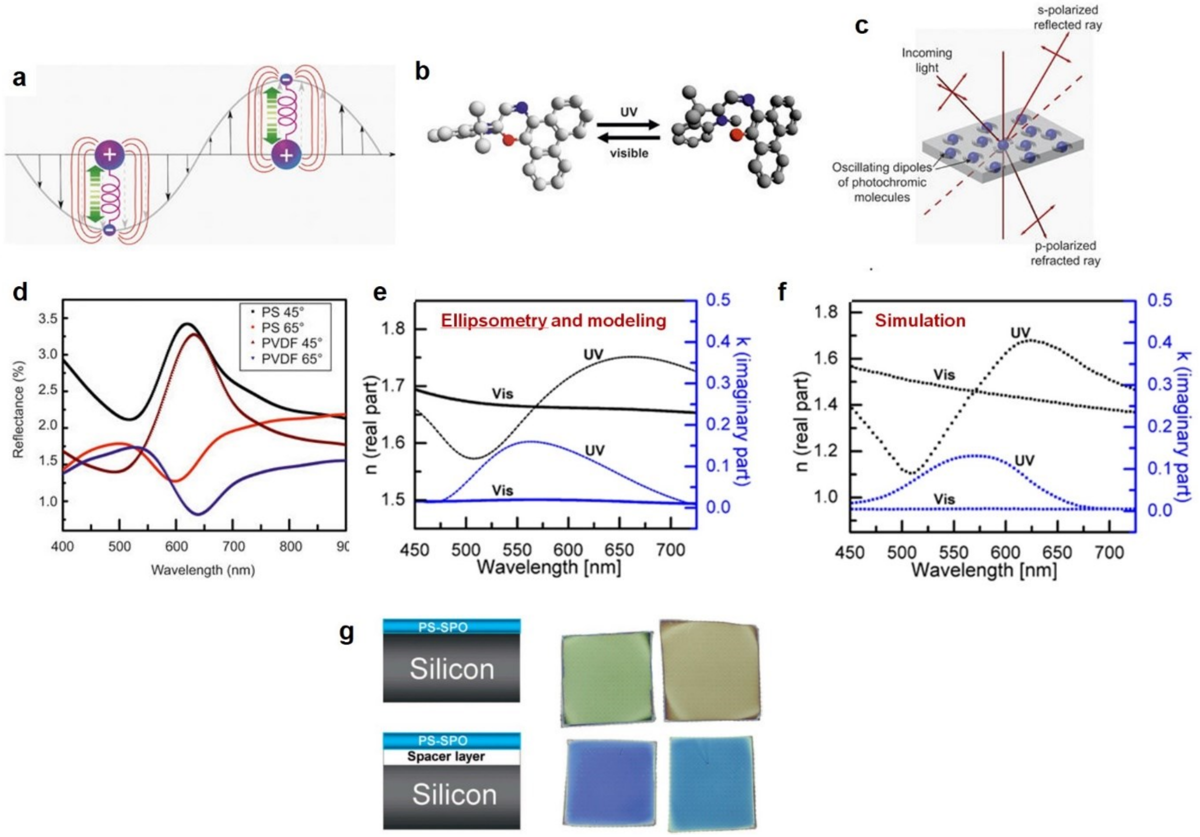

Figure 20. Specular reflection and Brewster effect in photoswitchable optical nanocomposites. a) Schematic demonstration of the Rayleigh effect where a fluctuating electric field moves a dipole's charges relative to each other. b) Schematic demonstrates the photoswitchable C-O bond cleavage in a spirooxazine (SPO) molecule subject to UV radiation. c) Schematic illustration of the Brewster effect caused by the oscillating dipoles (blue spheres) in an encompassing material. d) Reflectivity spectra of the SPO/polymer samples after UV exposure imply a noticeable matrix sensitive alteration in the Brewster wavelength (at 65° and under p-polarized light illumination). e,f) Real and imaginary parts of the RI of the SPO incorporated PS film when illuminated by UV-Vis light: obtained via (e) ellipsometry; (f) numerical simulation. g) Enhancement and weakening of photonic coupling effect by inclusion of a thin SiO_2 layer between the SPO incorporated PS film and silicon wafer, represented by the reflected colors with respect to the OFF (prior to UV irradiation) and ON states (after UV irradiation). Reproduced with permission[41]. Copyright 2015, Springer Nature.

Within the past few years, several SPNs based on a combination of plasmonic photochromic molecules and metal plasmonic metasurfaces or nanoparticles have been suggested (Figure 21a). In such systems, each component offers particular properties when light irradiated. While SPR i.e. local field enhancement occurs in the metal phase, the photochromic plasmonic molecule shows a photoswitching dynamic polarizonic effect, as stated above. These two optical behaviors affect each other, due to close proximity of the constituents of such a nanohybrid system. For instance, Elbahri et al. [42] developed a photoresponsive, transparent, and notably conducting system that could perform through the nanophotonic interplay of a Ag film underlying a spirophenanthrooxazine (SPO) molecules embedded polymer. Such a hybrid structure could be employed as a photobleaching gas sensor, as well. As we showed, utilizing the photoswitchable molecules, one can couple light to the plasmon of the film and therefore tune its transparency by illumination. As seen in Figure 21b, the clarity of the logo of the "*Nanochemistry and Nanoengineering*" group behind a 20 nm Ag film coated glass alone (right) and with a SPO-PS overlay (left) is quite different. This discrepancy stems from the low and high transmissions of the films, respectively. Optical measurements have shown that transparency of the system is 100% more than that of a bare Ag film, Figure 21c. The observed effect can be attributed to the coupling of the light to the plasmon resonance of the base layer reducing the reflection of the film thereby optimizing the transmission. In addition, the transparency of the film significantly drops upon UV illumination due to the strong absorption of Spiro molecules (Figure 21d). While transparency can be recovered after around 24 hours, we could notably accelerate it to only few seconds by subjecting the system to given organic gases including toluene and acetone, demonstrating a photobleaching gas sensor, Figure 21e. In fact, the gases act as plasticizers for the polymer matrix and ease the reversible isomerization of SPO molecules. Conclusively, benefitting from the absorption of the photoswitchable molecules coupled with plasmon resonance, a new class of optical systems is realized whose transmission level can be reversibly tuned by light. In another relevant study, Elbahri et al. [43] showed that an optically stimulated highly absorptive device can be made based on deposition of a thin photoswitchable molecules embedded polymer film (SPO-PS) on a metal mirror (an optically thick gold film). It is worthy to mention that the substrate for this layered structure is glass. In this configuration, the reflectivity of the mirror can decline to a few percent or increase to over 95% dynamically by UV or visible irradiation, respectively. In addition, the absorption band of this system can be extended over 150 nm or be narrowed by UV or visible irradiation, respectively. Figure 21f compares the absorption of a Au film overlaid by the SPO-PS one in *off* and *on* modes. In this Figure, the Au's SPR peak appears at 530 nm (in the *off* mode), implying that the SPO molecules have excited the SPP (solid line). By UV irradiation, an insignificant plasmon–molecular coupling takes place and an extensive asymmetric shaped resonance emerges (dashed line). The strong absorption spectrum of the irradiated sample arises from the coupling as well as several times interlayer reflections i.e. interference also plays a notable role in the reflection loss (absorption rise) in the system. Figure 21g implies that when the thickness of the SPO/PS composite varies on the Au mirror, the coupling does not change proportionally. The reflection drop for all the thicknesses follows a similar trend and occurs at a fixed frequency. Taking into account the subwavelength thickness of the coating and its switchable reflection drop (upon illumination), the developed device could be regarded as a novel absorbing antireflector for various applications with respect to remote sensing and plasmonic switches, amongst others.

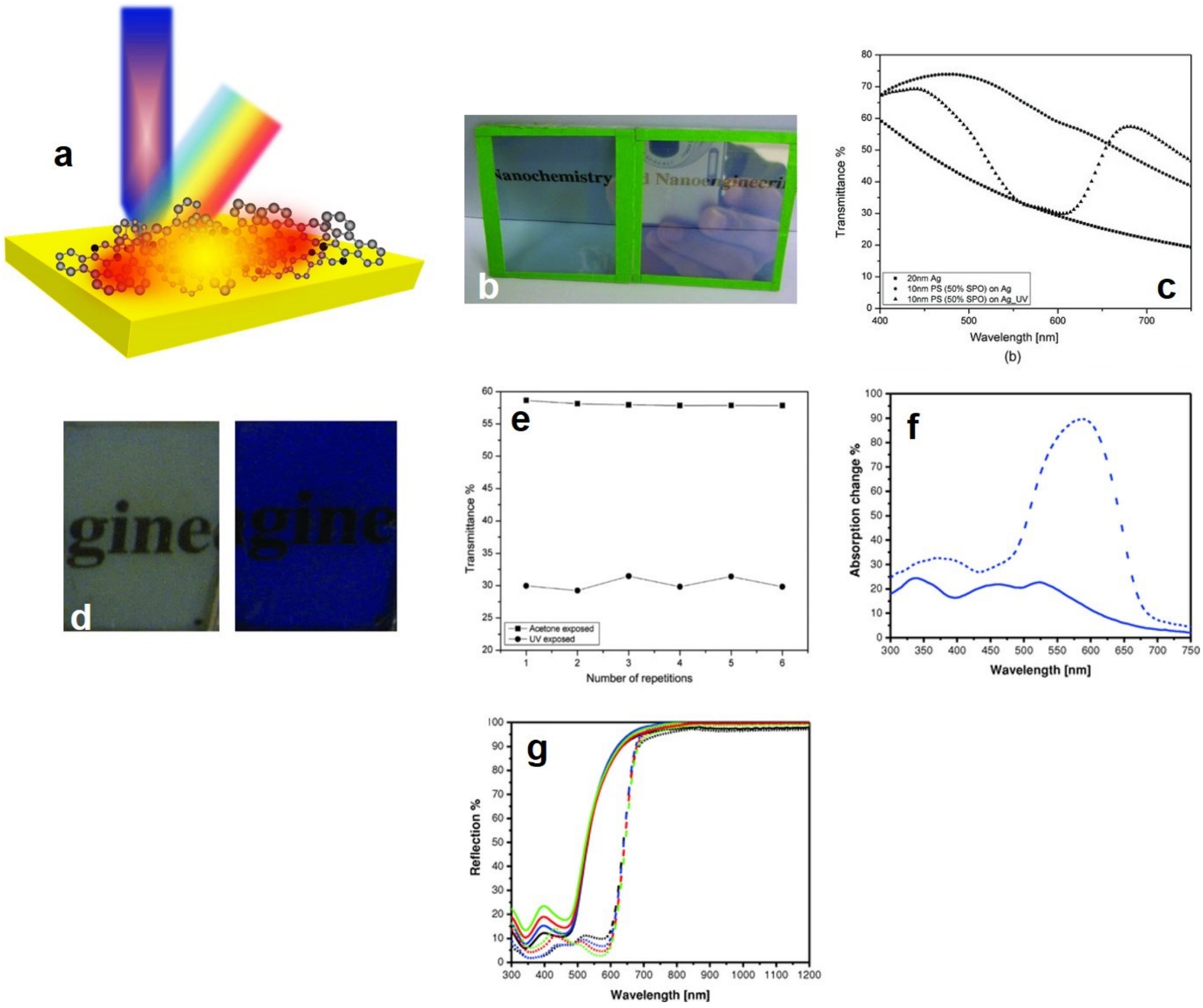

Figure 21. Plasmonic molecule based SPNs. a) Schematic illustration of a hybrid structure comprising photoswitchable molecules mounted on a metal film. b) Camera images show the "*Nanochemistry and Nanoengineering"* group's logo observed behind a piece of glass coated with a 20 nm silver film (right) and 10 nm PS (50 vol.% SPO) coated on a 20 nm silver film (left). c) Transmittance spectra of 10 nm PS films doped with 50 vol.% SPO coated on a 20 nm silver film under visible light and UV illumination. The references here include an uncoated 20 nm silver film and a10 nm PS film coated on a 20 nm silver film. d) Camera images show a 20 nm silver film coated with 10 nm PS (50 vol.% SPO) before (left) and after UV illumination (right). e) The photoswitchability of the system is verified by exposing it to the acetone vapor after UV illumination for up to six times. Reproduced with permission.[42] Copyright 2011, John Wiley and Sons. f) A comparison between the absorption measured in the *on* (dashed line) and *off* (solid line) modes of the SPO-PS layer mounted on a Au film versus the absorption of bare Au. g) Reflection spectra of the SPO-PS coated gold films whose coating thickness varies as: 15 nm (black), 30 nm (blue), 40 nm (red) and 50 nm (green). Solid and dashed lines represent the as-deposited and illuminated structures, respectively. Reproduced with permission. [43] Copyright 2014, John Wiley and Sons.

5. Summary, Challenges and Outlook

Here, we reported recent researches and progresses on the polymeric switchable nanocomposites in two main classes. While the classic SPNs contain a diluted regime of plasmonic NPs and the switchability does not bring about a notable change in optical properties, the modern SPNs performing via structural reconfiguration of the NPs can encompass a concentrated regime of the NPs and induce a large enhancement of the properties. This promising, advanced class of reconfigurable materials are based on the closely spaced ultrafine nanoparticles that can offer extraordinary reversible properties thanks to the available strong and cooperative near field coupling between them. Despite such merits, these nanostructures are mostly in the suspension form that restricts their wide applicability. The research must be thus directed towards the novel approaches enabling creation of such switchable structures in a solid frame and as scalable. We believe that inspired by several natural creatures e.g. sea cucumbers that are able to rapidly and reversibly alter their structure, the next generation of reconfigurable materials as 3D adaptive materials should be equipped with the physiological stimuli induced reversibility occurring slowly, without excessive expansion, and from a rigid, solid state to a soft one.

With no doubt, the area of the reconfiguration based SPNs holds a great promise for next generation of optical devices. However, there are still many challenges ahead to develop such controllable systems in large scale. For instance, control of the IS of ultrafine particles at high filling factors is a bottleneck. Moreover, there is a lack of theoretical models for prediction of the behavior of the strongly interacting non-periodic particle assemblies, and also very advanced characterizations are needed. As a consequence of widely different chemistry of the polymer host and plasmonic NPs, the strong aggregation tendency of the ultrafine densely packed nanoparticles has to be overcome. Thus, despite the enormous potential of SPNs in advanced optical utilities, the future research on such materials should be focused on the fabrication, characterization, simulation, and tailoring of functions based on the synergetic action of the main structural elements.

Our review has also highlighted a new generation of SPNs based on plasmonic molecules that are believed to play a notable role in the future research in this area. The conjugated molecules among others, for example, with the HOMO→LUMO-1 excitations give rise to a dipolar polarizonic state along the longitudinal axis of the molecule hence govern an electron density oscillation between the ends of the molecule [172, 173]and set up a plasmonic response as seen in the metallic NPs. This oscillating dipole is capable not only to absorb light but also to reflect the electromagnetic wave in the specular manner. Such a concept was proved for photoswitschable molecules[41] and extended to metal plasmonic NPs recently by our group[14]. In this context, we believe that a new class of active nano/molecular plasmonic composites will be developed that employ the finely tuned, engineered microscopic near field coupling for a customized macroscopic function.

Acknowledgements

M. E. thanks the School of Chemical Engineering at the Aalto University, Finland, the Helmholtz Association (the Initiative and Networking Fund, No. VH-NG-523), and Helmholtz-Zentrum Geesthacht, Germany, for providing financial support to his research group. The authors gratefully acknowledge partial financial supports from the Academy of Finland and the German Research Foundation (DFG) through SFB677 (C01).

Received: ((will be filled in by the editorial staff))
Revised: ((will be filled in by the editorial staff))
Published online: ((will be filled in by the editorial staff))

References

[1] S. Homaeigohar, Y. Davoudpour, Y. Habibi, M. Elbahri, *Nanomaterials* **2017**, *7(11),* 383.

[2] R. Khalil, S. Homaeigohar, D. Häuβler, M. Elbahri, *Sci. Rep.* **2016**, *6*, 33895.

[3] A. Yari Sadi, M. A. Shokrgozar, S. S. Homaeigohar, A. Khavandi, *J. Mater. Sci.: Mater. Med.* **2008**, *19*, 2359.

[4] F. Faupel, V. Zaporojtchenko, T. Strunskus, M. Elbahri, *Adv. Eng. Mater.* **2010**, *12*, 1177.

[5] K.-I. Jang, H. U. Chung, S. Xu, C. H. Lee, H. Luan, J. Jeong, H. Cheng, G.-T. Kim, S. Y. Han, J. W. Lee, J. Kim, M. Cho, F. Miao, Y. Yang, H. N. Jung, M. Flavin, H. Liu, G. W. Kong, K. J. Yu, S. I. Rhee, J. Chung, B. Kim, J. W. Kwak, M. H. Yun, J. Y. Kim, Y. M. Song, U. Paik, Y. Zhang, Y. Huang, J. A. Rogers, *Nat. Commun.* **2015**, *6*, 6566.

[6] S. Homaeigohar, A. U. Zillohu, R. Abdelaziz, M. K. Hedayati, M. Elbahri, *Materials* **2016**, *9*, 848.

[7] S. Behrens, *Nanoscale* **2011**, *3*, 877.

[8] M. Hedayati, F. Faupel, M. Elbahri, *Materials* **2014**, *7*, 1221.

[9] M. K. Hedayati, M. Elbahri, *Plasmonics* **2017**, *12*, 1463.

[10] S. Homaeigohar, M. Elbahri, *Materials* **2014**, *7*, 1017.

[11] S. Kango, S. Kalia, A. Celli, J. Njuguna, Y. Habibi, R. Kumar, *Prog. Polym. Sci.* **2013**, *38*, 1232.

[12] H. Goesmann, C. Feldmann, *Angew. Chem. Int. Ed.* **2010**, *49*, 1362.

[13] S.-W. Hsu, A. L. Rodarte, M. Som, G. Arya, A. R. Tao, *Chem. Rev.* **2018**, *118*, 3100.

[14] M. Elbahri, M. Abdelaziz, S. Homaeigohar, A. Elsharawy, M. Keshavarz Hedayati, C. Röder, M. El Haj Assad, R. Abdelaziz, *Adv. Mater.* **2018**, *30*, 1704442.

[15] H. Yongxing, L. Yuzi, L. Zheng, S. Yugang, *Adv. Funct. Mater.* **2014**, *24*, 2828.

[16] R. Schreiber, N. Luong, Z. Fan, A. Kuzyk, P. C. Nickels, T. Zhang, D. M. Smith, B. Yurke, W. Kuang, A. O. Govorov, T. Liedl, *Nat. Commun*. **2013**, *4*, 2948.

[17] S. Homaeigohar, D. Disci-Zayed, T. Dai, M. Elbahri, *Bioinspired, Biomimetic Nanobiomater.* **2013**, *2*, 186.

[18] S. Homaeigohar, T. Dai, M. Elbahri, *J. Colloid Interface Sci.* **2013**, *406*, 86.

[19] M. Elbahri, Sh. Homaeigohar, T. Dai, R. Abdelaziz, R. Khalil, A. U. Zillohu, *Adv. Funct. Mater.* **2012**, *22*, 4771.

[20] T. Xu, J. Xue, X. Zhang, G. He, H. Chen, *Appl. Surf. Sci.* **2017**, *402*, 294.

[21] S.-H. Bae, K. Karthikeyan, Y.-S. Lee, I.-K. Oh, *Carbon* **2013**, *64*, 527.

[22] A. Meldrum, J. H. R. F., L. A. Boatner, C. W. White, *Adv. Mater*. **2001**, *13*, 1431.

[23] W. A. Murray, W. L. Barnes, *Adv. Mater*. **2007**, *19*, 3771.

[24] R. C. McPhedran, I. V. Shadrivov, B. T. Kuhlmey, Y. S. Kivshar, *NPG Asia Mater.* **2011**, *3*, 100.

[25] F. E. Wagner, S. Haslbeck, L. Stievano, S. Calogero, Q. A. Pankhurst, K. P. Martinek, *Nature*. **2000**, *407*, 691.

[26] D. J. Barber, I. C. Freestone, *Archaeometry*. **1990**, *32*, 33.

[27] J. Roqué, J. Molera, P. Sciau, E. Pantos, M. Vendrell-Saz, *J. Eur. Ceram. Soc.* **2006**, *26*, 3813.

[28] J. Pérez-Arantegui, J. Molera, A. Larrea, T. Pradell, M. Vendrell-Saz, I. Borgia, B. G. Brunetti, F. Cariati, P. Fermo, M. Mellini, *J. Am. Ceram. Soc.* **2001**, *84*, 442.

[29] I. Reiche, S. Röhrs, J. Salomon, B. Kanngießer, Y. Höhn, W. Malzer, F. Voigt, *Anal. Bioanal. Chem.* **2009**, *393*, 1025.

[30] P. Mazzoldi, C. Sada, *Mater. Sci. Eng.: B* **2008**, *149*, 112.

[31] J. M. Garnett, *Phil. Trans. R. Soc. Lond. A* **1906**, *205*, 237.

[32] W. Caseri, *Chem. Eng. Commun*. **2008**, *196*, 549.

[33] F. Lüdersdorff, *Preussen* **1833**, *12*, 224.

[34] P. D. T. F. Kirchner, Universität Leipzig, Germany **1903**., in *Universität Leipzig*, 1903.

[35] J. Nina, S. Lei, W. Jianfang, *Adv. Mater.* **2014**, *26*, 3282.

[36] M. A. C. Stuart, W. T. Huck, J. Genzer, M. Müller, C. Ober, M. Stamm, G. B. Sukhorukov, I. Szleifer, V. V. Tsukruk, M. Urban, *Nat. Mater.* **2010**, *9*, 101.

[37] L. Ionov, *Adv. Funct. Mater.* **2013**, *23*, 4555.

[38] M. Ilčíková, J. Tkáč, P. Kasák, *Polymers* **2015**, *7*, 1518.

[39] N. Jiang, X. Zhuo, J. Wang, *Chem. Rev.* **2018**, *118*, 3054.

[40] W. Lewandowski, M. Fruhnert, J. Mieczkowski, C. Rockstuhl, E. Górecka, *Nat. Commun.* **2015**, *6*, 6590.

[41] M. Elbahri, A. U. Zillohu, B. Gothe, M. K. Hedayati, R. Abdelaziz, H. J. El-Khozondar, M. Bawa'aneh, M. Abdelaziz, A. Lavrinenko, S. Zhukovsky, S. Homaeigohar, *Light: Sci. Appl.* **2015**, *4*, e316.

[42] M. Jamali, M. K. Hedayati, B. Mozooni, M. Javaherirahim, R. Abdelaziz, A. U. Zillohu, M. Elbahri, *Adv. Mater.* **2011**, *23*, 4243.

[43] M. K. Hedayati, M. Javaheri, A. U. Zillohu, H. J. El-Khozondar, M. S. Bawa'aneh, A. Lavrinenko, F. Faupel, M. Elbahri, *Adv. Opt. Mater.* **2014**, *2*, 705.

[44] M. Großmann, A. Klick, C. Lemke, J. Falke, M. Black, J. Fiutowski, A. J. Goszczak, E. Sobolewska, A. U. Zillohu, M. K. Hedayati, H.-G. Rubahn, F. Faupel, M. Elbahri, M. Bauer, *ACS Photonics* **2015**, *2*, 1327.

[45] S. Hayashi, T. Okamoto, *J. Phys. D: Appl. Phys.* **2012**, *45*, 433001.

[46] C. Etrich, S. Fahr, M. K. Hedayati, F. Faupel, M. Elbahri, C. Rockstuhl, *Materials* **2014**, *7*, 727.

[47] M. K. Hedayati, S. Fahr, C. Etrich, F. Faupel, C. Rockstuhl, M. Elbahri, *Nanoscale* **2014**, *6*, 6037.

[48] B. Luk'yanchuk, N. I. Zheludev, S. A. Maier, N. J. Halas, P. Nordlander, H. Giessen, C. T. Chong, *Nat. Mater.* **2010**, *9*, 707.

[49] N. J. Halas, S. Lal, W.-S. Chang, S. Link, P. Nordlander, *Chem. Rev.* **2011**, *111*, 3913.

[50] P. K. Jain, W. Huang, M. A. El-Sayed, *Nano Lett.* **2007**, *7*, 2080.

[51] K. C. Woo, L. Shao, H. Chen, Y. Liang, J. Wang, H.-Q. Lin, *ACS Nano* **2011**, *5*, 5976.

[52] K. M. Mayer, J. H. Hafner, *Chem. Rev.* **2011**, *111*, 3828.

[53] Z. Qian, K. N. Guye, D. J. Masiello, D. S. Ginger, *J. Phys. Chem. B* **2017**, *121*, 1092.

[54] S. Samai, Z. Qian, J. Ling, K. N. Guye, D. S. Ginger, *ACS Appl. Mater. Interfaces* **2018**, *10*, 8976.

[55] K. Juyeong, S. Xiaohui, K. Ahyoung, L. Binbin, S. J. W., O. Zihao, W. Zixuan, C. Qian, *Macromol. Rapid Commun.* **2018**, *0*, 1800101.

[56] L. Dilong, F. Lingling, Z. Fei, L. Huilin, Z. Tao, L. Cuncheng, C. Weiping, D. Zhaoxiang, L. Liangbin, L. Yue, *Adv. Funct. Mater.* **2018**, *28*, 1707392.

[57] I. Ryo, M. Hideyuki, N. Kenichi, M. Yasutaka, I. Kuniharu, *Small* **2018**, *14*, 1704230.

[58] Z. Dai, P. K. Lo, *Nanoscale* **2018**, *10*, 5431.

[59] L. Li, R. Niu, Y. Zhang, *RSC Adv.* **2018**, *8*, 12428.

[60] Y. Zhang, Q. Liu, H. Mundoor, Y. Yuan, I. I. Smalyukh, *ACS Nano* **2015**, *9*, 3097.

[61] L. Jiang, H. Mundoor, Q. Liu, I. I. Smalyukh, *ACS Nano* **2016**, *10*, 7064.

[62] X. Liu, X. Wang, L. Zha, D. Lin, J. Yang, J. Zhou, L. Zhang, *J. Mater. Chem. C* **2014**, *2*, 7326.

[63] X. Liu, C. Zhang, J. Yang, D. Lin, L. Zhang, X. Chen, L. Zha, *Rsc Adv.* **2013**, *3*, 3384.

[64] N. Jiang, Q. Ruan, F. Qin, J. Wang, H.-Q. Lin, *Nanoscale* **2015**, *7*, 12516.

[65] L. Wenzheng, J. Nina, W. Jianfang, *Adv. Mater.* **2017**, *29*, 1604862.

[66] R. S. Silva, P. B. de Melo, L. Omena, A. M. Nunes, M. G. A. da Silva, M. R. Meneghetti, I. N. de Oliveira, *Phys. Rev. E* **2017**, *96*, 062703.

[67] H. Mundoor, G. H. Sheetah, S. Park, P. J. Ackerman, I. I. Smalyukh, J. van de Lagemaat, *ACS Nano* **2018**, *12*, 2580.

[68] A. W. Hauser, D. Liu, K. C. Bryson, R. C. Hayward, D. J. Broer, *Macromolecules* **2016**, *49*, 1575.

[69] G. H. Sheetah, Q. Liu, I. I. Smalyukh, *Opt. Lett.* **2016**, *41*, 4899.

[70] C. Fernández-López, C. Pérez-Balado, J. Pérez-Juste, I. Pastoriza-Santos, Á. R. de Lera, L. M. Liz-Marzán, *Soft Matter* **2012**, *8*, 4165.

[71] B. Rožič, J. Fresnais, C. Molinaro, J. Calixte, S. Umadevi, S. Lau-Truong, N. Felidj, T. Kraus, F. Charra, V. Dupuis, T. Hegmann, C. Fiorini-Debuisschert, B. Gallas, E. Lacaze, *ACS Nano* **2017**, *11*, 6728.

[72] Q. Liu, Y. Yuan, I. I. Smalyukh, *Nano Lett.* **2014**, *14*, 4071.

[73] R. Kempaiah, Y. Liu, Z. Nie, R. Basu, *Appl. Phys. Lett.* **2016**, *108*, 083105.

[74] M. Mishra, S. Kumar, R. Dhar, *Soft Mater.* **2017**, *15*, 34.

[75] M. Middha, R. Kumar, K. Raina, *Liq. Cryst.* **2016**, *43*, 1002.

[76] A. Kuzyk, M. J. Urban, A. Idili, F. Ricci, N. Liu, *Sci. Adv.* **2017**, *3*, e1602803.

[77] W. Caseri, *J. Mater. Chem.* **2010**, *20*, 5582.

[78] Y. Dirix, C. Bastiaansen, W. Caseri, P. Smith, *J. Mater. Sci.* **1999**, *34*, 3859.

[79] G. Carotenuto, G. L. Peruta, L. Nicolais, *Sens. Actuators, B* **2006**, *114*, 1092.

[80] G. Carotenuto, L. Nicolais, P. Perlo, *Polym. Eng. Sci.* **2006**, *46*, 1016.

[81] X. Lang, A. D. Patrick, B. Hammouda, M. J. A. Hore, *Polymer* **2018**, *145*, 137.

[82] M. Karg, Y. Lu, E. Carbó-Argibay, I. Pastoriza-Santos, J. Pérez-Juste, L. M. Liz-Marzán, T. Hellweg, *Langmuir* **2009**, *25*, 3163.

[83] C. Liu, H. Liu, C. Lu, K. Tang, Y. Zhang, *J. Mater. Sci.* **2017**, *52*, 11715.

[84] H. Gehan, C. Mangeney, J. Aubard, G. Lévi, A. Hohenau, J. R. Krenn, E. Lacaze, N. Félidj, *J. Phys. Chem. Lett.* **2011**, *2*, 926.

[85] K. Matthias, H. Thomas, M. Paul, *Adv. Funct. Mater.* **2011**, *21*, 4668.

[86] D. Tao, R. Christian, Z. Xuezhi, B. Felix, O. Hamid, V. G. A. E., M. V. V., G. Markus, B. J. J., *Adv. Opt. Mater.* **2016**, *4*, 877.

[87] T. Ding, A. W. Rudrum, L. O. Herrmann, V. Turek, J. J. Baumberg, *Nanoscale* **2016**, *8*, 15864.

[88] K. Gawlitza, S. T. Turner, F. Polzer, S. Wellert, M. Karg, P. Mulvaney, R. von Klitzing, *Phys. Chem. Chem. Phys.* **2013**, *15*, 15623.

[89] G. Si, Y. Zhao, E. S. P. Leong, Y. J. Liu, *Materials* **2014**, *7*, 1296.

[90] K. Yujie, Z. Chengzhi, Z. Yang, W. Shancheng, C. S. Hwa, L. Yi, *Adv. Funct. Mater.* **2018**, *0*, 1800113.

[91] E. Lee, Y. Xia, R. C. Ferrier, H.-N. Kim, M. A. Gharbi, K. J. Stebe, R. D. Kamien, R. J. Composto, S. Yang, *Adv. Mater.* **2016**, *28*, 2731.

[92] A. Querejeta-Fernández, G. Chauve, M. Methot, J. Bouchard, E. Kumacheva, *J. Am. Chem. Soc.* **2014**, *136*, 4788.

[93] Y. Zuo, J. Zhao, Y. Gao, Y. Zhang, *J. Mater. Sci.* **2017**, *52*, 9584.

[94] M. Muratalin, P. F. Luckham, *J. Colloid Interface Sci.* **2013**, *396*, 1.

[95] Q. M. Zhang, W. Wang, Y.-Q. Su, E. J. Hensen, M. J. Serpe, *Chem. Mater.* **2015**, *28*, 259.

[96] L. Wenzheng, J. Nina, W. Jianfang, *Adv. Mater.* **2017**, *29*, 1604862.

[97] J. Xu, Y. Zhang, T.-T. Zhai, Z. Kuang, J. Li, Y. Wang, Z. Gao, Y.-Y. Song, X.-H. Xia, *ACS Nano* **2018**, *12*, 6895.

[98] J. Kim, H. Son, D. J. Cho, B. Geng, W. Regan, S. Shi, K. Kim, A. Zettl, Y.-R. Shen, F. Wang, *Nano Lett.* **2012**, *12*, 5598.

[99] Y. Yao, M. A. Kats, P. Genevet, N. Yu, Y. Song, J. Kong, F. Capasso, *Nano Lett.* **2013**, 13, 1257.

[100] S. Homaeigohar, M. Elbahri, *NPG Asia Mater.* **2017**, *9*, e427.

[101] S. Khatua, W.-S. Chang, P. Swanglap, J. Olson, S. Link, *Nano Lett.* **2011**, *11*, 3797.

[102] C. P. Byers, H. Zhang, D. F. Swearer, M. Yorulmaz, B. S. Hoener, D. Huang, A. Hoggard, W.-S. Chang, P. Mulvaney, E. Ringe, N. J. Halas, P. Nordlander, S. Link, C. F. Landes, *Sci. Adv.* **2015**, *1*.

[103] V. Stockhausen, P. Martin, J. Ghilane, Y. Leroux, H. Randriamahazaka, J. Grand, N. Felidj, J. C. Lacroix, *J. Am. Chem. Soc.* **2010**, *132*, 10224.

[104] Y. Leroux, J. C. Lacroix, C. Fave, G. Trippe, N. Félidj, J. Aubard, A. Hohenau, J. R. Krenn, *ACS Nano* **2008**, *2*, 728.

[105] Y. R. Leroux, J. C. Lacroix, K. I. Chane-Ching, C. Fave, N. Félidj, G. Lévi, J. Aubard, J. R. Krenn, A. Hohenau, *J. Am. Chem. Soc.* **2005**, *127*, 16022.

[106] Y. Leroux, E. Eang, C. Fave, G. Trippe, J. C. Lacroix, *Electrochem. Commun.* **2007**, *9*, 1258.

[107] C. Bechinger, S. Ferrere, A. Zaban, J. Sprague, B. A. Gregg, *Nature* **1996**, *383*, 608.

[108] W. Yue, X. Yongshu, Z. Qiong, T. He, Z. Weihong, L. A. D. Q., *Angew. Chem. Int. Ed.* **2014**, *53*, 2090.

[109] S. Sun, C. B. Murray, D. Weller, L. Folks, A. Moser, *Science* **2000**, *287*, 1989.

[110] J. F. Stoddart, *Nat. Chem.* **2009**, *1*, 14.

[111] J. Andréasson, U. Pischel, S. D. Straight, T. A. Moore, A. L. Moore, D. Gust, *J. Am. Chem. Soc.* **2011**, *133*, 11641.

[112] J. Chen, R. J. Patton, *Robust model-based fault diagnosis for dynamic systems*, Vol. 3, Springer Science & Business Media, **2012**.

[113] D. Kitagawa, S. Kobatake, *Chem. Sci.* **2012**, *3*, 1445.

[114] S. Pu, D. Jiang, W. Liu, G. Liu, S. Cui, *J. Mater. Chem.* **2012**, *22*, 3517.

[115] J. Kärnbratt, M. Hammarson, S. Li, H. L. Anderson, B. Albinsson, J. Andréasson, *Angew. Chem.* **2010**, *122*, 1898.

[116] H. Cahová, A. Jäschke, *Angew. Chem. Int. Ed.* **2013**, *52*, 3186.

[117] T. Pace, V. Müller, S. Li, P. Lincoln, J. Andréasson, *Angew. Chem. Int. Ed.* **2013**, *52*, 4393.

[118] C. Jia, J. Wang, C. Yao, Y. Cao, Y. Zhong, Z. Liu, Z. Liu, X. Guo, *Angew. Chem. Int. Ed.* **2013**, *52*, 8666.

[119] S. Kobatake, S. Takami, H. Muto, T. Ishikawa, M. Irie, *Nature* **2007**, *446*, 778.

[120] R. Klajn, *Chem. Soc. Rev.* **2014**, *43*, 148.

[121] A. Spangenberg, R. Métivier, R. Yasukuni, K. Shibata, A. Brosseau, J. Grand, J. Aubard, P. Yu, T. Asahi, K. Nakatani, *Phys. Chem. Chem. Phys.* **2013**, *15*, 9670.

[122] M. Wang, G. Hartmann, Z. Wu, L. Scarabelli, B. B. Rajeeva, J. W. Jarrett, E. P. Perillo, A. K. Dunn, L. M. Liz-Marzán, G. S. Hwang, Y. Zheng, *Small* **2017**, *13*, 1701763.

[123] S. Murphy, S. Jaber, C. Ritchie, M. Karg, P. Mulvaney, *Langmuir* **2016**, *32*, 12497.

[124] J. R. Morones, W. Frey, *J. Nanopart. Res.* **2010**, *12*, 1401.

[125] Y. Yan, L. Liu, Z. Cai, J. Xu, Z. Xu, D. Zhang, X. Hu, *Sci. Rep.* **2016**, *6*, 31328.

[126] Y. B. Zheng, B. Kiraly, S. Cheunkar, T. J. Huang, P. S. Weiss, *Nano lett.* **2011**, *11*, 2061.

[127] D. Cao, C. Xu, W. Lu, C. Qin, S. Cheng, *Sol. RRL* **2018**, *2*, 1700219.

[128] W. Fuan, L. Xiaoqing, W. Itamar, *Angew. Chem. Int. Ed.* **2015**, *54*, 1098.

[129] K. L. Young, M. R. Jones, J. Zhang, R. J. Macfarlane, R. Esquivel-Sirvent, R. J. Nap, J. Wu, G. C. Schatz, B. Lee, C. A. Mirkin, *Proc. Natl. Acad. Sci.* **2012**, *109*, 2240.

[130] V. Sashuk, K. Winkler, A. Żywociński, T. Wojciechowski, E. Górecka, M. Fiałkowski, *ACS Nano* **2013**, *7*, 8833.

[131] I. Lagzi, B. Kowalczyk, D. Wang, B. A. Grzybowski, *Angew. Chem.* **2010**, *122*, 8798.

[132] S. Basu, S. Panigrahi, S. Praharaj, S. K. Ghosh, S. Pande, S. Jana, T. Pal, *New J. Chem.* **2006**, *30*, 1333.

[133] Z. Sun, W. Ni, Z. Yang, X. Kou, L. Li, J. Wang, *Small* **2008**, *4*, 1287.

[134] X. Qian, J. Li, S. Nie, *J. Am. Chem. Soc.* **2009**, *131*, 7540.

[135] W. Li, I. Kanyo, C.-H. Kuo, S. Thanneeru, J. He, *Nanoscale* **2015**, *7*, 956.

[136] Y. Torii, N. Sugimura, H. Mitomo, K. Niikura, K. Ijiro, *Langmuir* **2017**, *33*, 5537.

[137] C.-H. Lu, A. Cecconello, I. Willner, *J. Am. Chem. Soc.* **2016**, *138*, 5172.

[138] W. Chunyan, H. Zhenzhen, L. Youhui, R. Jinsong, Q. Xiaogang, *Adv. Mater.* **2010**, *22*, 2792.

[139] K. Saha, S. S. Agasti, C. Kim, X. Li, V. M. Rotello, *Chem. Rev.* **2012**, *112*, 2739.

[140] X. Liu, C.-H. Lu, I. Willner, *Acc. Chem. Res.* **2014**, *47*, 1673.

[141] Y. Zhao, L. Cao, J. Ouyang, M. Wang, K. Wang, X.-H. Xia, *Anal. Chem.* **2013**, *85*, 1053.

[142] A. Kuzyk, R. Jungmann, G. P. Acuna, N. Liu, *ACS Photonics* **2018**, *5*, 1151.

[143] N. Liu, T. Liedl, *Chem. Rev.* **2018**, *118*, 3032.

[144] J. Chao, Y. Lin, H. Liu, L. Wang, C. Fan, *Mater. Today* **2015**, *18*, 326.

[145] L. Zhang, L. Dai, Y. Rong, Z. Liu, D. Tong, Y. Huang, T. Chen, *Langmuir* **2015**, *31*, 1164.

[146] J. He, P. Zhang, T. Babu, Y. Liu, J. Gong, Z. Nie, *Chem. Commun.* **2013**, *49*, 576.

[147] Y. Wei, S. Han, J. Kim, S. Soh, B. A. Grzybowski, *J. Am. Chem. Soc.* **2010**, *132*, 11018.

[148] B. Tong, S. Lu, Y. Huijun, P. M. Teresa, W. Li-Zhu, T. Chen-Ho, N. Zhihong, T. Zhiyong, Z. Tierui, *Adv. Mater.* **2014**, *26*, 5613.

[149] Y. Yan, J. I. L. Chen, D. S. Ginger, *Nano Lett.* **2012**, *12*, 2530.

[150] K. Watanabe, K. Kuroda, D. Nagao, *Materials* **2018**, *11*, 794.

[151] L. De Sio, A. Cunningham, V. Verrina, C. M. Tone, R. Caputo, T. Bürgi, C. Umeton, *Nanoscale* **2012**, *4*, 7619.

[152] K. Wang, S.-M. Jin, J. Xu, R. Liang, K. Shezad, Z. Xue, X. Xie, E. Lee, J. Zhu, *ACS Nano* **2016**, *10*, 4954.

[153] T. A. F. König, P. A. Ledin, J. Kerszulis, M. A. Mahmoud, M. A. El-Sayed, J. R. Reynolds, V. V. Tsukruk, *ACS Nano* **2014**, *8*, 6182.

[154] K. R. Jeong, I. Lee, J. Y. Park, C. S. Choi, S.-H. Cho, J.-L. Lee, *Npg Asia Mater.* **2017**, *9*, e362.

[155] J.-L. Wang, Y.-R. Lu, H.-H. Li, J.-W. Liu, S.-H. Yu, *J. Am. Chem. Soc.* **2017**, *139*, 9921.

[156] Y. Montelongo, D. Sikdar, Y. Ma, A. J. S. McIntosh, L. Velleman, Anthony R. Kucernak, J. B. Edel, A. A. Kornyshev, *Nat. Mater.* **2017**, *16*, 1127.

[157] B. Comiskey, J. D. Albert, H. Yoshizawa, J. Jacobson, *Nature* **1998**, *394*, 253.

[158] S. J. Telfer, M. D. McCreary, *SID Symp. Dig. Tech. Pap.* **2016**, *47*, 574.

[159] H. D. C. Lin, M. Wang (E Ink California, LLc), US20160041448 A1. , **2016**.

[160] L. Shao, X. Zhuo, J. Wang, *Adv. Mater.* **2018**, *30*, 1704338.

[161] X. Xue, K. Liu, E. P. Furlani, *J. Phys. Chem. C* **2017**, *121*, 9489.

[162] J. He, X. Huang, Y.-C. Li, Y. Liu, T. Babu, M. A. Aronova, S. Wang, Z. Lu, X. Chen, Z. Nie, *J. Am. Chem. Soc.* **2013**, *135*, 7974.

[163] R. M. Choueiri, E. Galati, H. Thérien-Aubin, A. Klinkova, E. M. Larin, A. Querejeta-Fernández, L. Han, H. L. Xin, O. Gang, E. B. Zhulina, M. Rubinstein, E. Kumacheva, *Nature* **2016**, *538*, 79.

[164] A. B. Serrano-Montes, D. Jimenez de Aberasturi, J. Langer, J. J. Giner-Casares, L. Scarabelli, A. Herrero, L. M. Liz-Marzán, *Langmuir* **2015**, *31*, 9205.

[165] F. Brouers, D. Rauw, J. P. Clerc, G. Giraud, *Phys. Rev. B* **1994**, *49*, 14582.

[166] G. A. Niklasson, *J. Appl. Phys.* **1987**, *62*, 258.

[167] V. A. Markel, L. S. Muratov, M. I. Stockman, T. F. George, *Phys. Rev. B* **1991**, *43*, 8183.

[168] V. M. Shalaev, R. Botet, *Phys. Rev. B* **1994**, *50*, 12987.

[169] V. M. Shalaev, *Optical properties of nanostructured random media*, Vol. 82, Springer, **2002**.

[170] V. Astapenko, *Polarization Bremsstrahlung on Atoms, Plasmas, Nanostructures and Solids*, Vol. 72, Springer Science & Business Media, **2013**.

[171] J. I. Pankove, *Optical processes in semiconductors*, Courier Corporation, **1975**.

[172] A. Manjavacas, F. Marchesin, S. Thongrattanasiri, P. Koval, P. Nordlander, D. Sánchez-Portal, F. J. García de Abajo, *ACS Nano* **2013**, *7*, 3635.

[173] E. B. Guidez, C. M. Aikens, *J. Phys. Chem. C* **2013**, *117*, 21466.

Table of Content:

Inspired by Nature, the nanocomposites with a smart behavior evolve the area of advanced materials for optical technologies. Such materials have progressed from classic nanocomposites with a limited fraction of optical nanofillers towards advanced systems operating by reconfiguration of a large number of nanoparticles tethered by switchable amphiphilic copolymers, DNA etc. This review introduces such systems and also the advanced plasmonic molecules based switchable nanocomposites.

Keyword: ((switchability, optical nanomaterials, nanocomposites, plasmonics, external stimuli))

S. Homaeigohar, M. Elbahri*

Switchable Plasmonic Nanocomposites

ToC figure